The Application of Data Mining and Machine Learning in the Diagnosis of Mental Disorders

by

Mohammed A. Syed

A dissertation submitted to the Graduate Faculty of
Auburn University
in partial fulfillment of the
requirements for the Degree of
Doctor of Philosophy

Auburn, Alabama
August 5, 2017

Keywords: Autism, PTSD, fMRI, Independent Components, Reproducibility, Clustering

Approved by

Gopikrishna Deshpande, Committee Chair, Auburn University MRI Research Center
Sanjeev Baskiyar, Associate Professor, Committee Co-chair, Dept. of Computer Science & Software Eng., Auburn University
Cheryl Seals, Associate Professor, Dept. of Computer Science & Software Eng., Auburn University
Myoung An, Associate Research Professor, Dept. of Computer Science & Software Eng., Auburn University

Abstract

Autism is a developmental disorder that is currently diagnosed using behavioral tests which can be subjective. Consequently, objective non-invasive imaging biomarkers of Autism are being actively researched. The common theme emerging from previous functional magnetic resonance imaging (fMRI) studies is that Autism is characterized by alterations of fMRI-derived functional connections in certain brain networks which may provide a biomarker for objective diagnosis. However, identification of individuals with Autism solely based on these measures has not been reliable, especially when larger sample sizes are taken into consideration. There is a lack of objective biomarkers to accurately identify the underlying etiology and related pathophysiology of disparate brain-based disorders that are less distinguishable clinically. Brain networks derived from resting-state functional magnetic resonance imaging (R-fMRI) has been a popular tool for discovering candidate biomarkers. Specifically, independent component analysis (ICA) of R-fMRI data is a powerful multivariate technique for investigating brain networks. However, ICA-derived brain networks that are not highly reproducible within heterogeneous clinical populations may provide mean statistical separation between groups, and yet not be very discriminative at the individual subject level. We hypothesize that functional brain networks that are most reproducible in subjects within clinical and control groups separately, but not when the two groups are merged, may possess the ability to discriminate effectively between the groups.

In this study, we propose a “discover-confirm” scheme based upon the assessment of the reproducibility of independent components (representing brain networks) obtained from R-fMRI

(discover phase) using the gRAICAR (generalized Ranking and Averaging Independent Component Analysis by Reproducibility) algorithm followed by unsupervised clustering analysis of these components to evaluate their ability to discriminate between groups (confirm phase). followed by a clustering analysis of these components to evaluate their ability to discriminate between groups in an unsupervised way (confirm).

Furthermore, we present gMedICA, a software package that implements the methodology in in support of our hypothesis. The unique feature of our software package is its ability to seamlessly interface with other software packages such as FSL so that all related analyses utilizing features of other software can be performed within the same package, thus providing a one-stop software solution starting with raw DICOM images to the results.

We obtained cluster purity of up to 0.971 or 97.1% accuracy in a data set of 799 subjects comprising Autism Spectrum Disorders (ASD) and healthy controls acquired from multiple sites, using our proposed methodology. In addition, we showcase our software using R-fMRI data acquired from US Army soldiers returning from the wars in Iraq and Afghanistan who were clinically grouped into the following groups: PTSD (posttraumatic stress disorder), comorbid PCS (post-concussion syndrome) + PTSD, and matched healthy combat controls. Using our methodology, we obtained cluster purity of up to 1 or all groups were identified with 100% accuracy.

Acknowledgments

This research project was recommended by Dr. Deshpande and his indefatigable mentorship, exceptional guidance every step of the way, and extraordinary patience made it possible for me to start, progress and complete it. I would like to express my sincerest gratitude to Dr. Deshpande for giving me this opportunity. I am grateful to Dr. Umphress, our graduate program mentor, for introducing me to this great program and encouragement throughout. Dr. Baskiyar's encouragement and support was monumental in overcoming seemingly insurmountable challenges. I am grateful to him for that and an excellent academic experience as my very first course at Auburn was under his tutelage. Drs. Seals and An are owed a debt of gratitude by me for their kind thoughts and guidance that showed a clear path forward. Our IT team members, Shannon and Jim, and graduate school team members, Clint, Ms. Young and Ms. Ray, were always available and happy to help regardless of the nature of request and I offer my gratitude to them. I highly appreciate Dr. D. Rangaprakash's tireless help, support and patience throughout this project. I would like to thank Dr. Yang for his support and clarifying complex concepts which made this accomplishment possible. I am also grateful to Drs. Hu, Dretsch, Denney and Katz for their guidance and support. I acknowledge NSF and the Department of Computer Science and Software Engineering (S-STEM grant # 0966278) for funding this study.

I would also like to thank the people from my inner circle for their support during my doctoral studies. My mother, late father, grandfather and aunt established in me an unquenchable thirst for

knowledge that lead me down the path to my doctoral studies. My siblings offered moral support and an ear throughout the progression of my thesis. My children, who shared their enthusiasm for learning about my areas of study, served as a necessary distraction when I needed a break. My spouse and administrative head provided much needed balance among the challenges that arose during a term focused on the completion of this degree.

Finally, I would like to thank the Almighty, Most Gracious and Merciful, for helping me to realize my strengths and providing me with the means to see this harrowing, yet fulfilling, endeavor to its fruition.

Table of Contents

List of Tables

List of Figures

List of Abbreviations

AC	Aligned Component
ADDM	Autism and Developmental Disabilities Monitoring
ADHD	Attention Deficit Hyperactivity Disorder
AN	Auditory Network
ASD	Autism Spectrum Disorders
BOLD	Blood Oxygenation Level Dependent signal
CEN	Central-executive network
DLPFC	Dorsolateral Prefrontal Cortex
DMN	Default Mode Network
DPARSF	Data Processing Assistant for Resting-State fMRI
DTI	Diffusion Tensor Imaging
fMRI	Functional Magnetic Resonance Imaging
FSL	fMRIB Software Library
FSM	Full Similarity Matrix
FT	Functional Trees
FWHM	Full-Width at Half-Max
gRAICAR	Generalized Ranking and Averaging Independent Component Analysis by Reproducibility
HRF	Hemodynamic Response Function
IC	Independent Components

ICA	Independent Component Analysis
IPL	Inferior parietal lobe
LMT	Logical Model Trees
MELODIC	Multivariate Exploratory Linear Optimized Decomposition into Independent Components
MLP	Multi-layer Perceptron
MNI	Montreal Neurological Institute
MPFC	Medial prefrontal cortex
MRI	Magnetic Resonance Imaging
mTBI	Mild-Traumatic Brain Injury
MVPA	Multi-voxel pattern analysis
NIfTI	Data Format
NMI	Normalized Mutual Information
NSI	Neurobehavioral Symptom Inventory
PCA	Principal Component Analysis
RB	Realization Block
RZ	Realization Component (Used interchangeably)
PCL5	PTSD Checklist-5 score
PCS	Post-Concussion Syndrome
PTSD + PCS	Comorbid PTSD and PCS (subjects with both these disorders)
PTSD	Posttraumatic Stress Disorder

ROI	Region of Interest
R-fMRI	Resting-State fMRI
SBL	Subject Block
SBM	Surface-based Morphometry
SMN	Somato Motor Network
SOM	Self-organizing Map
SPM	Statistical Parametric Mapping
SVM	Support Vector Machine
TC	Typical Control
TE	Echo Time
TPN	Task-positive Network
TR	Repetition Time
VN	Visual Network

CHAPTER 1

Introduction

1.1 Motivation

It is a very challenging task to fully comprehend the workings of the human brain. Non-invasive techniques to study cognitive functions unique to humans are required to understand the human brain in vivo from a functional perspective. Technical advances have made it possible to eliminate the invasive nature of conventional neuroimaging techniques and study human brain functionality with high spatiotemporal resolution [1]. While magnetic resonance imaging of anatomic structures has long been considered an integral part of the diagnostic process, functional magnetic resonance imaging or fMRI methodologies to localize brain activity are significantly increasing the clinical role of MRI [2]. These methodologies are sensitive to cerebral blood flow, cerebral blood volume and blood oxygenation which may then be used to build functional maps of mental processes and define activity in the healthy and diseased human brain. fMRI can detect local fluctuations or increases in relative blood oxygenation, most likely indicating neurotransmitter action and local neuronal signaling. It can be utilized to characterize normal or pathological patterns of brain functioning, classify pathological traits, and measure treatment responses among others [3]. Since its introduction, fMRI has been successfully used in a wide variety of settings from identifying human brain language areas [4], detecting changes in the brain in response to complex human movements [5], measuring signal changes accompanying sensory stimulation [6] to such monumental tasks as studying brain networks shaping religious beliefs [7]. Its application has not been

limited to humans and recently been expanded to canines studying the enhancement of odor-induced activity in the canine brain [8] as an example.

Fig. 1.1 Siemens Magnetom 7T Actively-Shielded MRI Scanner at the Auburn MRI Research Center

The utilization of fMRI in diagnostics has significantly expanded. We provide some recent examples of how it is being applied in the fields of general diagnostics, psychiatry and neurology. Brain activity changes in patients with Crohn's disease were detected by blood oxygenation level dependent fMRI or BOLD-fMRI [9]. fMRI studies showed that patients with bulimia nervosa do not have characteristic neurodevelopment of cognitive control under emotional influences [10]. Hubbard et al. [11] investigated a new diagnostic marker, visual-

evoked cerebral metabolic rate of oxygen ($veCMRO_2$), to classify patients with multiple sclerosis using fMRI. Jin et al. [12] studied the characterization of patients with post-traumatic stress disorder or PTSD using resting-state fMRI. Rangaprakash et al. [13] presented a diagnostic biomarker of mild-traumatic brain injury and posttraumatic stress disorder. fMRI studies have also been providing valuable insight into the diagnostics and management of Autism Spectrum Disorders or ASD [14] [15] [16] [17]. This leads us to another challenge which is the diagnostics of heterogeneous neurological disorders such as Autism. A heterogeneous medical disorder is defined as having several etiologies or causes. In more generalized terms, this also refers to a group of patients where the disease is not the same for all of them, yet they all share some loosely defined common characteristics. Neurological/Psychiatric conditions that are categorized as such pose diagnostic challenges since we are not defining the condition pathologically (such as a lesion, inflammation etc.) or clinically (such as pain, excessive vomiting etc.), but by a broad set of behavioral manifestations.

Autism is considered a developmental disability that can lead to significant social, communication, and behavioral challenges. Considering the societal implications of Autism, it is imperative that this disorder is diagnosed early and definitively. Autism is currently diagnosed using behavioral tests that can be subjective but objective non-invasive biomarkers of Autism are being actively researched. Previous and current research studies have been focusing on combining functional magnetic resonance imaging (fMRI) with machine learning and data mining techniques to reach definitive classification of Autism. The common theme emerging is that Autism is characterized by alterations of functional connections in certain brain networks and that appropriately using MRI-based methods to characterize this altered connectivity may provide a biomarker for classification and objective diagnosis. However, identification of

individuals with Autism solely based on these measures has not been reliable especially when larger sample sizes are taken into consideration.

Similarly, Posttraumatic stress disorder (PTSD) and Post-concussion syndrome (PCS) are heterogeneous neurological disorders where fMRI connectivity metrics derived from them may not be highly reproducible, leading to poor generalizability and consequently lower classification accuracies. Posttraumatic Stress Disorder or PTSD symptoms can either start soon after experiencing a traumatic event or years after the event thus leading to its classification as a heterogeneous disorder not only from the standpoint of the occurrence following a trauma but also from that of symptoms experienced. Mild traumatic brain injury (mTBI) presents a broad range of clinical features indicating that its underlying pathologic features are highly heterogeneous. Military service members sustaining mTBI are also at the risk of developing post-concussion syndrome (PCS) and PSTD. Even though PTSD can be characterized by functional hyper-connectivity, making such a determination in PCS has led to mixed or inconclusive results.

We surmise that one of the contributing factors may be that these disorders are highly heterogeneous, hence metrics derived from the affected group may not be highly reproducible within that group leading to poor generalizability, which in turn leads to lower classification accuracies.

We hypothesize that functional brain networks that are most reproducible within these groups and healthy Control groups separately, but not when the groups are merged, may possess the ability to distinguish effectively between the groups. In this dissertation, we propose a methodology to discover the biomarkers of such mental disorders using non-invasive imaging and neuroinformatics tools, and show that such biomarkers possess good discriminative ability

for classifying healthy individuals from those with the disorder. We combine data mining and machine learning techniques, by first assessing the reproducibility of independent components obtained from resting-state fMRI followed by a clustering analysis of these components to evaluate their ability to discriminate between groups in an unsupervised way. We also propose a self-organizing map (SOM) based approach to visualize high-dimension subject population and the separation between groups. Furthermore, we present gMedICA, a software package implementing this methodology to illustrate its power and utility.

Our proposed methodology produced cluster purities of up to 0.97 or 97.1% accuracy when applied to a subject population comprising Autism Spectrum Disorders and healthy controls. Cluster purities of up to 1 were obtained when we applied this methodology to a subject population comprising Posttraumatic stress disorder (PTSD), Post-concussion syndrome, and healthy controls. In other words, all 3 groups were identified with 100% accuracy.

1.2 This Work in Relation to Prior Literature

Significant progress has been made towards investigating biomarkers in the diagnostics of heterogeneous neurological disorders including Autism and PTSD. Main deficits observed in ASD patients have been attributed to decreased functional connectivity in default mode subnetworks (DMN) [18]. Also, there is reduced activity in the ventral medial prefrontal cortex and ventral anterior cingulate cortex [19]. Adolescents with ASD were found to have visuospatial working memory deficiency within the DMN [20] and the regions of DMN functional connectivity are smaller in the bilateral inferior parietal lobule and posterior cingulate cortex in ASD patients [21]. Similarly, brain regions involved in executive control are impaired in PTSD and PCS [22] [23] [24] [25]. In addition, previous studies implicate the prefrontal

cortex [26] [27] [28] [29], parietal lobe [30] [31] [32] [33], and caudate [34] [35] [36] [37] in these disorders. Although we have these invaluable insights into such disorders, identifying patients based on these measures has not been reliable especially in larger sized samples [38] [39].

We attempt to generate reliable metrics, for both small and large samples, by delving deeper into the arena of data mining and machine learning. We employ independent component analysis, a blind source separation technique commonly used to extract functional brain networks [40] [41] [42] [18]. We examine the reproducibility of independent components separately using a novel algorithm, gRAICAR (Generalized Ranking and Averaging Independent Component Analysis by Reproducibility) [43], within groups, and cluster results to discover the ability of highly reproducible components to distinguish between patients and healthy controls. In addition, we present a software package that implements this methodology.

1.3 Organization of the Dissertation

This dissertation has a total of 6 chapters. Chapter 1 provides an introduction and motivation behind this study. Chapter 2 presents general methods which in our case include an overview of the gRAICAR algorithm we have used to analyze the reproducibility of independent components. Chapters 3 and 4 present work on our projects. Each chapter first introduces the topic and the motivation behind the project followed by materials and methods used in the study, its results, and a discussion section. Chapter 3 presents our methodology to investigate brain connectomic alterations in Autism using the reproducibility of independent components derived from Resting State functional MRI. Chapter 4 presents an implementation of our methodology in gMedICA, a software package for assessing the reproducibility of brain networks and their discriminability across disorders, followed by its evaluation in a study involving PTSD, PCS and

healthy control subjects. Chapter 5 provides concluding remarks on our projects whereas chapter 6 lists peer-reviewed publications as a result of our studies.

CHAPTER 2

General Methods

In this chapter, we introduce the gRAICAR algorithm to review the reproducibility of independent components.

2.1 gRAICAR Algorithm

In this section, we summarize the conceptual underpinnings of the gRAICAR algorithm. We refer our readers to the original paper by Yang et al. [43], should they need a more comprehensive review.

We can represent the pre-processed dataset from subject i (i=1,2,$\cdots$,n) as a matrix A_i, of dimensions $\alpha_i \times \beta_i$, with α_i representing the number of time points and β_i the number of voxels. A_i, the data matrix, can now be decomposed into c_i independent components (ICs) in the spatial domain forming a matrix B_i, of dimensions $c_i \times \beta_i$, and their corresponding mixing time courses forming a matrix, C_i, of dimensions $c_i \times \alpha_i$.

The four main processing phases in the gRAICAR algorithm have been summarized in Fig. 2.1. We will include a high-level overview of this algorithm referring the readers to the original work by Yang et al. [43] for a more comprehensive description. The first phase involves performing ICA decomposition k (~5000 for this study) times for each subject using random initial values leading to $k \times n$ realizations where n represents the number of subjects. We refer to these realizations as *RZ*s where RZ_{ab} refers to the ICs obtained from the b^{th} realization of subject a. A full similarity matrix (*FSM*) that has relational measures between all *RZ*s is constructed in the second phase. Normalized mutual information or *NMI* quantifies the similarity between two *RZ*s in this algorithm. *RZ*s that are found to be highly reproducible

across subjects and ICA realizations are extracted and aligned in the third phase. Two related *RZ*s are treated as individual-level components with the same primary group-level component or an aligned component, *AC*. For each *AC*, the algorithm generates a $kn \times kn$ reproducibility matrix within which *NMI*s between all pairs of *RZ*s relevant to the *AC* are collected. The algorithm now aligns *AC*s to obtain group-level component maps and examines the inter-subject consistency in the fourth phase. Fig. 2.1 demonstrates the algorithm in general terms and we illustrate the specific implementation of this algorithm for an example of three subjects in Fig. 2.2, each with a set of four subject-level ICs.

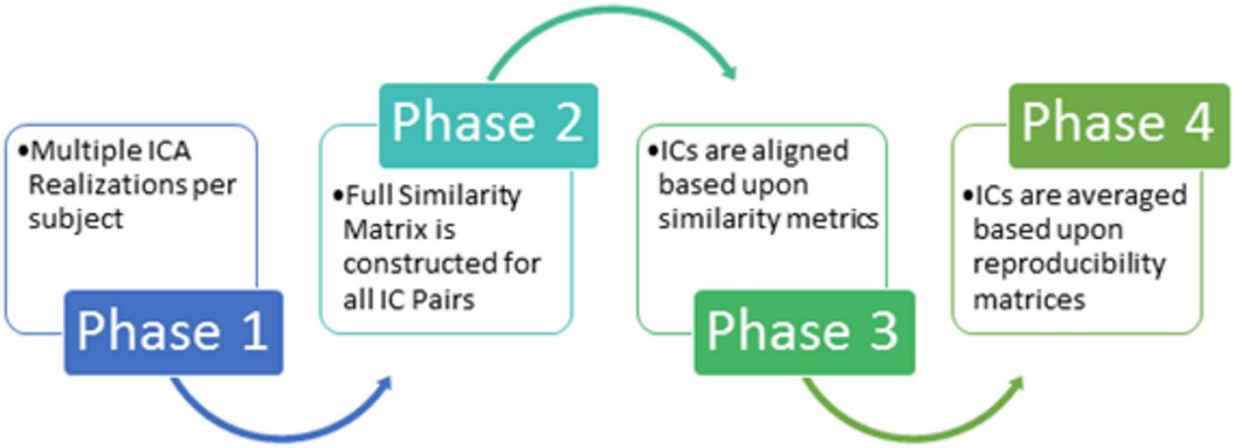

Fig. 2.1 Work flow diagram illustrating the 4 phases of gRAICAR algorithm.

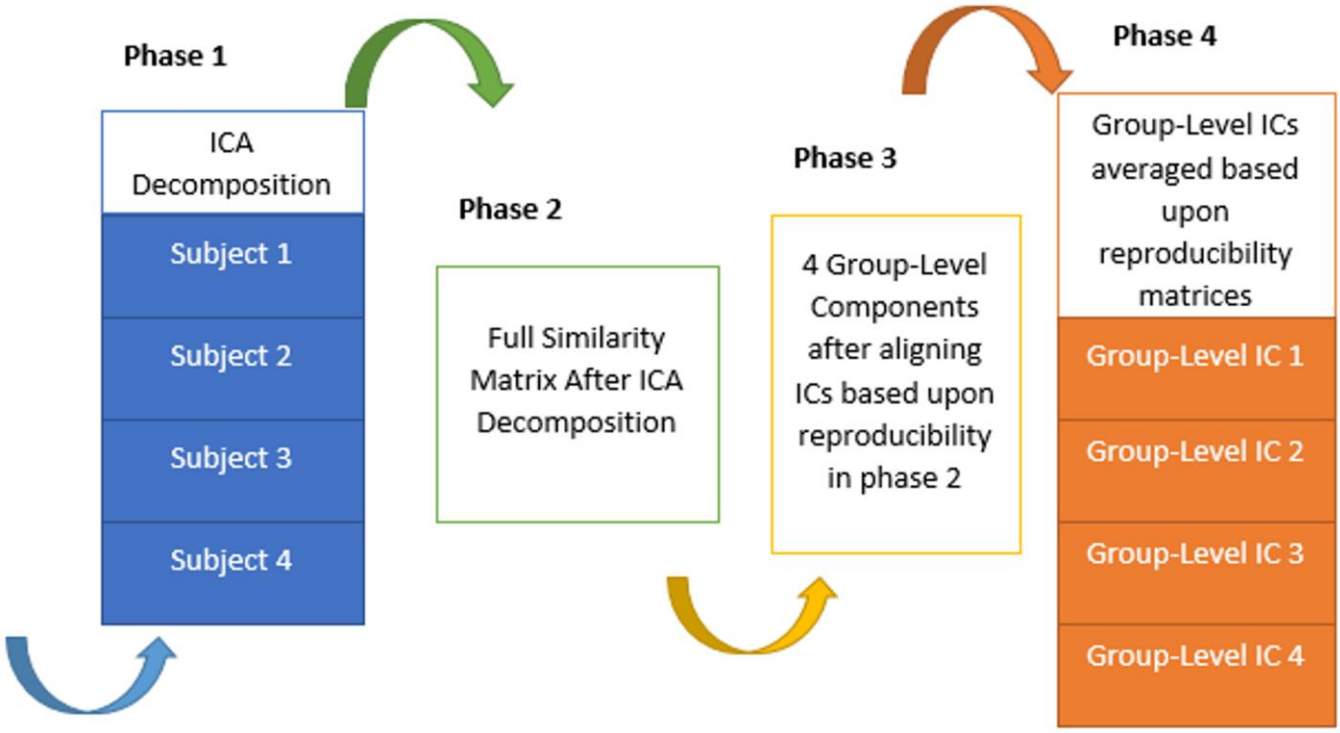

Fig. 2.2. An illustration of the implementation of gRAICAR algorithm using a sample data set of 3 subjects, each with 4 subject-level ICs. Phase 1 involves multiple ICA decompositions for each subject. Phase 2 involves creating a full similarity matrix (FSM). ICs are aligned based upon similarity metrics in phase 3. In phase 4, ICs are averaged based upon reproducibility matrices.

Continuing our discussion of the algorithm, we now delve into the high-level technical underpinnings of the algorithm. The FSM constructed in the second phase of the algorithm includes relational measures between all *RZ*s. Block structure of this *FSM* shows subject blocks (*SBL*s) which in turn represent subject-wise relationships. Elements within these blocks are able to determine similarity between *RZ*s from the same subject or pairs of *RZ*s from different subjects depending upon the block location. In these *SBL*s, there are $k \times k$ realization blocks (*RB*s) providing pair-wise similarity between *RZ*s from different ICA realizations. Similarity between two *RB*s can be quantified by using normalized mutual information or *NMI*

[44]. If two variables are identical, *NMI* is set to 1 and 0 if the two variables are statistically independent. This reveals higher order statistical similarity as opposed to second order similarity as defined by correlation or covariance [45]. The gRAICAR algorithm computes *NMI*s between each IC pair using mutual information based upon the algorithm proposed by Kraskov et al. [46]. *NMI*s are then standardized within an *RB*, leading to standardized *NMI* or *SNMI*. Fig. 2.3 shows the block structure as implemented in a *FSM* with 3 artificial subjects having two ICA realizations each i.e. $n = 3$ and $k = 2$.

	SUBJECT 1	SUBJECT 2	SUBJECT 3
SUBJECT 1	RZ 11 – 11 RZ 11 – 12 RZ 12 – 11 RZ 12 – 12	RZ 11 – 21 RZ 11 – 22 RZ 12 – 21 RZ 12 – 22	RZ 11 – 31 RZ 11 – 32 RZ 12 – 31 RZ 12 – 32
SUBJECT 2	RZ 21 – 11 RZ 21 – 12 RZ 22 – 11 RZ 22 – 12	RZ 21 – 21 RZ 21 – 22 RZ 22 – 21 RZ 22 – 22	RZ 21 – 31 RZ 21 – 32 RZ 22 – 31 RZ 22 – 32
SUBJECT 3	RZ 31 – 11 RZ 31 – 12 RZ 32 – 11 RZ 32 – 12	RZ 31 – 21 RZ 31 – 22 RZ 32 – 21 RZ 32 – 22	RZ 31 – 31 RZ 31 – 32 RZ 32 – 31 RZ 32 – 32

Fig. 2.3 Block structure of full similarity matrix (FSM) based upon an example set with 3 subjects and 2 sets of subject-level components (RZ, a set of ICs produced after two ICA decompositions). In this example, each block shows similarity between 2 pairs of RZs from the same subject or two different subjects. Also, RZ 11-31 indicates inter-subject similarity between RZ 1 of subject 1 and RZ 1 of subject 3. The first digit in 11 is an index to the subject whereas the second is an index to the RZ. Highlighted, on the diagonal blocks indicate similarity within the components of a subject or intra-subject similarity whereas off diagonal ones indicate that between the components of two different subjects.

In this representation, solid lines mark subject blocks or *SBL*s. Off the diagonal *SBL*s reflect the similarity between pairs of *RZ*s from different subjects whereas those on the diagonal reflect those from the same subject. The *RB* represented as a matrix, $R_{ab\text{-}cd}$ with dimensions $c_a \times c_c$, reflects the similarity between RZ_{ab} and RZ_{cd} ($a, c: 1,2,\ldots n, b,d: 1,2,\ldots k$). In the algorithm, *NMI* for two *RZ*s is now calculated as:

$$RZ_{ab-cd}[y,z] = NMI\left(RZ_y \in RZ_{ab}, RZ_z \in RZ_{cd}\right) = \frac{H(RZ_y) + H(RZ_z)}{H(RZ_y, RZ_z)} - 1 \qquad (2.1)$$

$H(RZ_y)$, $H(RZ_z)$, $H(RZ_y, RZ_z)$ in (2.1) represent the entropies of random variables, RZ_y and RZ_z, and the mutual entropy between RZ_y and RZ_z ($1 \leq y \leq c_a$, $1 \leq z \leq c_c$).

To obtain standardized *NMI* in the alignment procedure, the *NMI*s are further standardized using the formula:

$$RZ_{ab-cd}[y,z] = \frac{RZ_{ab-cd}[y,z] - mean(RZ_{ab-cd}[y,*] \cup RZ_{ab-cd}[*,z])}{std(RZ_{ab-cd}[y,.] \cup RZ_{ab-cd}[.,z])} \quad (2.2)$$

* denotes all *NMI* values in row *y* or column *z* of the *RB* in (2.2). This standardized *NMI* or *SNMI* is used to compute the specificity of individual similarity values related to a given *RZ* within the *RB*. Diagonal *RB*s are generally set to zero because they represent identity matrices and are not of interest.

The gRAICAR algorithm then extracts highly reproducible *RZ*s across subjects and ICA realizations and aligns them in its third phase of execution. To accomplish this, the algorithm searches all *SNMI* values within *SB*s indicating the similarity between pairs of *RZ*s from different subjects to find a global maximum. Two *RZ*s found to be related are considered subject-level components but with the same underlying group-level component, which we refer to as an aligned component (*AC*). These *RB*s are then examined to locate the local maxima within them as this reflects possible locations of the aligned component within different ICA realizations and subjects. Rows and columns that contain these maxima are eliminated from the *FSM* after all *RZ*s associated with this aligned component are located. This task is repeated until $c_m = max(c_{1 \leq i \leq n})$ *AC*s have been found where *c* represents the number of ICs. The number of components is not the same among subjects, and hence empty matches for some subjects are allowed. A *kn* × *kn* reproducibility matrix for each *AC* is produced, thus collecting

*NMI*s between all pairs of *RZ*s associated with the *AC*. *NMI*s are then utilized to provide a more direct interpretation of similarity. In order to form its reproducibility matrix, a maximum of one *RZ* is selected per *AC* in each ICA realization. The algorithm divides information contained within the reproducibility matrix into two metrics: inter-subject consistency and intra-subject reliability. Inter-subject consistency is defined as the mean of all *NMI*s within inter-subject blocks. The inter-subject consistency for a given *AC* between subjects *a* and *c* can be calculated as:

$$\propto_{ac} = mean(RZ_{a'-c'}) = \frac{\sum_{b=1}^{k}\sum_{d=1}^{k} RZ_{ab-cd}[y(a,b),z(c,d)]}{K^2}, \qquad 1 \leq a,\ c \leq n,\ a \neq c \tag{2.3}$$

Equation (2.3) represents the mean *NMI* within the inter-subject block '*a*–*c*' in the reproducibility matrix, since it averages all the *NMI* values located at the intersection between realization *b* of subject *a* and realization *d* of subject *c*.

Fig. 2.4, a continuation of Fig. 2.3, provides an example of the third phase of the gRAICAR algorithm summarizing the description presented above using the same scenario as in Fig. 2.3. The circle mark represents a global maximum, which is computed by searching all *SNMI*s within the off-diagonal *SB*s. Doing so provides compatibility with larger variations across subjects than within subjects. In this example, the global maximum was located at $RZ_{ab-cd}[y, z]$, which represents the *y*-th row and the *z*-th column of the *RB*. Two related *RZ*s, $RZ_{y(a,b)}$ and $RZ_{z(c,d)}$, are treated as subject-level components with the same underlying group-level component or *AC*. $RZ_{y(a,b)}$ is a representation of the *y*-th component of the *b*-th realization of the *a*-th subject.

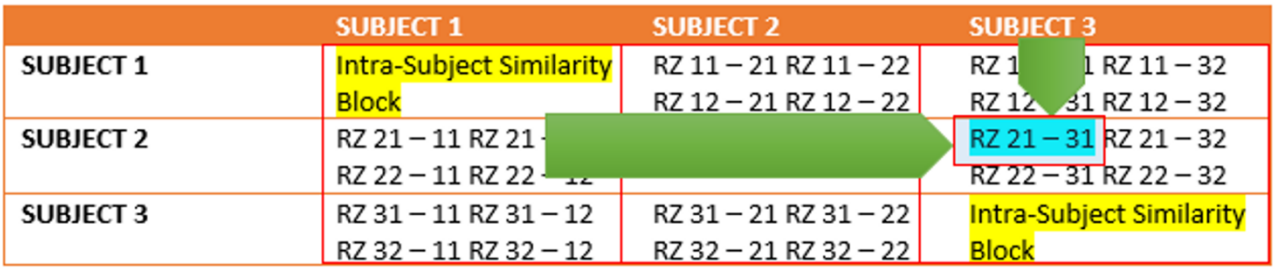

Fig. 2.4 RZ 21-31 represents RZ 1 of subject 2 and RZ 1 of subject 3 and has been found to be the global maximum in this example.

This identifies the aligned component in different ICA realizations and subjects. These locations have been identified in Fig. 2.5 as *R22-11[s, v1]* and *R11-31[w1, t]* where *v1* and *w1* represent relevant *RZ* positions in individual *RB*s indicating the largest similarity with $RZ_{y(a,b)}$ and $RZ_{z(c,d)}$ respectively. *v1 = w1* here means [*y, v1*] and [*w1, z*] favor the same *RZ* and the component formed as a result is considered to be related to the aligned component determined by $RZ_{y(a,b)}$ and $RZ_{z(c,d)}$. If *v1* and *w1* are unequal, either *v1* or *w1* is chosen based upon a voting mechanism to determine the proximity of one or the other to more of those *RZ*s investigated as the *v1 = w1* case.

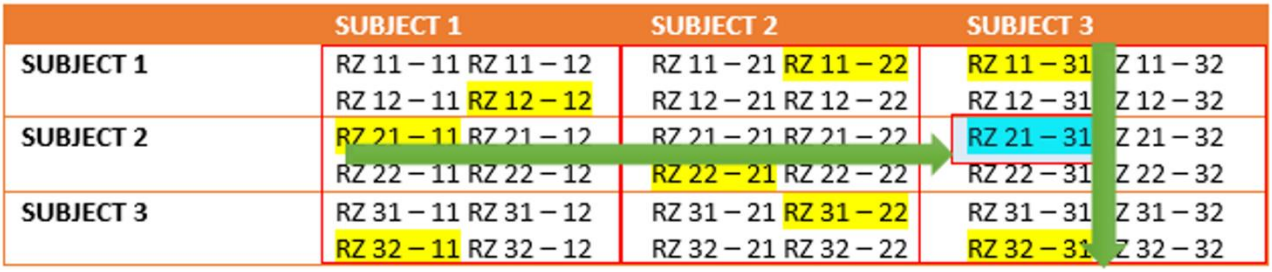

Fig. 2.5 Determine block-wise maxima with highlighting in each block such as RZ 21-11 in row 2 and column 1. Global maximum in this figure has been highlighted in addition.

In its fourth phase, the gRAICAR algorithm estimates *AC* maps and corresponding mixing time courses by utilizing weighted averages of their related *RZ*s. To calculate the weighted

average of the *RZ*s, the first step is to define a subject load on inter-subject consistency reflecting the contribution or inter-subject centrality of a given subject to a given *AC*.

$$\gamma_i = \frac{1}{n-1} \sum_{c=1,c\neq a}^{n} \propto_{ac} \ , 1 \leq a \leq n \quad (2.4)$$

Equation (2.4) can also be described as the inter-subject centrality of a subject in a given *AC*, and is the mean of the inter-subject consistency metrics between the given subject and the rest of the subjects. In (2.4), $\propto_{ac}$ is a reference to the inter-subject consistency metric between subjects *a* and *c*. Spatial maps and mixing time courses of an *AC* are calculated by merging this subject load on inter-subject consistency and the intra-subject reliability, as follows:

$$grpIC_\tau = \frac{\sum_{a=1}^{n}[\beta_a \ \gamma_a \sum_{b=1}^{k} RZ_{p(a,b,n)}]}{K \sum_{a=1}^{n} \beta_a \ \gamma_a} \ , 1 \leq \tau \leq c_m \quad (2.5)$$

$RZ_{p(a,b,n)}$ represents the *RZ* or the spatial map of the IC identified in the *b*-th realization of the *a*-th subject. *p* sets an index on the location of the *RZ*s and can differ with different realizations and subjects. The weights vary for each *AC*, calculated by the *AC*-specific reproducibility matrix.

The algorithm now statistically detects *AC*s found consistently across subjects. It explores the significance of cross-subject consistency of the resulting *AC* in two steps. It applies a non-parametric test to select the *AC* consistent across all subjects. One *RZ* from each ICA

realization in the *FSM* is randomly tested with replacement and the mean of inter-subject consistency metrics is calculated after a non-participating subject is artificially generated. This procedure is repeated ~500 times. The resulting means of inter-subject consistency metrics are combined to yield a null-distribution of the inter-subject consistency. The 95^{th} percentile, equivalent to a significance level of $p = 0.05$, of the null distribution provides a threshold at this point. *AC*s with mean inter-subject consistency metrics greater than the threshold value mentioned earlier are treated as common *AC*s across subjects. Null distributions of the subject loads on inter-subject consistency and intra-subject reliability for each one of the *AC*s mentioned earlier are produced by randomly assigning *RZ*s with replacement in the reproducibility matrix to subjects generated artificially. In the algorithm, thresholds for aforesaid metrics are determined at 95^{th} percentile of the equivalent null distributions, corresponding to a significance level of $p = 0.05$. Subjects above these two threshold levels are treated as representing the *AC* under consideration. The main tasks in the fourth phase of gRAICAR algorithm include estimating *AC* maps and corresponding time courses after weighted averaging of their related *RZ*s, statistically detecting *AC*s that are consistent across all subjects, and constructing a graph for each *AC* to characterize relationships among subjects from the standpoint of inter-subject consistency.

CHAPTER 3

Investigating Brain Connectomic Alterations in Autism using the Reproducibility of Independent Components derived from Resting State functional MRI Data

3.1 Introduction

Autism Spectrum Disorder (ASD) is characterized as a developmental disability leading to significant social, communication and behavioral challenges [47]. In 2010, an estimate from the Autism and Developmental Disabilities Monitoring (ADDM) Network involving 11 sites revealed that 14.7 per 1000 or 1 in 68 children aged 8 years were affected by this disorder [48] [49]. In addition, this study discovered that one in 54 males and one in 252 females in the ADDM communities had Autism. These disorders have been found to be very heritable [50]. In addition, approximately 18.7% of infants with at least one older sibling with Autism developed this disorder [51]. Given the societal implications of Autism, early diagnosis and intervention has become paramount. However, Autism is currently diagnosed using behavioral tests which can be subjective. Consequently, objective non-invasive biomarkers of Autism are being actively researched.

In order to find objective biomarkers of Autism, studies have used information from brain imaging techniques such as structural Magnetic Resonance Imaging (MRI). Ecker et al. [52] used a multiparameter classification approach involving a support vector machine (SVM) to characterize the structural pattern of gray matter anatomy in adults with ASD and examined a set of five morphological parameters such as volumetric and geometric features at each spatial location on the cortical surface to discriminate between people with ASD and controls. Jiao et al. [53] built diagnostic models for ASD based upon regional thickness measurements extracted from

surface-based morphometry (SBM) and compared these models to diagnostic models based on volumetric morphometry using four machine learning techniques: support vector machines (SVM), multilayer perceptrons (MLPs), functional trees (FTs), and logistic model trees (LMTs). Voxel-based morphometry along with a multivariate pattern analysis approach was used by Uddin et al. [54] to determine multiple brain regions showing atypical structural organization in children with Autism. Calderoni et al. [55] examined whole brain volumes of female subjects with ASD using mass-univariate and pattern classification approaches. Sato et al. [56] extracted individual subject features from inter-regional thickness correlations based on structural MRI which were later used in a machine learning framework to obtain subject level prediction of severity scores based upon neurobiological criteria rather than behavioral information. Libero et al. [57] examined multiple brain imaging modalities to investigate the neural architecture in the same set of subjects using techniques such as decision tree classification analysis. Functional (as opposed to structural) MRI has been used in several studies on Autism as well. The feasibility of a functional MRI connectivity diagnostic assay for Autism was investigated by Anderson et al [38] after obtaining pairwise functional connectivity measurements from a lattice of 7266 regions of interest covering the entire gray matter and using a single resting state blood oxygen level-dependent scan of 8 minutes for classification in each subject. Coutanche et al. [58] used data from an fMRI study of the neural basis for face processing in subjects with ASD to illustrate that multi-voxel pattern analysis (MVPA) may provide a sensitive functional biomarker of clinical symptom severity. Wang et al. [59] used a multi-scale clustering methodology known as "data cloud geometry" to extract functional connectivity patterns from fMRI for the recognition of ASD subjects by applying it to correlation matrices of 106 regions of interest (ROIs) in subjects with ASD and controls. Deshpande et al. [60] used supervised machine learning and fMRI to show

alterations in causal connectivity in the brain could serve as a potential non-invasive neuroimaging signature for Autism. Nielsen et al. [61] also used pairwise functional connectivity measurements from a lattice of 7266 regions of interest covering the gray matter for 964 subjects to conclude that multisite classification based on functional connectivity derived from resting state fMRI of Autism performed better than chance using a simple leave-one-out classifier. Maximo et al. [62] used regional homogeneity and local density approaches at different spatial scales and examined local connectivity in ASD, while Supekar et al. [63] showed hyper-connectivity in a sample of relatively younger Autistic kids using resting state fMRI. The common theme emerging from the studies mentioned above is that Autism is characterized by altered functional connectivity in certain brain networks and that characterizing this appropriately using MRI-based methods may provide a biomarker for objective diagnosis.

Independent Component Analysis (ICA) is a blind source separation technique which is commonly employed for extracting brain networks involving spatially distributed regions with similar/correlated temporal activity [40], especially in the baseline resting state. Consequently, it has been applied to investigate altered brain networks in Autism using fMRI. Specifically, Von dem Hagen et al. [41] employed ICA to demonstrate that individuals with Autism had reduced functional connectivity within the Default Mode Network (DMN), an important resting state brain network [42]. Assaf et al. [18] studied the role of altered functional connectivity of the default mode sub-networks in ASDs using short resting fMRI scans and ICA. In spite of these studies showing reduced connectivity in certain brain networks in Autism, identification of individuals with Autism solely based on these measures has not been reliable, especially in samples of large sizes [61]. We surmise that one major factor contributing to this state of affairs may be that metrics derived from Autism and/or Control subjects may not be highly reproducible within their

respective group. Consequently, such metrics have poor generalizability, leading to lower cluster purities. Therefore, in this paper, we hypothesize that functional brain networks which are most reproducible separately within Autism and healthy Control groups, but not reproducible when both groups are merged, may possess the ability to effectively discriminate between the groups. The basis for this hypothesis is illustrated in Fig. 3.1 which shows an imagined feature space where we want to discriminate between the two groups (Autism and healthy Control). Please note that Fig. 3.1 has not been drawn to scale and is an illustrative schematic.

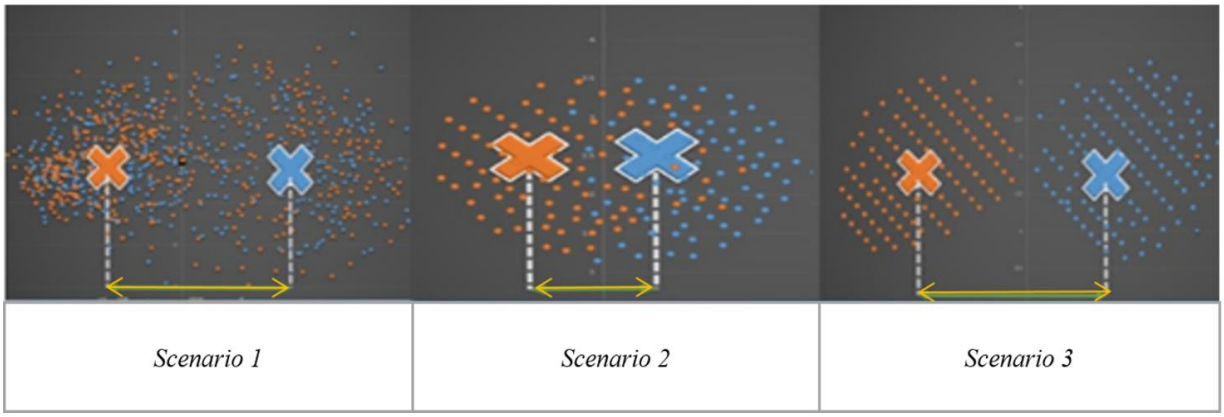

Fig. 3.1. Imaginary feature space showing three different scenarios while discriminating between two groups (indicated by two colors orange and blue): Autism and Healthy Control. Scenario 1: Significant group difference in means, say, x. Scenario 2: Non-significant difference in group means. Scenario 3: Significant mean difference comparable to x in scenario 1.

Scenario-1 corresponds to the situation wherein the two groups have significantly different means (say, x) in the feature space. However, within each group, the features have poor reproducibility (i.e. they are more scattered in the feature space), likely due to the heterogeneity of the disorder. Therefore, even if the group means are statistically separated, such features will give poor cluster purity. Scenario-2 is a situation where there is no significant difference between means, but the features are reproducible in the combined group (i.e. Autism + Control group), i.e. they are less scattered in the feature space even when both groups are combined. These two

scenarios indicate that features which are highly reproducible separately in each group but are not reproducible in the combined (Autism + Control) group are likely to provide purer clusters while discriminating between the Autism and Control groups. In the third scenario, the features are not only statistically separated between the groups (with the difference between the group means comparable to "x" in Scenario-1), but also reproducible within each group, i.e. less scattered in feature space within each group. In order to test our hypothesis, traditional ICA-based characterization of the functional brain needs to be modified such that reproducibility information is considered while choosing independent components. Therefore, we propose a methodology involving assessment of reproducibility of independent components, followed by clustering analysis of such components for evaluating their discriminability between groups in an unsupervised way. Accordingly, we applied a recently introduced algorithm, "generalized Ranking and Averaging Independent Component Analysis by Reproducibility" (gRAICAR, https://github.com/yangzhi-psy/gRAICAR) [64], which can provide independent components that are highly reproducible within a given group of subjects. This technique is an extension of a framework previously developed for single subject analysis called Ranking and averaging independent component analysis by reproducibility – RAICAR [65] and has been successfully used in a number of applications [66] [67]. In this work, gRAICAR was applied to Autism Brain Imaging Data Exchange (ABIDE) data [68] to estimate the independent components which are most reproducible, in Autism and Control groups, respectively, but not reproducible in the combined group. We input the spatial maps of such independent components into a k-means clustering algorithm and determined the purity of each cluster with respect to the a priori clinical diagnosis received by subjects.

3.2 Composition of the Subject Sample

We utilized resting-state functional magnetic resonance imaging (R-fMRI) data from 799 individuals provided by Autism Brain Imaging Data Exchange (ABIDE). The data we used had 392 individuals with Autism spectrum disorders and 407 age- and sex-matched typical controls (TCs). These data came from 13 different imaging sites and included 700 male and 99 female subjects (Table. 3.1) between 7 and 64 years of age. Data were fully anonymized wherein all 18 HIPAA (Health Insurance Portability and Accountability)-protected health information identifiers were removed. Data contributions were based on studies approved by the local Institutional Review Boards. Detailed information regarding the imaging data sets and associated phenotypic protocols can be found at http://fcon_1000.projects.nitrc.org/indi/abide. Data acquisition parameters and individual site details are also available on this web site.

Table 3.1. Institute names used in our study from ABIDE data and subject distribution by diagnosis code, Autism and Control.

ID	Institute Name	Autism	Control
1	California Institute of Technology	19	19
2	Kennedy Krieger Institute	22	33
3	University of Leuven	29	35
4	Ludwig Maximilians University Munich	24	33
5	Oregon Health and Science University	12	14
6	University of Pittsburgh	30	27
7	Social Brain Lab UMC Groningen NIN	15	15
8	San Diego State University	14	21
9	Stanford University	17	18
10	Trinity College Dublin	24	25
11	University of California Los Angeles	62	47
12	University of Michigan	68	77
13	University of Utah	56	43

3.3 Data Pre-processing

3.3.1 Acquisition and Conversion of Raw Data Set

We first converted the data downloaded from ABIDE database, which was in DICOM format, to Neuroimaging Informatics Technology Initiative (NIfTI) format. In order to complete the first step, we used dcm2nii software which is freely available at http://www.mccauslandcenter.sc.edu/mricro/ mricron/dcm2nii.html.

3.3.2 Standardization Process

In the next step, we used a combination of Data Processing Assistant for Resting-State fMRI [69] (DPARSF, http://www.restfmri.net)), which is a plug-in software based on Statistical Parametric Mapping or SPM (http://www.fil.ion.ucl.ac.uk/spm), and uses functionality from Resting-State fMRI Data Analysis Toolkit (REST 1.7) [70], both of which run on MATLAB. DPARSF was used to perform realignment of 3D brain volumes at each instant relative to the initial volume using 6-parameter rigid body registration, normalization to MNI (Montreal Neurological Institute) template using nonlinear warping, spatial smoothing using a Gaussian kernel with full width at half maximum of 4 mm × 4 mm × 4 mm, de-trending using linear polynomial and temporal band-pass filtering using the frequency range of 0.01 – 0.1 Hz.

3.3.3 Independent Component Analysis

Four Dimensional NIfTI-1 format images (http://nifti.nimh. nih.gov/nifti-1) from the pre-processing described above were then used in FMRIB Software Library v5.0 [71] [72] (FSL by Analysis Group, FMRIB, Oxford, UK) to obtain a set of independent components for each subject using Multivariate Exploratory Linear Optimized Decomposition into Independent Components

(MELODIC) algorithm [73] [74]. FSL provides analysis tools for fMRI, MRI and DTI brain imaging data, including ICA for decomposing single or multiple 4D data sets into linearly independent spatial components. More information on MELODIC is available at http://fsl.fmrib.ox.ac.uk/fsl/ fslwiki/MELODIC. We used the MELODIC analysis tool to perform standard 2D spatial ICA on each subject resulting in time courses (one per component) in the mixing matrix and spatial maps (one per component). The number of components for each subject was determined by MELODIC through automatic dimensionality estimation. We saved MELODIC results for each subject and used them in the algorithm we describe in the following section, for finding reproducible independent components.

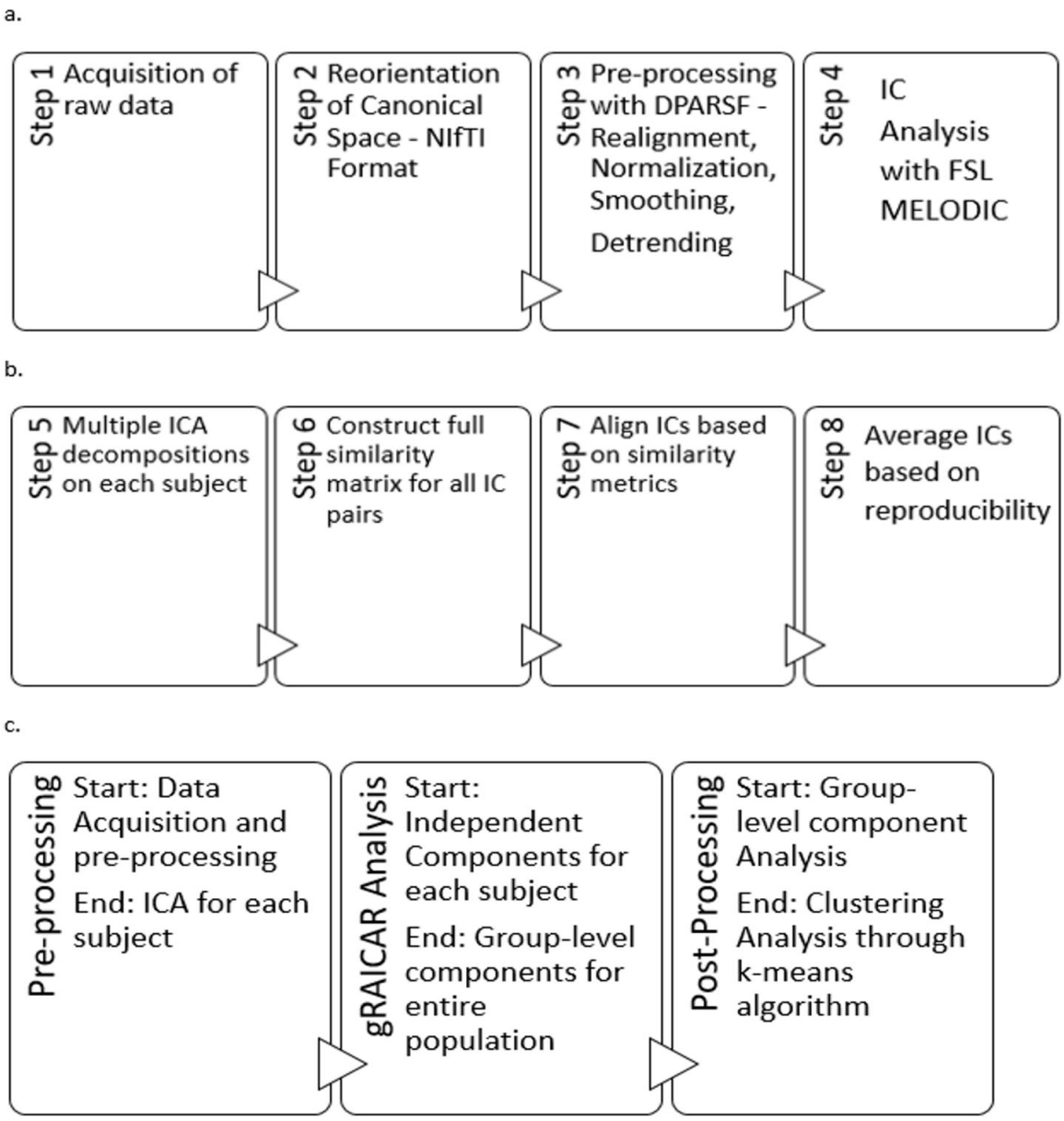

Fig. 3.2. a. Steps used in our pre-processing methodology have been summarized. Step 1 involved obtaining raw multi-site data for each subject in .nii.gz format. Step 2 involved converting raw data to NIfTI format which resulted in pairs of header and image files (hdr/.img) for each subject, using dcm2nii software. Step 3 involved processing data for each subject using a combination of MATLAB, DPARSF, SPM and REST to obtain a 4D .nii file for each subject based upon the input .hdr/.img files. Step 4 included the processing of 4D files obtained from step 3 in FSL - MELODIC using group ICA for each site leading to independent components or ICs to be used in our algorithm. Step 4 was the last step in our pre-processing methodology. b. Schematic illustrating the 4 steps (5-8) of the gRAICAR algorithm once the pre-processing is complete. c. Workflow of our analysis

3.4 Methods

3.4.1 The Application of gRAICAR Algorithm

We applied the gRAICAR algorithm separately to Autism, Control and Combined groups. This process involved performing ICA decomposition d (~5000 for this study) times for each subject using random initial values leading to $d \times n$ realizations where n is the number of subjects. Specifically, $d \times n$ or $d \times 392$ realizations of ICs for Autism group, $d \times 407$ realizations in the TC group and $d \times 799$ realizations in the combined group were obtained. These ICA realizations are named *REs* and RE_{ij} is used to denote the set of ICs from the j^{th} realization of the i^{th} subject. All steps of the gRAICAR algorithm were completed according to the flow described earlier.

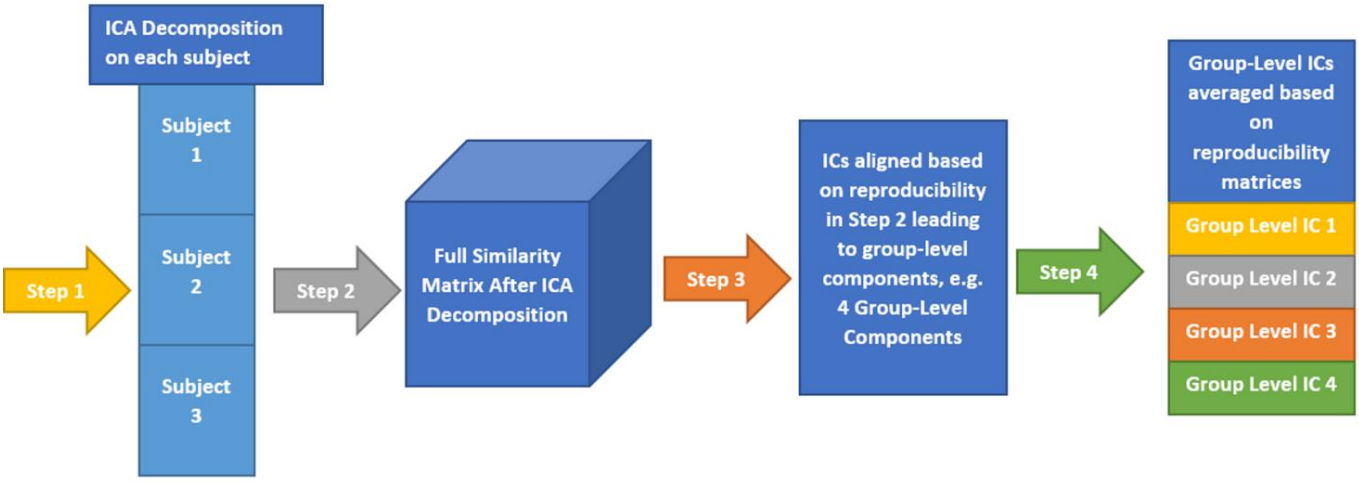

Fig. 3.3 This illustrates the implementation of gRAICAR algorithm using 3 subjects with 3 subject-level components each as an example. As discussed in fig. 4, step 1 involves multiple ICA realizations for each subject. Step 2 is used to create a full similarity matrix (FSM). In step 3, ICs are aligned based upon similarity metrics. In step 4, ICs are averaged based upon reproducibility matrices.

3.4.2 Clustering Analysis

K-means algorithm has been previously used in fMRI analysis in several studies [75] [76] [77]. We used this algorithm to examine the level of separation between Autism and TC groups for the

ICs which were reproducible within each group, but not reproducible in the combined group. Clustering was unsupervised without using *a priori* subject groupings. We determined cluster purity per cluster as shown below:

$$Purity = \frac{1}{N} \sum_{i=1}^{k} max_j \mid c_i \cap t_j \mid \quad (3.1)$$

In (3.1), *N* represents the number of data points or subjects, *k* the number of clusters, c_i the cluster in our analysis, and t_j the classification with maximum count for cluster c_i .

Equation (3.2) shows our approach to determine sensitivity values where *SEN* represents sensitivity, *TP* true positive, and *FN* true negative.

$$SEN = \frac{TP}{TP+FN} \quad (3.2)$$

Equation (3.3) shows our approach to determine specificity values where *SPC* represents specificity, *TN* true negative, and *FP* false positive.

$$SPC = \frac{TN}{TN+FP} \quad (3.3)$$

3.4.3 Analysis Workflow

This section presents our implementation and workflow. For technical details and the rationale behind every step, we have included a technical discussion in earlier sections of this paper. We

applied the gRAICAR algorithm thrice: first on the Autism group, second on the Control group, and then on the combined group. For the Autism and Control groups, we had 54 and 49 group-level components, respectively. For the combined (Autism + Control) group, we had 54 group-level components. We then examined these group-level components using criteria presented above describing the steps of gRAICAR algorithm and inter-subject consistency. These criteria gave us 11 group-level components in the Autism group and 3 in the Control group. For all subjects, we accessed post-MELODIC analysis results and retrieved spatial maps associated with the ICs corresponding to each selected group-level component. MELODIC analysis was a part of data pre-processing and described earlier in this paper. We then processed these spatial maps in MATLAB wherein the spatial map associated with the IC index of the current subject was retrieved and singleton dimensions were removed. The resulting array was reshaped using MATLAB's reshape function (http://www. mathworks.com/help/matlab/ref/reshape.html) thus giving us an $m \times n$ matrix where m is 1 for the current subject and n is $61 \times 73 \times 61$ (=271633) which was the size of each spatial map associated with the current IC index. After all subjects were processed, we had a 392×271633 matrix for the Autism group and 407×271633 matrix for the Control group. Suppose the resulting matrix for Autism is *A* while that for TC is *C*. We then combined *A* and *C* giving us a 799×271633 matrix. We applied the k-means algorithm using this matrix to examine how subjects were clustered based on their spatial maps without *a priori* groupings. The aforementioned process was repeated for all permutations of group-level components selected based on pairing a component from the Autism group with one from the Control group resulting in 33 k-means clustering analyses (Autism Group: 11 × Control Group: 3). We had set up the algorithm to partition the data set into two clusters since we had two subject groups, Autism and Control. For each of these clustering permutations, the purity of clusters was

identified based on how many subjects were correctly (or wrongly) clustered along with other subjects with the same diagnosis.

3.4.4 Covariance Analysis and Post-processing

From the above analysis, the pair with maximum cluster purity was identified. Let the corresponding components be A^x and C^x in Autism and Control groups, respectively. The component in Controls with maximum spatial correlation with A^x (say, $C_a{}^x$) and the component in Autism with the maximum spatial correlation with C^x (say, $A_c{}^x$), were identified using the following approach:

$$\lambda = max \sum_{i=1}^{k} cov(\omega, \omega_i) \tag{3.4}$$

λ represents maximum covariance in (3.4), between group level component, ω, from the group being analyzed and ω_i, that from the opposite group with k being the total number of group level components in the opposite group.

Two more k-means clustering analyses were performed by pairing A^x with $C_a{}^x$, and C^x with $A_c{}^x$. This analysis was carried out to ascertain whether the reproducible components in each group, when paired with the corresponding component with similar spatial distribution in the other group, can effectively discriminate between the groups. The entire analysis pipeline is illustrated in Fig. 7(a-d).

Steps I-IV presented in Fig. 7illustrate the concepts and summarize the processing by gRAICAR algorithm and k-means clustering analysis. For demonstration purposes, 6 artificial subjects, 3 from the Autism group (denoted by *A*) and the other 3 from Control group (denoted by *C*) are shown. Each example subject is assigned 4 ICs as shown. This is an arbitrary number

illustrating the concept and the number of ICs was not constant in actual processing. In actual processing, 799 subjects were used with a variable number of ICs. (I) This step shows gRAICAR processing on all subjects in the combined group (Autism + Control groups) and the resulting list of group-level components, 3 in this case: *x*, *y*, and *z*. (II) This step shows gRAICAR analysis on Autism group only from the example and the list of group-level components obtained as in step I. Component *x* was found in step I as well and is discarded after visual examination. (II) This step shows gRAICAR analysis on Control group only and the list of group-level components obtained as in steps I and II. Component *y* was found in step I hence discarded. (IV) In this step, we completed multiple tasks. We combined the group-level components x_1 and y_1 by mapping these to individual ICs for each subject. We then retrieved spatial maps for each IC representing a subject under the group-level component and linearly combined them using MATLAB creating a matrix we called '***M***'. Finally, we used k-means clustering algorithm in MATLAB using ***M*** to investigate the separation of components between groups.

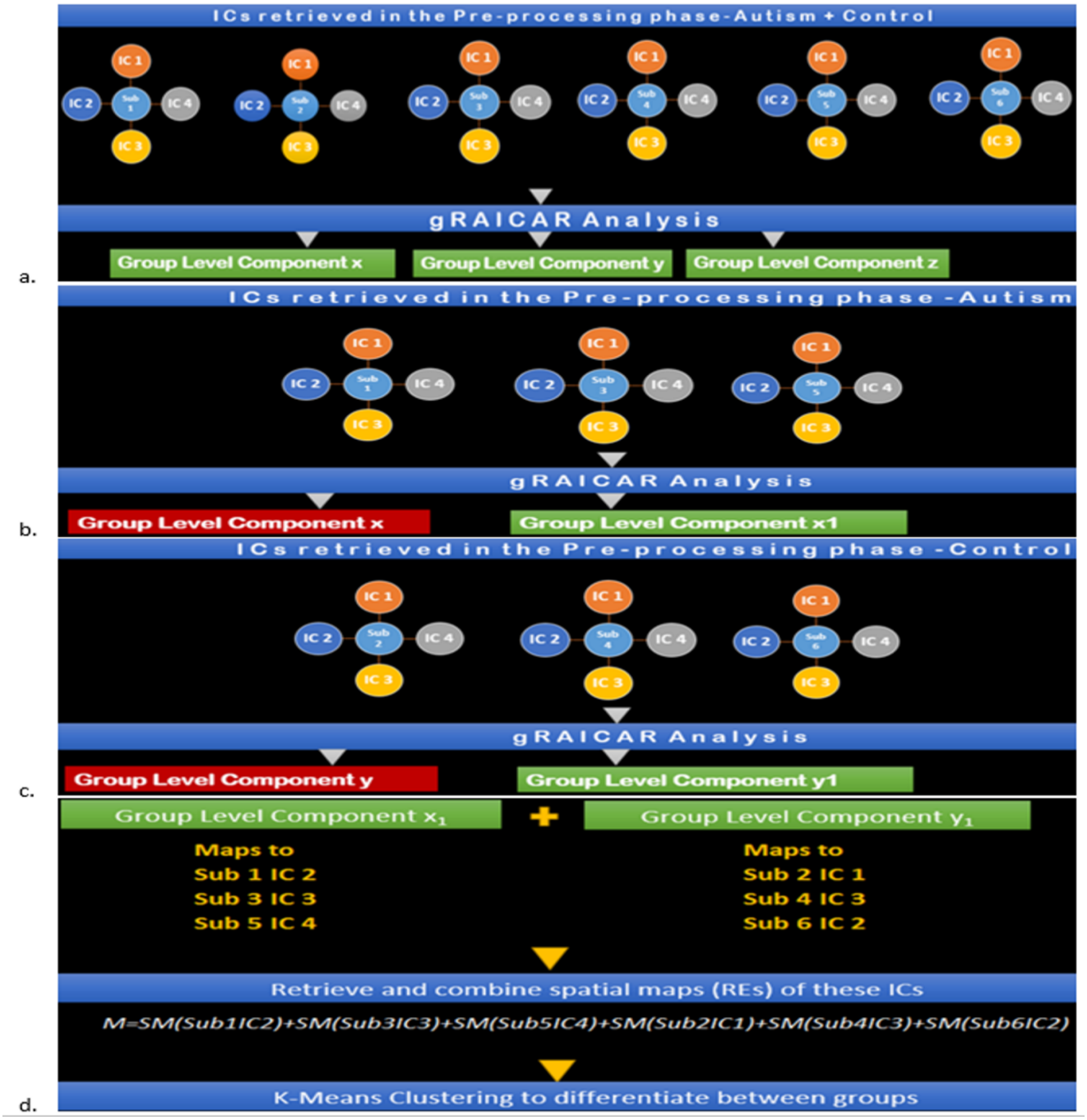

Fig. 3.4. a. Step I: gRAICAR Analysis on Combined (Autism + Control) Group producing group level components x, y, and z. b. Step II: gRAICAR Analysis on Autism Group Only, producing group-level components, x and x_1. x is discarded since it was produced in step I. c. Step III: gRAICAR Analysis on Control Group Only, producing group-level components, y and y_1. y is discarded since it was produced in step I. d. Step IV: Group level components from Steps II and III were combined by retrieving spatial maps corresponding to ICs these group-level components represented for each subject within each group as shown in the figure. Group level components reproducible in the combined group also found in individual analysis (steps II and III) were excluded.

Once the clustering was complete, we constructed an inter-subject Euclidean distance matrix within both Autism and Control groups using spatial maps associated with each subject for component pairings (C^x, A^x), (A_c^x, C^x), and (C_a^x, A^x). A self-organizing map or SOM analyzes input vectors in the input space and learns, in an unsupervised manner, to classify them accordingly [78] [79]. The result includes a low-dimensional (one- or two-) discretized representation of the input space of the training samples referred to as a map.

Neighboring neurons in SOMs learn recognizing neighboring sections of the input space which leads them to not only learn the distribution but the topology of the training vectors used as input. These neurons are arranged in physical positions based upon a topology function and distances between them are calculated using a distance function.

Adjacent neurons in the topology generally are close in the input space as well. In our study, we used SOMs to visualize the reproducibility and separation of the subjects in feature-space in additional to the numerical values given by k-means. High dimensionality in k-means was scaled using SOMs for optimal visualization. We obtained individual spatial maps for A^x and C^x and stacked them into a matrix. We then used this matrix as input to a 5×5 SOM for visualization as described earlier. This process was repeated for (A^x, C_a^x) and (A_c^x , C^x).

3.5 Results

Let us first examine the most reproducible group-level components within each group. We found 54 group-level components within the Autism group and 49 such components within the Control group. By combining selected components as described earlier, the range of cluster purity was 0.69 – 0.97 using unsupervised k-means clustering over all permutations of 11 group-level

components from Autism and 3 from Controls. The average purity value was 0.89 with a standard deviation of 0.06.

Figs. 3.5 and 3.6 show the spatial maps of A^x and C^x, respectively. The highest cluster purity value was 0.97 obtained by combining these two group-level components. Fig. 3.7 presents a map of pie charts based on a 5×5 SOM to visualize the reproducibility and separation of the two groups using A^x and C^x as described earlier. Each pie chart represents the number of subjects from a given group, Autism or Control. As an example, a solid red chart represents all subjects from the Autism group whereas a solid blue all from the Control group.

In the next step, we ascertained which group-level components in the opposite group had the highest spatial correlation to A^x and C^x, using all 54 components from Autism and 49 from Control groups depending upon the comparison being carried out. A^x was found to have the highest spatial correlation value of 0.29 ($p<0.001$) with $C_a{}^x$ in the Control group while C^x had the highest spatial correlation value of 0.63 ($p<0.001$) with $A_c{}^x$ in the Autism group. We then combined C^x with $A_c{}^x$ and subjected them to k-means clustering analysis. This produced cluster purity of 0.895 with a sensitivity of 0.893 and a specificity of 0.897. Similarly, we combined A^x with $C_a{}^x$ as described earlier and completed k–means clustering analysis. This resulted in a cluster purity of 0.607 with a sensitivity of 0.43 and specificity of 0.77. Figs. 3.8 and 3.9 show the spatial profiles of $A_c{}^x$ and $C_a{}^x$, respectively.

We also used pie charts to visualize the reproducibility and separation of subjects using 5×5 SOMs for these combinations: $A^x + C_a{}^x$ and $C^x + A_c{}^x$. These visualizations are presented in Figs. 3.10 and 3.11. In both cases, a dotted line represents the approximate separation observed between the two groups. Numbers on each pie chart represent the neuron in the SOM. It can be observed that the purity of individual pie charts drops when using spatial equivalents (Figs 3.10

and 3.11) as compared to the most reproducible components in each group (Fig. 3.7). This is a reflection of higher purity and separation in Fig. 9 (97.1%) to lower purity values and hence lower separation in Figs. 3.10 and 3.11 (0.607 and 0.895 respectively).

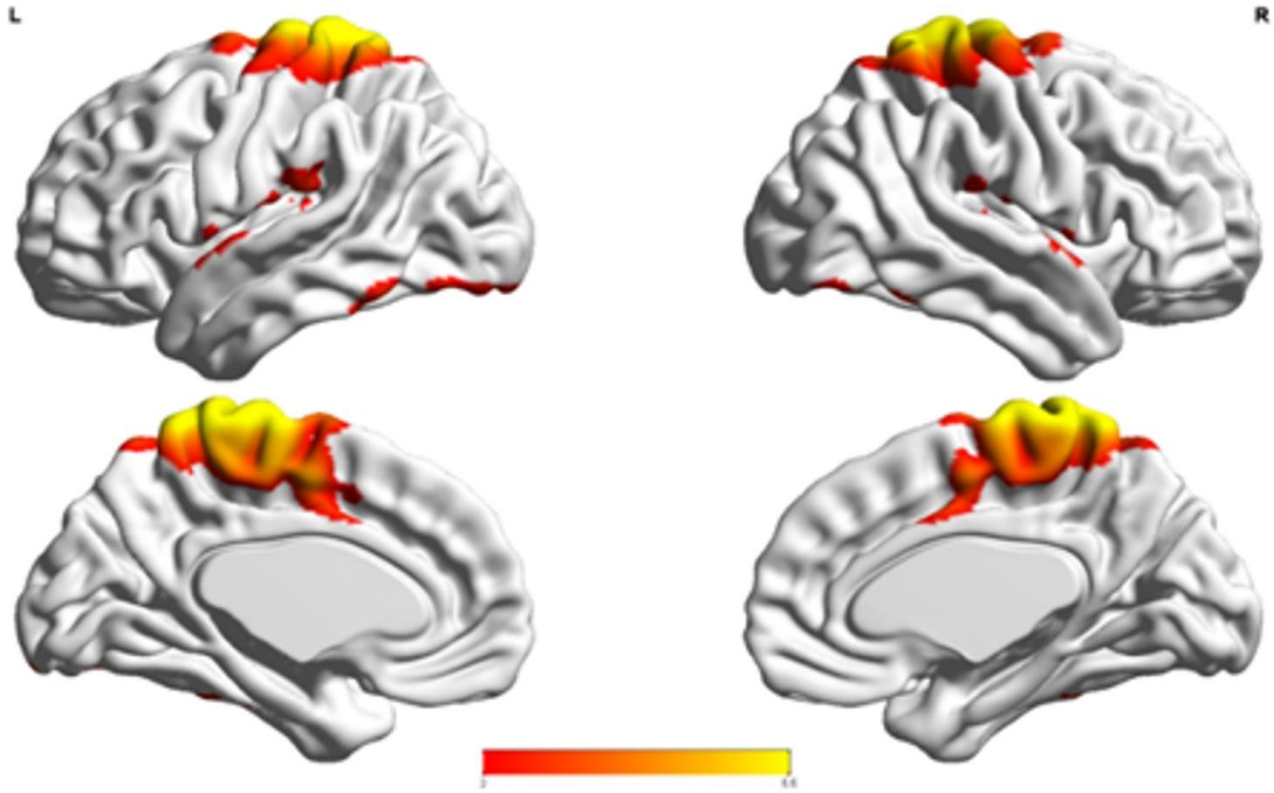

Fig. 3.5. The group-level component, A^x, from Autism group that produced the highest cluster purity value of 0.971 when combined with another group-level component from the Control group, C^x.

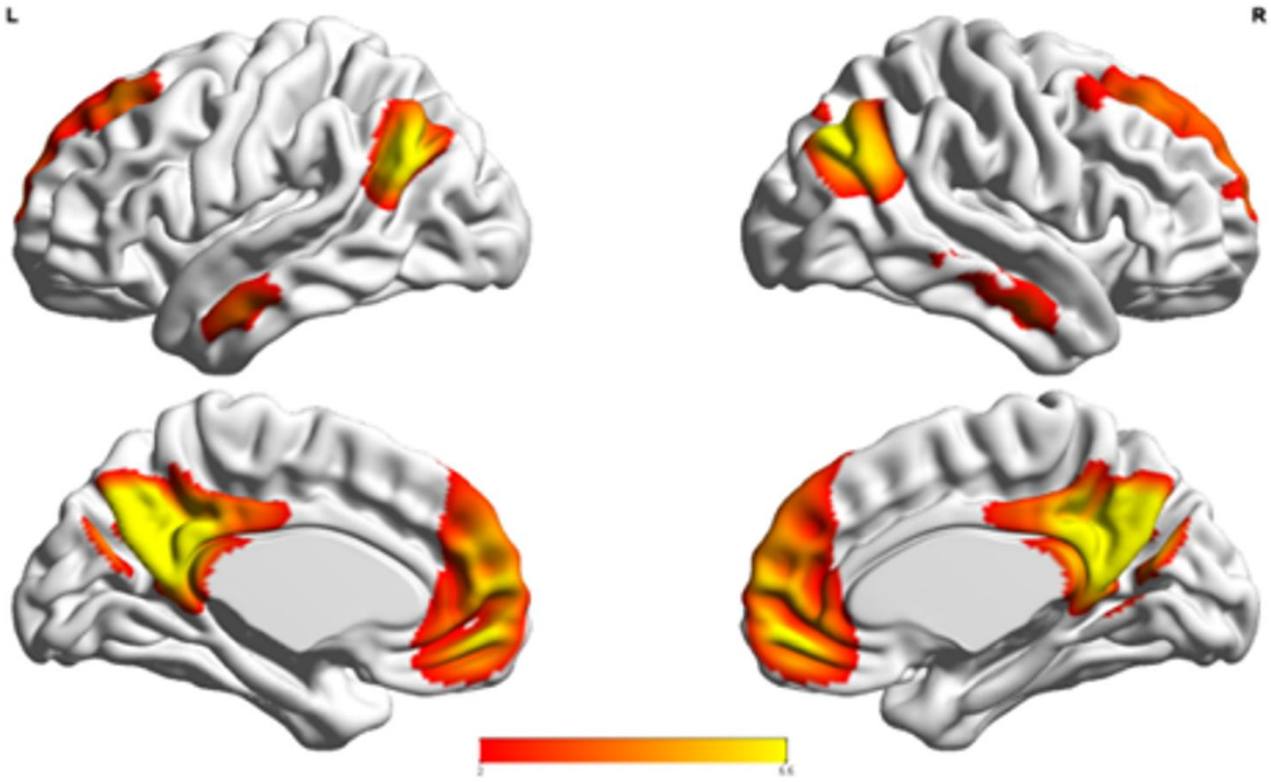

Fig. 3.6. The group-level component, C^x, from Control group that produced the highest cluster purity value of 0.971 when combined with another group-level component from the Autism group, A^x.

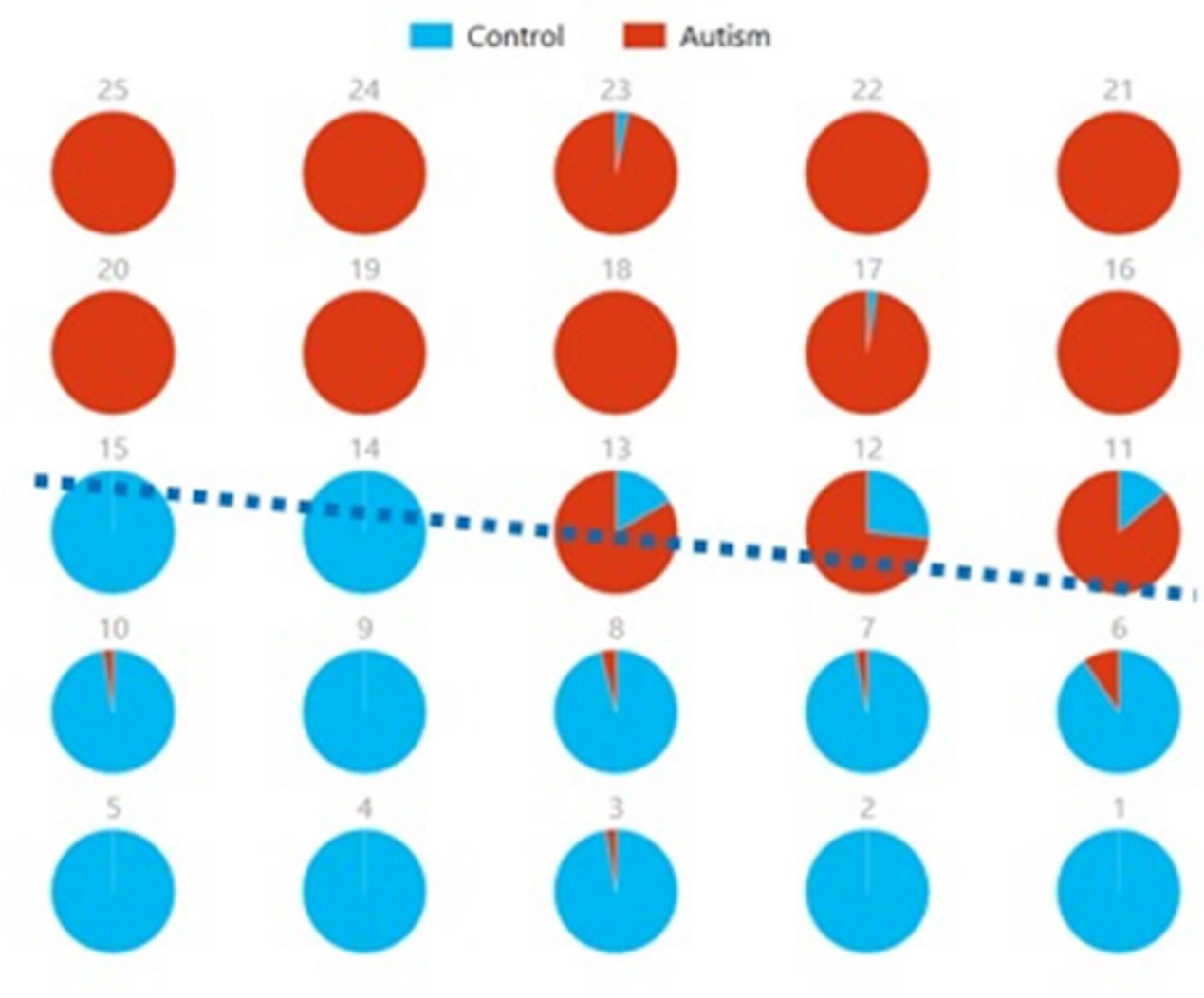

Fig. 3.7. Pie chart visualizations based on a 5×5 SOM for A^x and C^x showing Autism and Control groups by neuron. Each pie chart corresponds to a neuron, represented by the number on each chart, in the SOM map for these components. This map indicates group separation approximately in the middle with Autism group populating the upper while Control the lower half of the SOM, represented by the dotted blue line.

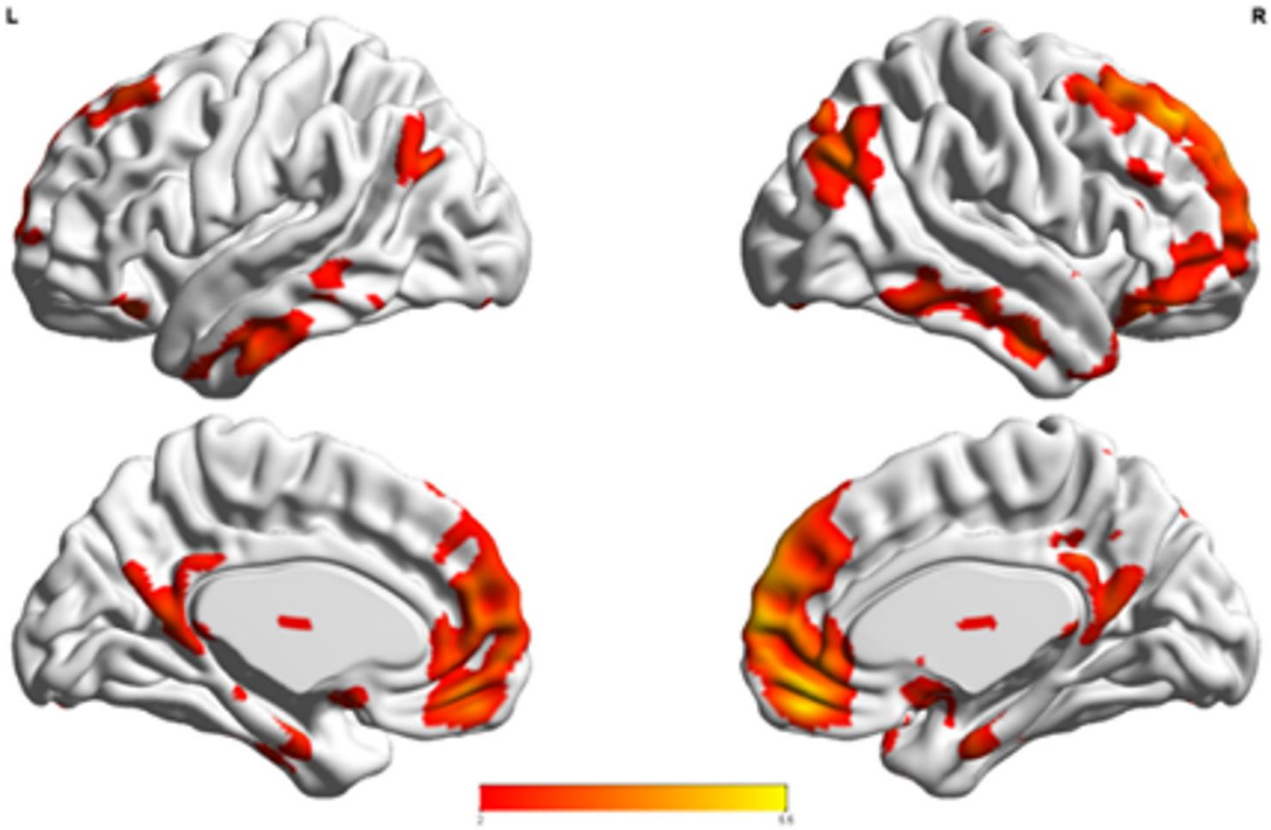

Fig. 3.8. This figure represents the spatial map for A_c^x, the group-level component in the Autism group with the highest spatial correlation with C^x.

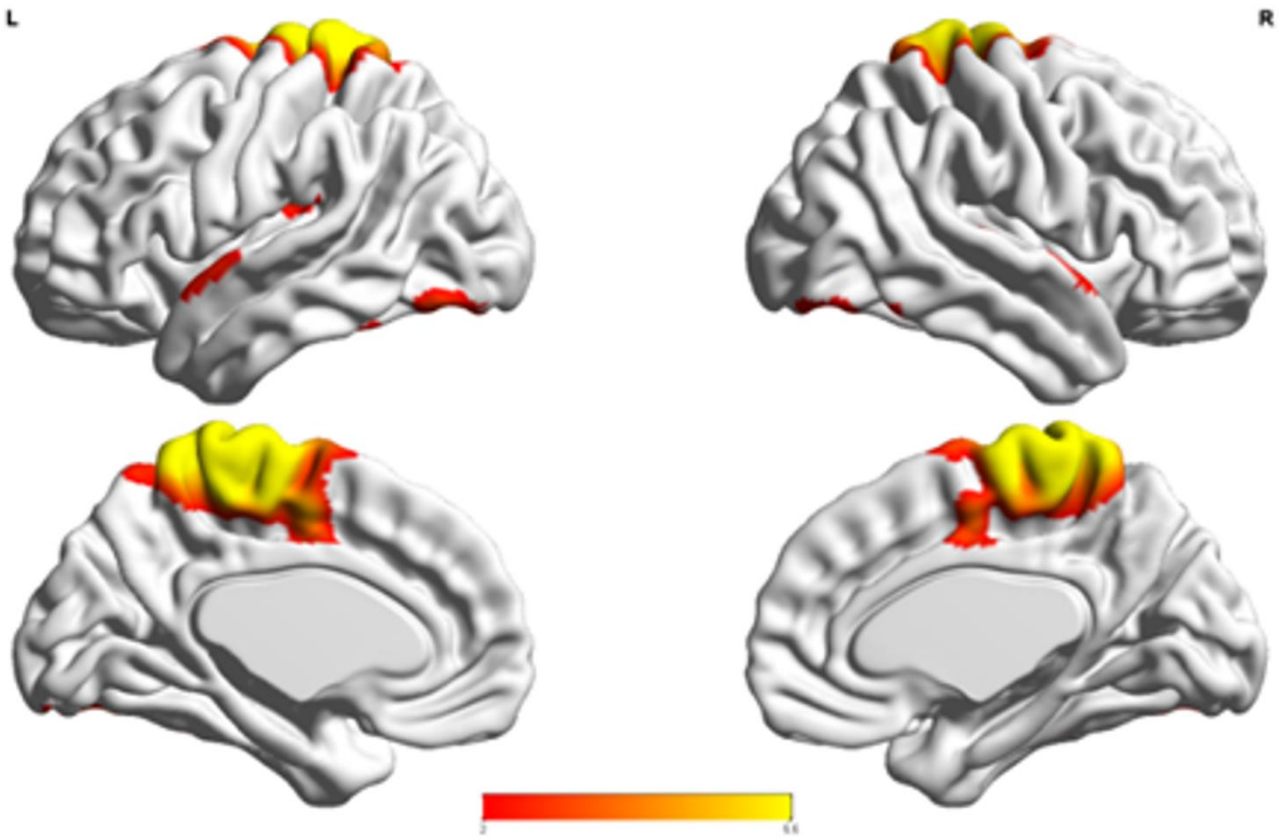

Fig. 3.9. This figure represents the spatial map for C_a^x, the group-level component in the Control group with the highest spatial correlation with A^x.

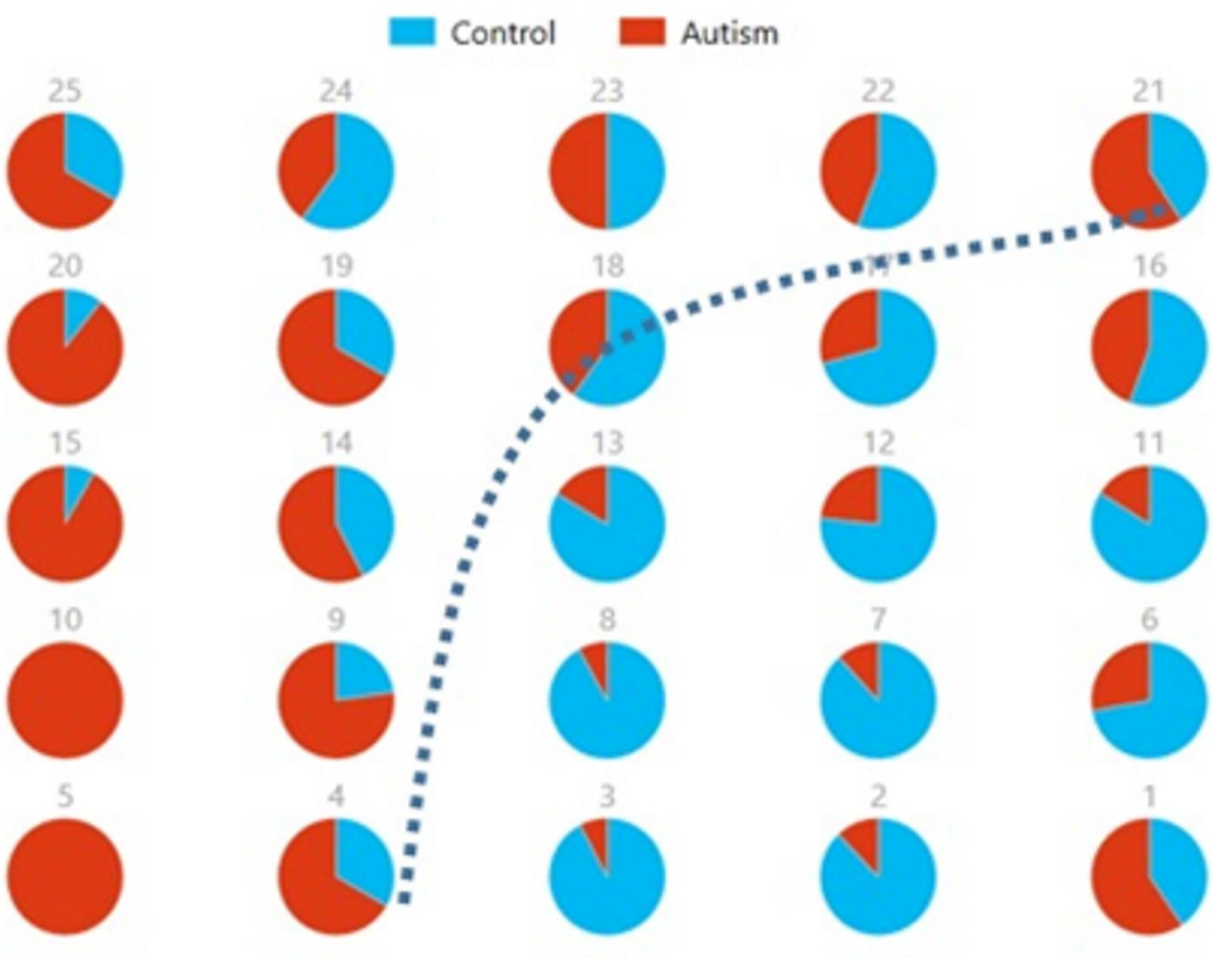

Fig. 3.10. Pie chart visualizations based on a 5×5 SOM for A^x and C_a^x showing Autism and Control groups by neuron where the number on each chart corresponds to a neuron in the SOM. The dotted line represents approximate separation between the two groups.

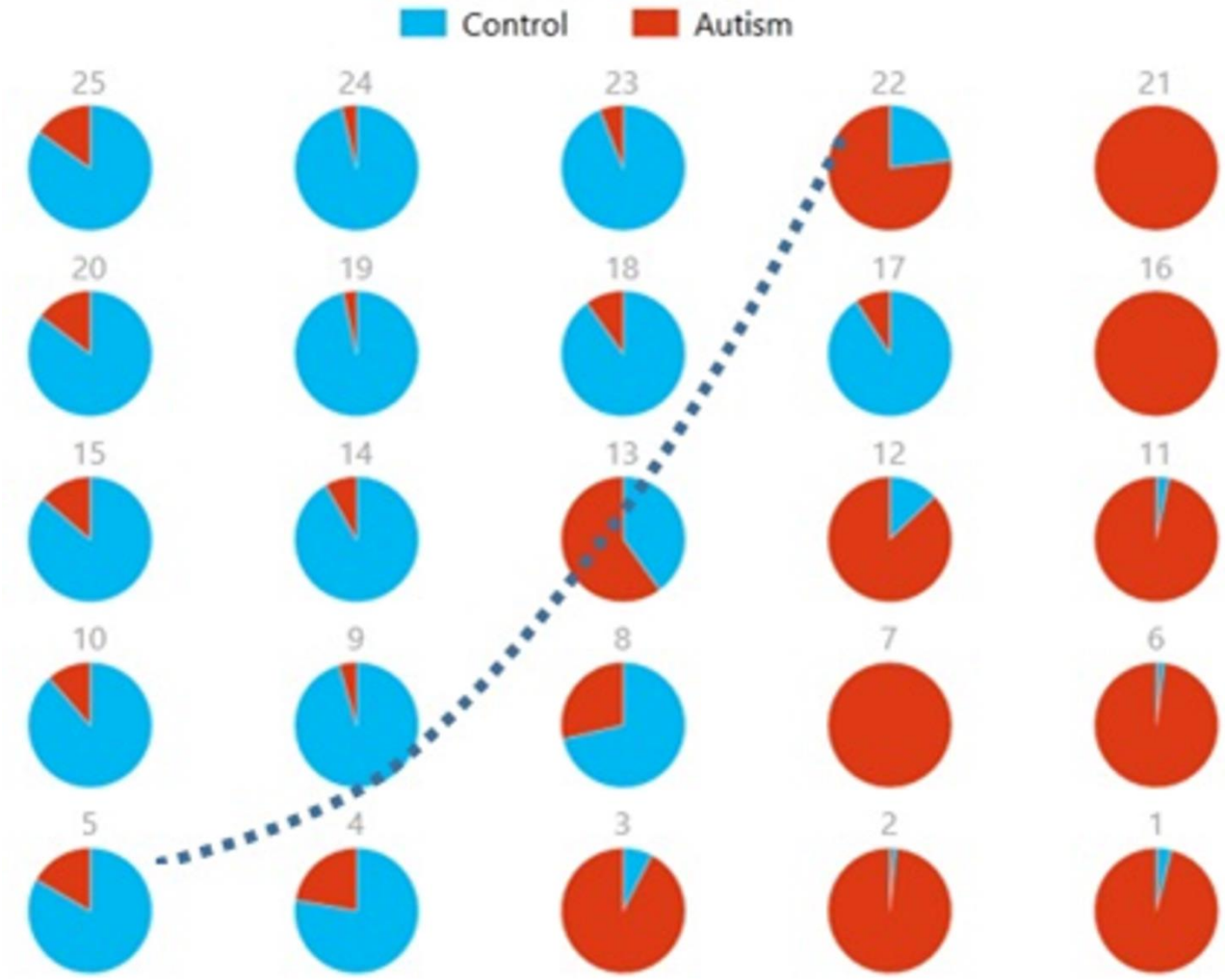

Fig. 3.11. Pie chart visualizations based on a 5×5 SOM for A_c^x and C^x showing Autism and Control groups by neuron where the number on each chart corresponds to a neuron in the SOM.. The dotted line represents approximate separation between the two groups.

3.6 Discussion

We used a discover-confirm scheme wherein during the “discover” phase, we used gRAICAR to retrieve reproducible components in each group and during the “confirm” phase, we used unsupervised clustering to determine the separation between groups based on the reproducible components in each group. Further, the separation was visualized using self-organizing maps or SOMs. This is a novel methodological framework for investigating discriminative features between diagnostic groups as opposed to performing group-wise statistical tests or supervised classification.

Even though multiple studies have shown altered fMRI-based connectivity in certain brain networks in Autism using machine learning techniques, identifying individuals with Autism based on these measures has not been reliable especially in larger sized samples [38] [39]. We hypothesized that functional brain networks which are most reproducible separately within Autism and Control groups, but not reproducible when analyzing both groups as merged, may lead to effective discrimination between the groups. We tested the above hypothesis by finding the most reproducible ICA components (which represent brain networks) first in the merged and then in separate Autism and Control groups. Our results, shown in the previous section, indeed support the above hypothesis. SOM visualizations provided along with spatial maps of the group-level components give further insight into the reproducibility of certain brain networks as well as their differences between groups based on our proposition.

The overall cluster purity we obtained from our multisite fMRI data set, obtained by averaging the results obtained from the three scenarios was 0.824 with a sensitivity of 0.77 and specificity of 0.87. Previous studies using the same data set, but supervised classification methods

instead of unsupervised clustering methods, have reported classification accuracies between 0.6 and 0.8 depending on whether they used a larger or smaller sub-sample of the ABIDE database [38] [61]. Given the fact that the methods used here are different from the previous studies mentioned above, it would not be fair to directly compare our cluster purity with theirs. Instead, we would like to make the point that characterizing reproducibility of brain networks in different groups as well as the merged sample is a novel idea which may hold promise, especially in the context of disorders such as Autism. This is because the most discriminative features identified via the proposed method are more likely to be generalizable to a larger sample given the reproducibility constraint.

C_x and A_c^x, which provided highest discriminability between the groups, represent the default mode network (DMN) in Control and Autism groups, respectively. The DMN in Autism appears less prominent and incohesive. Decreased functional connectivity in default mode subnetworks contributes to core deficits observed in ASD patients [18] whereas activity was reduced in the autism group in the ventral medial prefrontal cortex/ventral anterior cingulate cortex [19]. Visuospatial working memory deficiency within the DMN was discovered in adolescents with ASD [20] and the regions of DMN functional connectivity in the bilateral inferior parietal lobule and posterior cingulate cortex were found to be smaller in ASD patients [21]. On the other hand, A^X and C_A^X represent regions of the motor network, mid cingulate cortex and temporal-parietal junction. Even though these regions have been implicated in autism [80] [81] [82] [83], it was not as discriminatory as the DMN. To summarize, our methodology first discovered highly reproducible components separately in Autism and Control groups pointing to functional networks described in this section. These components or functional networks they pointed to from both groups, when combined and analyzed in clustering analysis as described, provided high

cluster purities, hence the ability to distinguish between the two groups. Functional networks discovered by applying our methodology separately in groups confirm earlier findings on alterations involving these networks in Autism. Results obtained from analyzing these networks support our hypothesis that functional networks highly reproducible separately in groups lead to higher cluster purities and discriminability.

3.6.1 Limitations and Future Directions

Despite the fact that the ABIDE database provides invaluable means to analyze multisite resting state fMRI data sets with significant statistical power, there are certain inherent limitations to this data set. Site to site variability in acquisition parameters, subject populations, scanner performance, and research protocols may all be cofounding factors when it comes to the sensitivity for detecting abnormalities [61]. It could be argued that the analysis of individual site data sets separately may provide a higher cluster purity. However, such results may be less easily translatable to the clinic because inter-site variability is something any potential clinical method will have to cope with. Both groups in ABIDE, Autism and healthy Control, appeared to have subjects with average to above-average range of IQ in addition to variation in diagnostic subtypes (Asperger's and PDD-NOS) across sites. A broader range of IQ levels need to be included in further studies since R-fMRI studies allow the inclusion of individuals with lower IQ than task based studies. In addition, not all sites spanned childhood to middle adulthood but further studies can include a deeper examination of the development of brain providing insight into developmental dynamics of Autism [68].

We used a novel analysis framework involving gRAICAR as described earlier *[64]*. Despite its robustness, there are several limitations including computational and physical memory costs. We were able to mitigate computational and physical memory concerns by using parallel processing and cloud computing. gRAICAR further provides the ability to parallelize one of the processing stages hence reducing the computational time and increasing efficiency. We had used gRAICAR code in a UNIX/ MATLAB environment. Also in the absence of a threshold in gRAICAR to determine the existence of a relationship, the RZs are forced to align with a group-level component even if there is low similarity with other RZs. In future studies, it would be interesting to investigate how gRAICAR performs in site-level analytics within Autism and ABIDE data sets. Our methodology can also be expanded to other neurological disorders to determine the utility of this algorithm in future studies.

CHAPTER 4

gMedICA: A Software Package for Assessing Reproducibility of Brain Networks and their Discriminability across Disorders

4.1 Introduction

Independent Component Analysis (ICA) is a blind source separation technique that is commonly employed for extracting brain networks involving spatially distributed regions with similar/correlated temporal activity [84], especially in the baseline resting state. Consequently, it has been applied to investigate altered brain networks in various heterogeneous neurological disorders using fMRI. Von dem Hagen et al. [85] employed ICA to demonstrate that individuals with Autism Spectrum Disorders (ASD) have reduced functional connectivity within the Default Mode Network (DMN), an important resting state brain network [86]. Assaf et al. [87] studied the role of altered functional connectivity of the default mode sub-networks in ASDs using short resting fMRI scans and ICA. von Rhein et al. [88] showed that subjects with ADHD exhibit alterations in connectivity of the salience and executive control networks and associated brain regions during task performance by using ICA as a part of their methodology. Patriat et al. [89] used ICA and discovered higher inverse correlation between the whole DMN and TPN networks in pediatric post-traumatic stress disorder (PTSD). Shang et al. [90] showed using ICA and chronic earthquake-related PTSD patients that the salience network (SN), central executive network (CEN), default mode network (DMN), somato-motor network (SMN), auditory network (AN), and visual network (VN) have both an increase and a decrease in functional connectivity in PTSD. Enhanced coupling of the amygdala and the insula within the SN was observed by Thome et al. [91] in subjects with PTSD by using ICA to evaluate connectivity within SN. The effects of

developing PTSD in combat personnel with mild traumatic brain injury (mTBI) exhibiting abnormal activation of distributed brain networks including the emotion network and DMN were studied by Shu et al. [92] using ICA as a part of their methodology. Cisler et al. [93] used ICA in a study involving the characterization of the relationships of assault and PTSD severity with the organization of networks that are identified in emotion processing.

Another perspective we take into consideration is the general crisis of lack of reproducibility of findings reported in a given study using a different sample [94]. Often, preclinical research outcomes generate significant media attention while failing to translate into successful diagnoses or treatments [95] [96]. Although, there may be multiple potential reasons for these problems, basic scientific results frequently turn out to be irreproducible. A recent survey of more than 1500 scientists revealed that 70% had tried but failed to reproduce another scientist's experiment, whereas 52% thought that there was a crisis of reproducibility [96]. Up to 85% of the resources were wasted while producing and reporting research relevant to clinicians and patients [97]. Major contributors to research waste have been identified as irrelevant research questions, research design and conduct, inefficient regulation and management of research, failure to provide access to full research reports, and the lack of unbiased and useable reports [98]. Sharing code written to analyze neuroimaging data improves transparency and reproducibility in neuroimaging research, as this code is necessary for interpreting and validating results, and addressing new research questions [99]. Methods, in general, need to address the issue of reproducibility of results, at least within their sample. In this paper, we not only provide a methodology that analyzes the reproducibility of independent components obtained from resting state fMRI (representing brain networks), but also implements it in a software package which is freely distributed along with this article.

We surmise that the lack of reproducibility of brain networks across heterogeneous spectrum disorders not only hinders replicability of results as mentioned above, but also the ability of potential biomarkers based on such brain networks to effectively discriminate between disease groups and healthy controls. Therefore, we hypothesize that the functional brain networks most reproducible separately within disease and healthy control groups, but not reproducible when both groups are merged, can effectively discriminate between the groups.

Recently, an algorithm was proposed for modifying traditional ICA-based characterization of the functional brain networks such that reproducibility information is taken into consideration when we choose independent components. We utilize this method, namely "generalized Ranking and Averaging Independent Component Analysis by Reproducibility" (gRAICAR, https://github.com/yangzhi-psy/gRAICAR) [43], which can provide independent components that are highly reproducible within a given group of subjects. This methodology extends a framework developed initially for single subject analysis called "Ranking and averaging independent component analysis by reproducibility – RAICAR" [100], which has been used before in various neuroimaging applications [101] [102].

Our study builds upon these previous works by introducing gMedICA, a software package that implements a "discover-confirm" approach, wherein the "discover" phase entails estimating the reproducibility of independent components using the gRAICAR (generalized Ranking and Averaging Independent Component Analysis by Reproducibility) algorithm [43], and subsequently the "confirm" phase involves evaluating the ability of highly reproducible components thus obtained to effectively discriminate between groups of subjects or participants with heterogeneous neurological disorders. This software package implements a work flow not available previously in literature, and utilizes a system-of-systems design approach [103] that

minimizes user workload. It accepts fMRI data from individual participants as input, completes pre-, para-, and post-processing of these data sets, and presents results to the user. Using results obtained from gMedICA, we can examine the reproducibility of group-level independent components, alterations in functional connectivity, and the ability of functional brain networks discovered by gMedICA to discriminate between different groups of participants in an unsupervised way.

4.2 Materials and Methods

This section is organized as follows. First we present a conceptual explanation of data pre-processing, main analysis and post-processing, including clustering. Next, the details of the software package which implements these conceptual steps are presented. Finally, we illustrate the conceptual steps as well as the capabilities of the software package using experimental fMRI data obtained from Soldiers with PTSD and mTBI.

4.2.1 Pre-processing

In the first step of our pre-processing phase, we utilize a combination of Data Processing Assistant for Resting-State fMRI [104] (DPARSF, http://www.restfmri.net), which is a plug-in software based upon Statistical Parametric Mapping or SPM version 8 (http://www.fil.ion.ucl.ac.uk/spm), Resting-State fMRI Data Analysis Toolkit (REST 1.7) [105], and MATLAB. Input data in this phase can either be in DICOM or .img/ .hdr file pair format, which is converted to NIfTI-1 format images (http://nifti.nimh.nih.gov/nifti-1, .nii files) before further processing. We use DPARSF to perform realignment of 3D brain volumes relative to the initial volume using 6-parameter rigid body registration, normalization to MNI (Montreal

Neurological Institute) template using nonlinear warping, spatial smoothing using a Gaussian kernel with full width at half maximum of 4 mm × 4 mm × 4 mm, de-trending using linear polynomial and temporal band-pass filtering in the frequency range of 0.01 – 0.1 Hz.

The next step of this phase picks up four dimensional NIfTI-1 format images (http://nifti.nimh.nih.gov/nifti-1, .nii files) from the previous step, and use them as input to FMRIB Software Library v5.0 [106] [107] (FSL by Analysis Group, FMRIB, Oxford, UK) to derive a set of independent components for each subject using Multivariate Exploratory Linear Optimized Decomposition into Independent Components (MELODIC) algorithm [108] [109]. Analysis tools for ICA are available within FSL for decomposing single or multiple 4D data sets into linearly independent spatial components. More information on MELODIC can be obtained at http://fsl.fmrib.ox.ac.uk/fsl/fslwiki/MELODIC. In our pre-processing, we use MELODIC analysis tool to perform standard 2D spatial ICA on each subject. In addition to one spatial map per component, this analysis also results in corresponding time course and a mixing matrix. MELODIC determines the number of components internally within FSL through a dimensionality estimation mechanism including principal component analysis technique or PCA [110]. We use MELODIC results for each subject in the main analysis section to determine the reproducibility of these components, and therefore, the highly reproducible ones within each group. One of the highlights of our proposed software, gMedICA is that the users do not have to deal directly with individual software packages mentioned in this phase since our software automates these tasks by seamlessly communicating with other software packages.

4.2.2 Main Analysis

Our main analysis comprised of the implementation of gRAICAR algorithm described earlier in this dissertation.

4.2.3 Post-processing

To review our workflow after gRAICAR processing, we present an example case with two diagnostic groups, 4 subjects in each group and 4 IC realizations per subject. For brevity, we assume gRAICAR produces two group-level components per group, $grpIC_{1,1}$ and $grpIC_{1,2}$ in group 1 as shown in Fig. 4.1, as well as $grpIC_{2,1}$ and $grpIC_{2,2}$ in group 2, as shown in Fig. 4.2. In this example, the first digit represents group enumeration and the second digit represents group-level component index. Suppose group-level components $grpIC_{1,1}$ and $grpIC_{2,2}$ had the highest inter-subject consistency according to gRAICAR analysis in groups 1 and 2, respectively, as shown in equations (4.1) and (4.2).

$$\propto_{(Sub\ 1\ \ldots Sub\ 4)} \left(grpIC_{1,1}\right) > \propto_{(Sub\ 1\ \ldots Sub\ 4)} \left(grpIC_{1,2}\right) \quad (4.1)$$

$$\propto_{(Sub\ 1\ \ldots Sub\ 4)} \left(grpIC_{2,2}\right) > \propto_{(Sub\ 1\ \ldots Sub\ 4)} \left(grpIC_{2,2}\right) \quad (4.2)$$

We now select these two components for further processing.

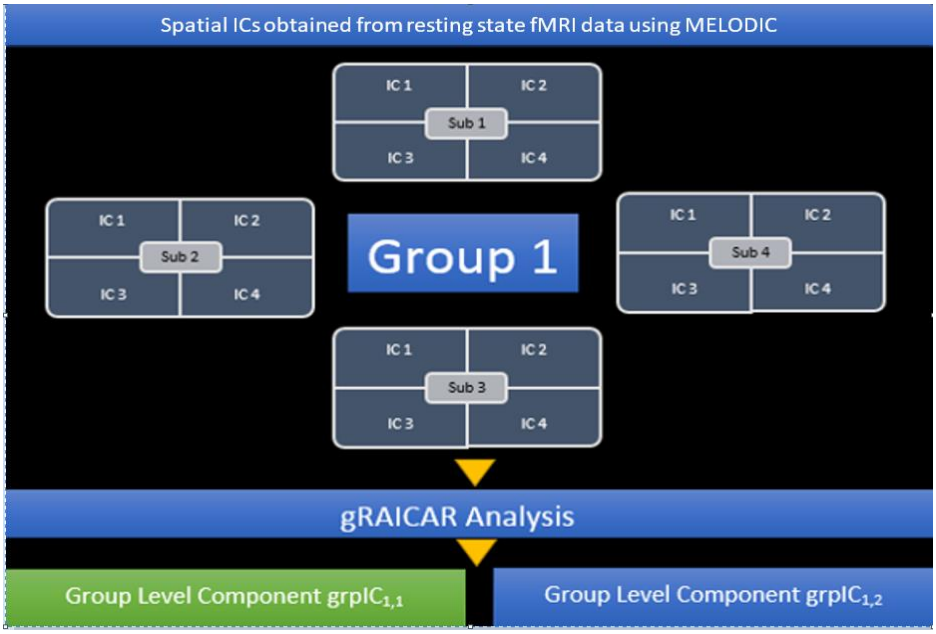

Fig. 4.1 A toy illustration of the analysis workflow. gRAICAR analysis on ICs estimated from fMRI data corresponding to Group 1 is assumed to produce group-level components $grpIC_{1,1}$ and $grpIC_{1,2}$. Let us suppose that $grpIC_{1,1}$ has highest inter-subject consistency in Group 1 and hence be selected for further processing.

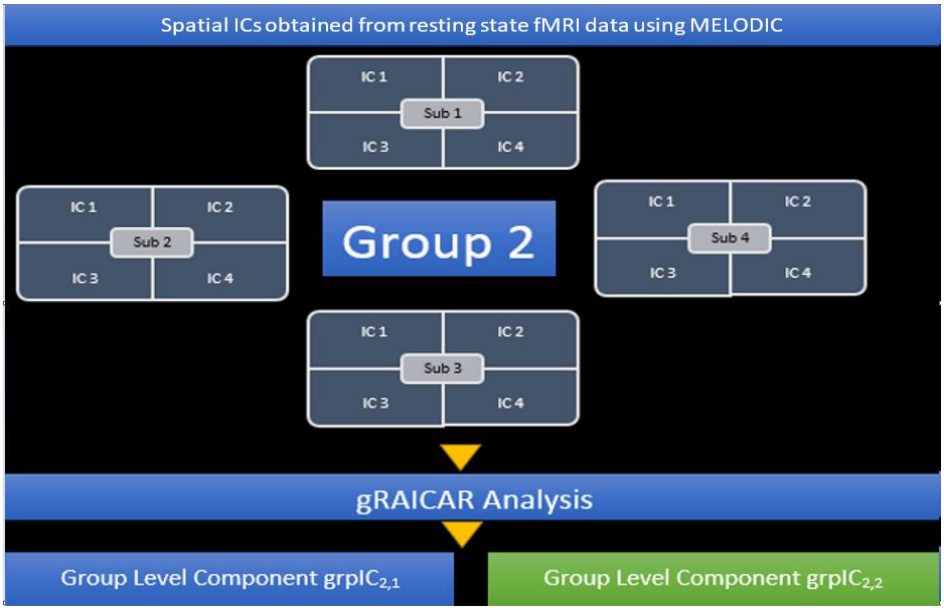

Fig. 4.2 A toy illustration of the analysis workflow. gRAICAR Analysis on ICs estimated from fMRI data corresponding to Group 2 is assumed to produce group-level components $grpIC_{2,1}$ and $grpIC_{2,2}$. Let us suppose that $grpIC_{2,2}$ has highest inter-subject consistency in Group 2 and hence be selected for further processing.

4.2.4 Clustering Analysis

For all subjects, we access post-MELODIC analysis results and retrieve spatial maps associated with the ICs for each subject corresponding to each selected group-level component. We then process these spatial maps in MATLAB wherein the spatial map associated with the IC index of the current subject is retrieved and singleton dimensions are removed. The resulting array is reshaped using MATLAB's reshape function (http://www. mathworks.com/help/matlab /ref/reshape.html) thus giving us a matrix ϕ_x with dimensions $p_x \times q$ where p_x is the number of subjects in group x and q is the size of each spatial map associated with the current IC index. Suppose the size of the spatial map size for each subject in this example is 61 × 73 × 61. For group 1 with 4 subjects, ϕ_1 is 4 × 61 × 73 × 61 and the same for group 2 and ϕ_2. After all subjects in both groups are processed, we combine ϕ_1 and ϕ_2 matrices from groups 1 and 2 resulting in ϕ_c, an 8 × 271633 matrix representing all individual subject-level maps from all groups. We apply the k-means algorithm, utilized by several studies in the analysis of fMRI data [111] [112] [113], to ϕ_c to examine how subjects were clustered based upon their spatial maps without *a priori* groupings, and how this corresponds to clinically determined diagnostic clusters. We minimize the objective function, *M*, as follows:

$$M = \sum_{b=1}^{x} |\phi_b - C_b|^2 \quad (4.3)$$

ϕ_b represents combined spatial maps from all subjects in group b, C_b represents the mean of all points in group b, and x represents the number of groups in the analysis.

We set up the k-means algorithm to partition ϕ_ϵ into two clusters since we have two example subject groups, continuing with the example we presented earlier. Cluster purity, referring to true positive rate obtained through k-means clustering analysis, provides us insight into the ability of $grpIC_{1,1}$ and $grpIC_{2,2}$ to accurately distinguish between the two diagnostic groups. If $grpIC_{1,1}$ and $grpIC_{2,2}$ do not represent the same functional brain network in both groups, or the spatial correlation value between the two group-level components is less than 0.9, we take $grpIC_{1,1}$ from group 1 and find the group-level component, $grpIC_{2,.}$, in group 2 having the highest spatial correlation with it thus giving us the same functional network in group 2. The '.' in $grpIC_{2,.}$ represents the index value of this new-found component. We then find $grpIC_{1,.}$, the group-level component in group 1 with the highest spatial correlation with $grpIC_{2,2}$ in group 2, or the component representing the same network as $grpIC_{2,2}$ in group 1. We now merge ($grpIC_{1,1}$ $grpIC_{2,.}$) and ($grpIC_{1,.}$ $grpIC_{2,2}$) and examine cluster purity in both cases using the k-means algorithm. The rationale behind this second round of analysis is to examine cluster purity values if similar functional brain networks from all groups are combined. In other words, this second round of analysis provides insight into the ability of similar functional networks to distinguish between the two groups. Having determined these reproducible networks and their ability to effectively discriminate between the groups also supports furthering our "discover-confirm" approach introduced earlier in this paper. In the following section, we review the implementation of this methodology in a software package named gMedICA.

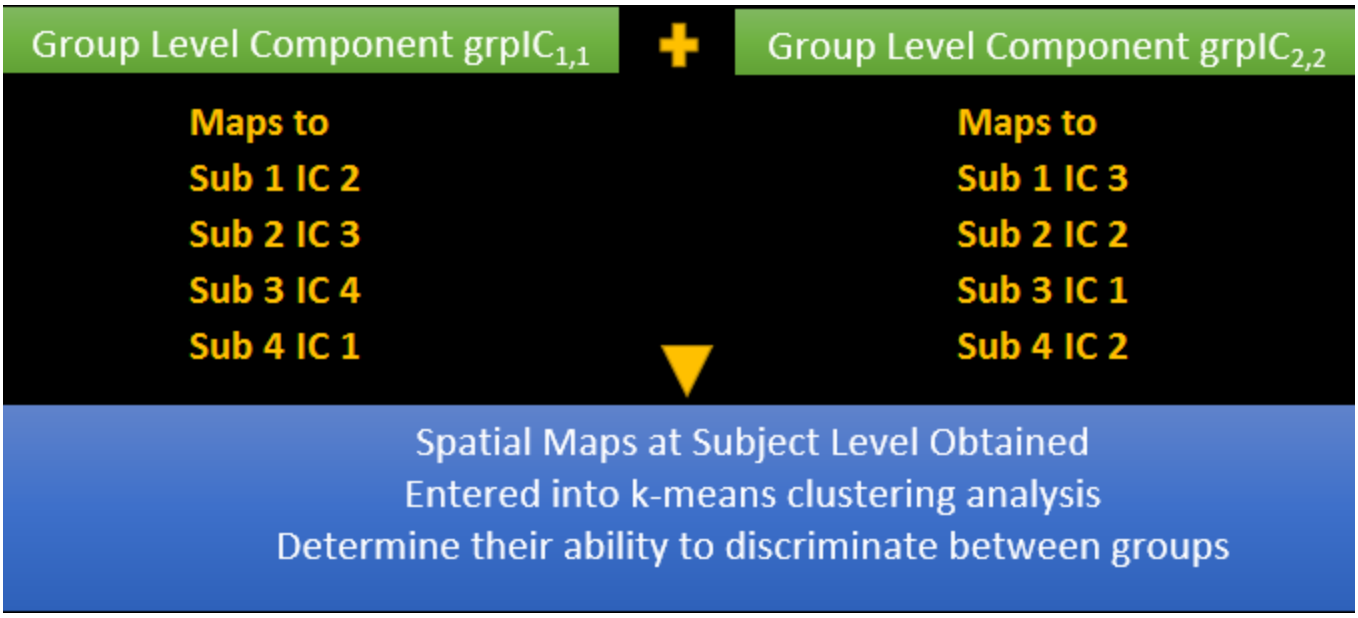

Fig. 4.3 The spatial maps at the individual subject level corresponding to group-level components from Fig. 4.1 and Fig. 4.3, i.e. the most reproducible ICs within each group, are obtained and entered into a k-means clustering analysis in order to determine their ability to discriminate between the groups.

4.3 Implementation

We have designed gMedICA software to allow users to examine their fMRI data sets using the "discover-confirm" approach we have proposed using the reproducibility of independent components. It is meant to provide functionality described in our analysis workflow and resulting components with minimal effort. The main application was developed in MATLAB with wrapped subsidiary applications. We have provided two starting formats for users, DICOM or .img/ .hdr file pairs.

4.3.1 Prerequisites

The first version of gMedICA was developed in MATLAB environment and hence MATLAB is required to run the software. Another pre-requisite is to define the location of FSL software

directory in the host system. If this has been accomplished per instructions in FSL software (FMRIB Software Library v5.0; https://fsl.fmrib.ox.ac.uk/fsl/fslwiki), the following command – "*echo $FSLDIR*" – should display the location of the above-mentioned directory. This gives the ability to run FSL's '*FEAT*' command described later in FSL analysis. Once the FSL location has been established in the environment, the user can execute gMedICA.

In order to utilize this approach, GMedICA is designed to read the following directory structure, which the user needs to create:

Main Directory

Group 1

Sub 1

Sub 2

Sub 3

Sub 4

.

.

.

Group 2

Sub 1

Sub 2

Sub 3

Sub 4

.

.

In this structure, each subject directory contains DICOM or NIfTI Hdr/Img pair files. The current version of gMedICA has been limited to three diagnostic groups due to external processing constraints. This limitation is discussed later in this paper. An example structure has been discussed under gRAICAR algorithm and we continue with the same example that includes two groups – Group 1 and Group 2. Consequently, the data structure should be set up as follows:

Main Directory/Group 1/Sub 1, Sub 2, Sub 3…,

and

Main Directory/Group 2/Sub 1, Sub 2, Sub 3...

Under each subject, we may have

Sub 1/ 1.dcm,2.dcm,3.dcm,...

or

Sub 1/1.img,1.hdr,2.img,2.hdr,...

4.3.2 Packaged Software

gMedICA wraps two software packages in addition to its native programming. These two packages are Data Processing Assistant for Resting-State fMRI [104] (DPARSF, http://www.restfmri.net) and fMRIB Software Library v5.0 [106] [107] (FSL by Analysis Group, FMRIB, Oxford, UK). DPARSF uses libraries from Statistical Parametric Mapping or SPM (http://www.fil.ion.ucl.ac.uk/spm) and Resting-State fMRI Data Analysis Toolkit (REST 1.7) [105]. DPARSF, SPM and REST are bundled with gMedICA software. This not only helps standardize inter-process communications, such as those to and from the gMedICA software

itself, but also resolves possible software conflicts. One of the highlights of gMedICA is that users do not have to deal directly with software packages mentioned in this section as gMedICA automates pre-processing whilst minimizing user effort.

4.3.3 User Interface

Minimal user effort was the philosophy behind gMedICA's user interface design. Fig. 4.4 shows the user interface corresponding to the starting point of the software. It was designed to accomplish its goals through methodology proposed in our paper with minimal effort on the user's part. Single stage user interface allows users to enter the location where the entire analysis is set to execute. This refers to the main directory as described in the prerequisites section. The user then enters repetition time (TR) and selects an input format. There are two input format options available: DICOM and .img/ .hdr file pairs. Once the user clicks 'Continue', background processing takes over.

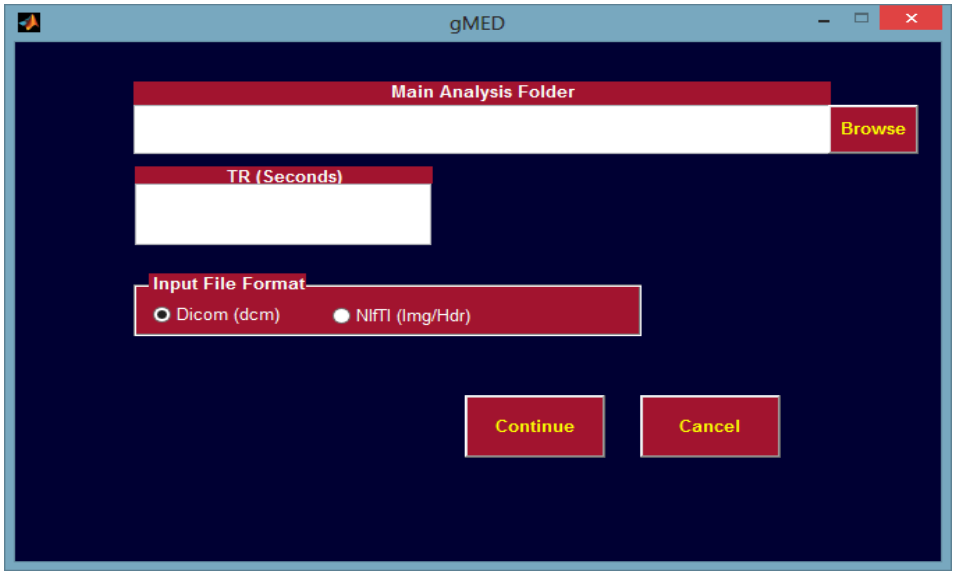

Fig. 4.4 gMedICA's user interface with options described under "User Interface" section of this paper.

4.3.4 Main Analysis

The software now ascertains a uniform number of input images or time points (DICOM or NIfTI) and alerts the user if any discrepancies are found, discontinuing the progress. If a uniform number of images or time points is found for each subject, the software sets the location of SPM, REST and DPARSF along with any NIfTI processing files necessary for the pre-processing phase. The program includes a separate interface to allow users to customize most DPARSF settings. Default settings are available in case customization is not needed. It communicates with DPARSF and completes the following tasks:

- Sets SPM, REST and DPARSF locations
- Disables options in these other software packages not used in our methodology
- Sets Time Points by examining files per subject
- Sets TR provided by the user
- Sets Slice Timing
- Sets Realignment
- Sets Normalization with Bounding Box [-90 -126 -72;90 90 108] and voxel size of 2×2×2
- Sets smoothing with FWHM of 4×4×4
- Sets de-trend and filter range 0.01 – 0.1 Hz

Once started, the software triggers SPM, REST and DPARSF. This processing completes steps set in the DPARSF module while the progress can be monitored through SPM and REST interfaces. Upon completion, the resulting 3D Img/Hdr pairs are saved in the following directory structure per subject:

MainDirectory/Group1/FunImgNormalizedSmoothedDetrendedFiltered/Subject1, Subject2, Subject3…

A similar structure is created for other groups. Once DPARSF steps are completed, the software finds locations as described above and collapses all 3D images per subject to a single 3D Img/ Hdr pair. This collapsed 3D Img/Hdr pair is now converted to 4D NIfTI format. The software now creates a directory per group under the main directory called 'Melodic' as:

MainDirectory/Group1/Melodic

4D NIfTI images created per subject are now moved to this directory. The software prepares to run the Multivariate Exploratory Linear Optimized Decomposition into Independent Components (MELODIC) algorithm [108] [109] which will decompose 4D data sets using Independent Component Analysis. More information on the MELODIC algorithm can be obtained at http://fsl.fmrib.ox.ac.uk/fsl/fslwiki/MELODIC. In order to run FSL MELODIC through gMedICA, the software first creates a design script file with the extension '*fsf*' (.fsf). This file defines the following steps, some of which are set by MELODIC as defaults:

- Location of each subject's 4D NIfTI (nii) file which is edited and adjusted by gMedICA
- High pass frequency cut off point at 100 seconds
- Linear Registration on input data using FEAT functionality before the statistical analysis with 12 degrees of freedom

- Resampling resolution which refers to the desired isotropic voxel dimension of the resampled data set to 4mm
- Variance normalize time courses so that the estimation is more influenced by voxel-wise temporal dynamics than a voxel's mean signal
- Automatic dimensionality estimation to avoid overfitting. This is achieved by using Bayesian estimators for the model order and PCA (principal component analysis) to reduce the data prior to IC estimation
- Single-session ICA
- Threshold IC maps at 0.5. MELODIC carries out inference on the estimated maps by default using a mixture model and an alternative hypothesis testing approach. This threshold level in alternative hypothesis testing refers to a voxel that survives thresholding as soon as the probability of being in the active class – modelled by the Gamma densities – exceeds the probability of being in the background noise class.

This design file is run in the environment using the '*FEAT*' command of FSL which reads the design script file (.fsf) and starts MELODIC IC analysis, e.g. '*feat design.fsf*'. MELODIC ICA results are stored under the '*Melodic*' directory where new directories are created by MELODIC for each subject. In this case, the file we specifically need for gRAICAR analysis is stored under each subject's MELODIC ICA directory created by FSL MELODIC and called '*melodic_IC.nii.gz'*. A sample location is as follows:

MainDirectory/Group1/Melodic/Subject1.ica/filtered_func_data/melodic_IC.nii.gz

In this location, *Subject1.ica* is a directory based upon Subject 1's 4D NIfTI file and holds FSL MELODIC analysis' results.

We now prepare to run the gRAICAR algorithm. In order to do so, the software creates a directory under '*Melodic*' called '*gR*'. All ICA directories are moved to *gR* directory as follows:

MainDirectory/Group1/Melodic/gR/Subject1.ica…

The software then creates a shell script to calculate the average mask of the group based upon individual masks created by FSL and stored in each subject's ICA directory. As mentioned earlier, users do not have to directly interact with FSL and once the script is created, it is run as an environment command from within the software. The result is a file called '*mask.nii.gz*' stored under gR directory of the group. In addition, the software creates a list file, *subjects.list*, that stores the names of subject directories. This list file is used by the gRAICAR algorithm. As an example, if we had four subjects in Group 1, the gR directory would have the following structure:

MainDirectory/Group1/Melodic/gR/Subject1.ica
MainDirectory/Group1/Melodic/gR/Subject2.ica
MainDirectory/Group1/Melodic/gR/Subject3.ica
MainDirectory/Group1/Melodic/gR/Subject4.ica
MainDirectory/Group1/Melodic/gR/mask.nii.gz
MainDirectory/Group1/Melodic/gR/subjects.list

Once the preparation is complete, the software calls the gRAICAR algorithm with the location of '*gR*' directory in addition to those of average mask and the subjects list which are also under '*gR*'. It also specifies an output directory name, *gROutput*, for the algorithm to store results in. Once gRAICAR processing is complete, results are stored under '*gROutput*' directory for each group. If we had two groups as an example, we should now have the structure created by the gRAICAR algorithm shown in Fig. 4.5 for each group:

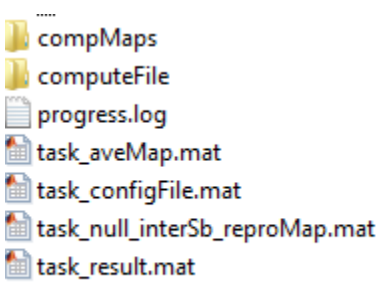

Fig. 4.5 *Directory structure created by the gRAICAR algorithm in MATLAB*

In our example, this structure is created under the following two directories:

MainDirectory/Group1/Melodic/gR/gROutput

MainDirectory/Group2/Melodic/gR/gROutput

The gRAICAR algorithm is run at the group-level and '*computeMaps*' directory holds NIfTI (.nii) files of group-level components discovered by the algorithm.

4.3.5 Post-Processing

Once the gRAICAR results are available, the software completes the following tasks:

1) Loads the '*task_result.mat*' file for each group looking at the result object in this file and, specifically, the field *obj.result.beta_rank_subjLoad*. The lower the value of a group-level component in this field, the greater the inter-subject consistency.

2) Picks the most reproducible component.

3) For this group-level component, it looks at the '*obj.result.foundComp*' field of the result object to determine which subject level component this group-level component maps to.

4) It then retrieves spatial maps for each subject's IC forming the group-level component and combines them. We can call this combination *x_vec*.

5) Steps 1-4 are repeated for the second and third group (if we have three groups).

6) *y_vec* is the result of step 4 from Group 2 and the software now combines *x_vec* and *y_vec*, resulting in a combined matrix, *A*.

7) The software now runs k-means algorithm on *A* after defining the centroids as the average of *x_vec* and *y_vec* respectively. We set the number of clusters equal to the number of groups in the analysis.

8) These steps are summarized by Eq. 6 or Deshpande-Syed's Equation for group distinction using ICA reproducibility and clustering.

9) The result of step 7 is a column vector where each row represents a subject along with the index of the cluster this subject has been assigned to. These indices help us determine cluster purity. Continuing our earlier example of two groups and 4 subjects in each group, k-means results refer to the following structure:

Group 1 Subject 1 – Cluster 1

Group 1 Subject 2 – Cluster 1

Group 1 Subject 3 – Cluster 1

Group 1 Subject 4 – Cluster 1

Group 2 Subject 1 – Cluster 2

Group 2 Subject 2 – Cluster 2

Group 2 Subject 3 – Cluster 2

Group 2 Subject 4 – Cluster 2

In this example, cluster purity is 1 as all subjects have been identified correctly.

If the most reproducible components selected per group do not represent the same network based upon their spatial correlation values being less than 0.9, the software can take the best component from Group 1 used in k-means and calculate its covariance against all group-level components in Group 2. This step provides the group-level component in Group 2 that represents the same functional network as and, therefore, has the highest covariance with our starting component from Group 1. This step is then repeated for the best component from Group 2 that was used in k-means. Now we have the group-level component in Group 1 that has the highest covariance value with the selected component in Group 2. This additional step ensures that the best components we had selected for k-means are matched with a component within the same brain network in the opposite group. In this case, the software runs k-means after combining an initial component from Group 1 and its counterpart from Group 2 and cluster purity is examined. The step is repeated for the initial component from Group 2. In our example, we have three cluster purity values. The software, therefore, calculates $x+1$ cluster purity values, where x is the number of groups.

4.4 Example Application

4.4.1 Data Overview

Post-traumatic stress disorder (PTSD) is categorized as an anxiety disorder and develops after a traumatic event has been experienced [114]. Veterans are at a higher risk for developing PTSD as many experience traumatic events during deployment and combat. The prevalence of PTSD among veterans deployed to Iraq and Afghanistan evaluated anonymously through questionnaires was found to be 6.2 – 12.9% [115]. We used a study that included 71 male participants who were also active duty soldiers, to evaluate gMedICA. Of these 71 participants, 15 had PTSD, 30 had both PTSD and PCS (post-concussion syndrome, a chronic sequalae of mild traumatic brain injury - mTBI), and 26 combat controls. All three groups were matched in age, race and education. In addition, all participants had combat experience in Iraq (Operation Iraqi Freedom, OIF) and/or Afghanistan (Operation Enduring Freedom, OEF). In this study, PTSD Checklist-5 (PCL-5) score, clinician referral, post-concussive symptoms using the Neurobehavioral Symptom Inventory (NSI), and medical history including documentation of mTBI(s) were used when grouping the subjects [23]. Details regarding inclusion and exclusion criteria for defining the three groups can be obtained from Rangaprakash et al, 2017.

4.4.2 Data Acquisition

A 3T Siemens MAGNETOM Verio scanner (Siemens Healthcare of Erlangen, Germany) was used for participant scanning using T2* weighted multiband echo planar imaging (MB-EPI) sequence in resting state. The participants were asked to keep their eyes open and fixated on a

white cross displayed with dark background on the screen using an Avotec projection system and not think of anything specific. Scanning parameters used included a TR (repetition time) of 600ms, TE (echo time) of 30ms, FA (flip angle) at 55˚, multiband factor of 2, anterior to posterior phase encoding direction, voxel size of 3×3×4 mm^3 and 1000 volumes or time points. We used a TR of 1900 ms, TE of 2.5ms, FA at 9˚ and voxel size of 1×1×1 mm^3 for acquiring anatomical scan using an MPRAGE (magnetization-prepared rapid gradient echo) sequence. Brain coverage was limited to the cerebral cortex, subcortical structures, midbrain and pons, excluding the cerebellum

4.4.3 Technical Implementation

In order to examine our PTSD dataset, gMedICA was provided three (3) input directories representing three subject groups: PTSD, PTSD + PCS, and matched combat controls. Each subject had 1000 time points saved in the form of DICOM (.dcm) images within each directory, as described in the pre-requisites section. All software and processing settings were the same as described in the workflow, processing and implementation phases of gMedICA. During the first stage, gMedICA pre-processed these sets using DPARSF. This step created a 4D NIfTI format output file per subject. gMedICA then used these 4D NIfTI images to run independent component analysis using FSL's MELODIC functionality. Once the ICs had been computed per subject, gMedICA used that information per subject in the gRAICAR algorithm to calculate group-level components per group. The most reproducible components were then selected as explained earlier by gMedICA, one component per group was then retrieved, combined with all selected ones in the other two groups, and k-mean clustering was performed for different combinations, ϕ_ϵ, where ϵ represents the permutational spatial combinations of 127 such components from the PTSD, 82

from the PTSD + PCS, and 111 from matched control groups. Resulting cluster purities were then determined for the three groups. The combination of group-level components, P^x from the PTSD group, S^x from the PTSD + PCS group, and C^x from the control group, which gave the the highest cluster purities was then examined further. We denote these as the primary group-level components. We examined the spatial correlation values of P^x with all group-level components in PTSD + PCS and control groups, those of S^x with all group-level components in PTSD and control groups, and finally those of C^x with all group-level components in the PTSD and control groups. Secondary group-level components with the highest spatial correlation with primary components were identified using the following approach.

$$\xi = \max \sum_{i=1}^{n_s} cov(\psi, \psi_i) \quad (4.4)$$

In Eq. (4.4), ξ denotes the highest covariance between the primary group-level component, and the secondary group-level component,ψ_i , from the opposite group with n_s identifying the total number of components in the opposite group. Secondary group-level components thus identified are presented in Table 2.

Table 4.1 Notations used to refer to group-level components used in our analysis and described in the technical implementation section. This table shows the secondary components, the groups they belong to, and the primary component most significantly spatially correlated to each secondary component.

Secondary Component	Group	Primary Component
$\boldsymbol{S_p^x}$	*PTSD + PCS*	P^x
$\boldsymbol{C_p^x}$	*Control*	P^x
$\boldsymbol{P_c^x}$	*PTSD*	C^x
$\boldsymbol{S_c^x}$	*PTSD + PCS*	C^x
$\boldsymbol{P_s^x}$	*PTSD*	S^x
$\boldsymbol{C_s^x}$	*Control*	S^x

We then performed another set of clustering analyses, on P^x combined with $S_p{}^x$ and $C_p{}^x$, on S^x combined with $P_s{}^x$ and $C_s{}^x$, and finally on C_x combined with $P_c{}^x$ and $S_c{}^x$. This second round of analyses determined whether the reproducible components in each group, when paired with the corresponding components with similar spatial distribution in the other groups, effectively discriminated between the groups. Finally, for components that effectively discriminated between the groups, we performed two-sample t-tests to determine whether they were stronger or weaker in the disease groups as compared to the control group.

4.5 Results

We first present the most reproducible components in the PTSD, PCS+PTSD and control groups, i.e. P^x, S^x, and C^x, respectively (Figs 4.6-4.8). These group-level components, when

combined and examined using k-means clustering, yielded a cluster purity value of 1 for all three clusters, one cluster per group. All three groups were identified with 100% accuracy.

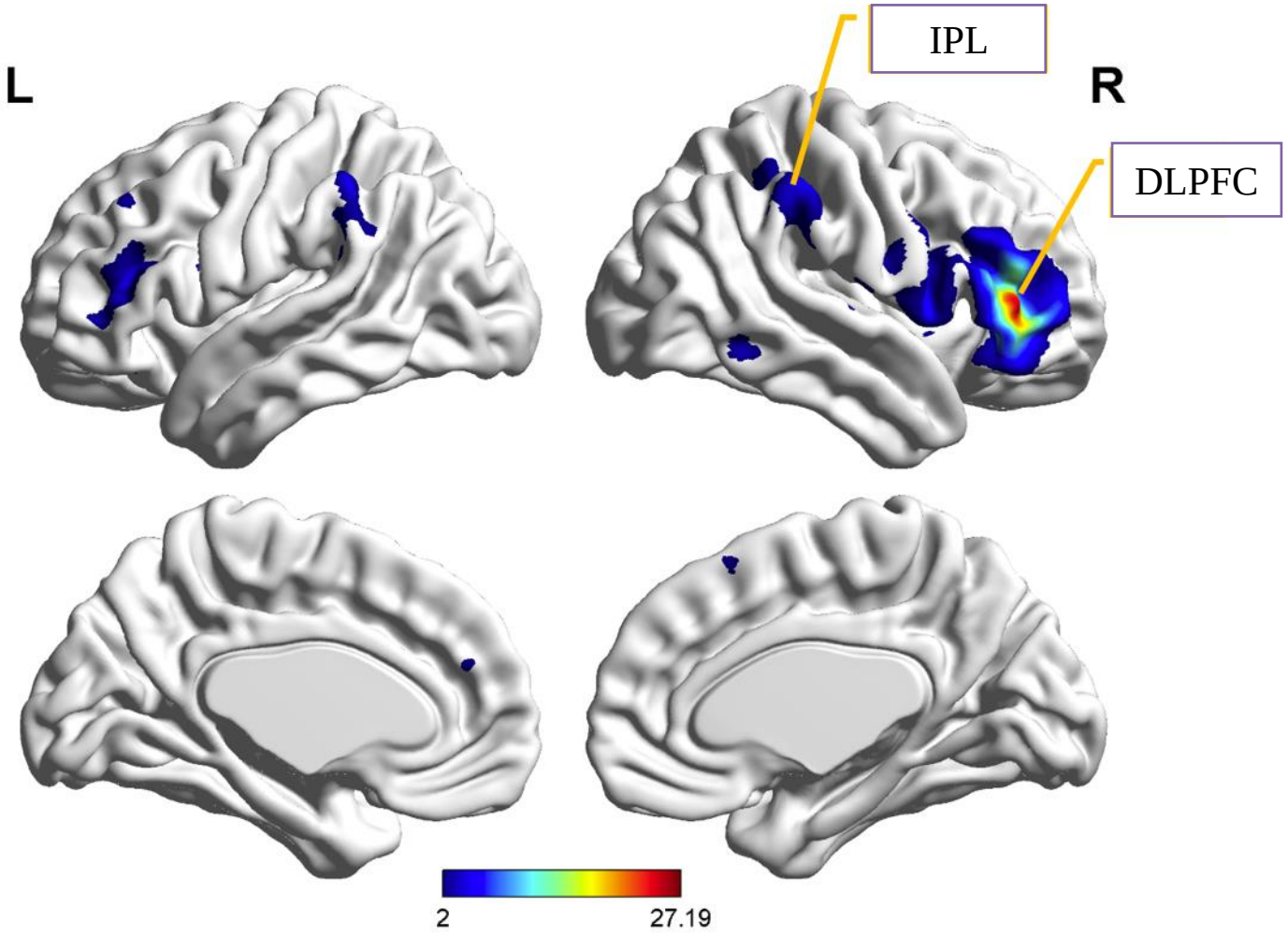

Fig. 4.6 Spatial map of the group-level component, P^x from PTSD group, that was most reproducible within the PTSD group as well as produced the highest cluster purity when combined with S^x from PTSD + PCS group and C^x from the controls group. DLPFC (Dorsolateral prefrontal cortex) and IPL (inferior parietal lobe) have been identified as well.

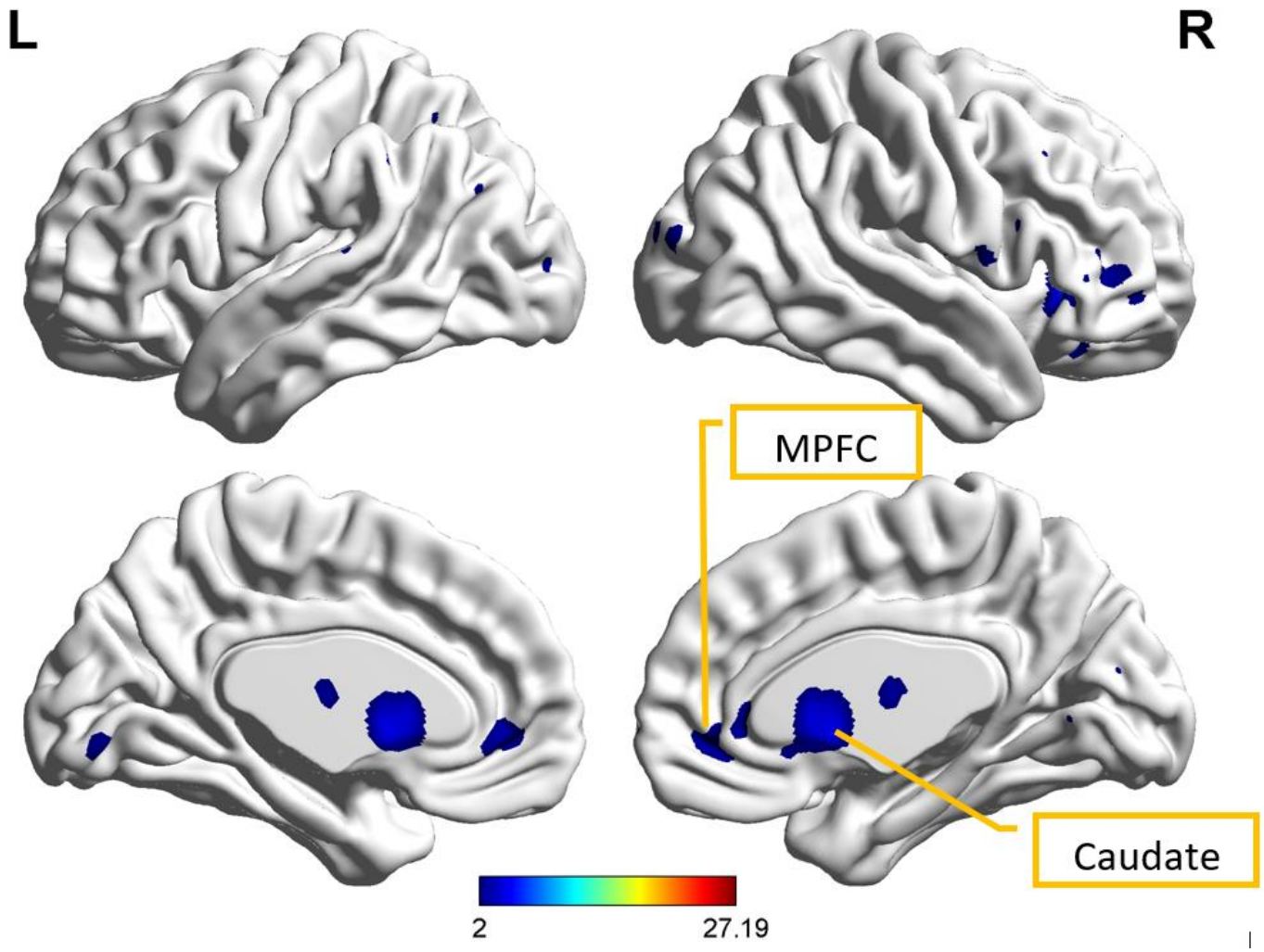

Fig. 4.7 Spatial map of the group-level component, S^x from PTSD + PCS group, that was most reproducible within the PCS+PTSD group as well as produced the highest cluster purity value when combined with P^x from PTSD group and C^x from the controls group. Caudate and MPFC (medial prefrontal cortex) have been identified as well.

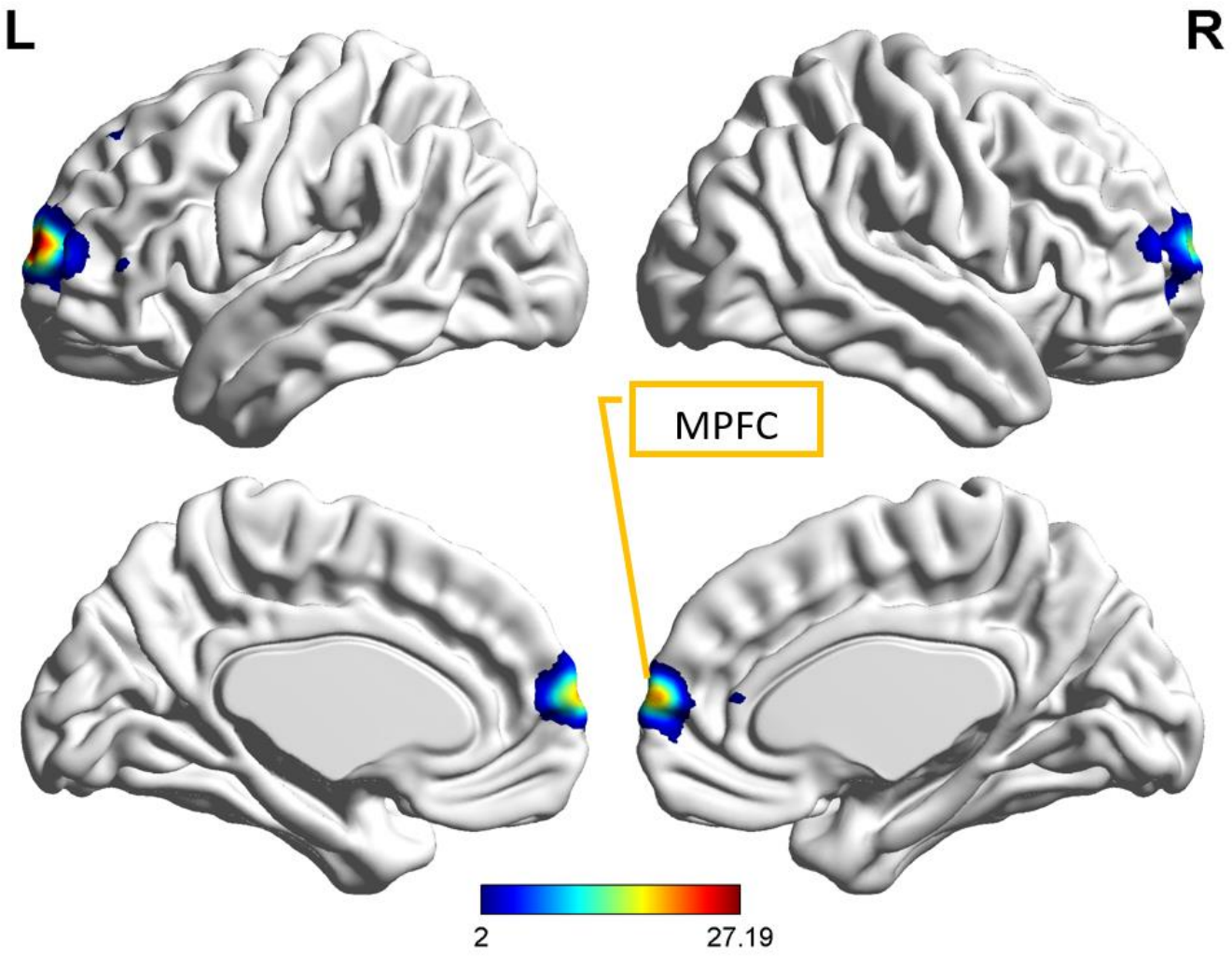

Fig. 4.8 Spatial map of the group-level component, C^x from controls group, that was most reproducible within the control group as well as produced the highest cluster purity value when combined with P^x from PTSD group and S^x from PTSD + PCS group. MPFC (Medial prefrontal cortex) has been identified as well.

We then combined P^x with $S_p{}^x$ and $C_p{}^x$ and examined this combination using k-means clustering. This combination produced cluster purity values of 0.93 for PTSD group, 0.83 for PTSD + PCS group, and 0.85 for the control group. The spatial correlation coefficient value between P^x and $S_p{}^x$ or $\rho(P^x, S_p{}^x)$ was 0.68 ($p < 0.005$) while $\rho(P^x, C_p{}^x)$ was 0.51($p < 0.005$).

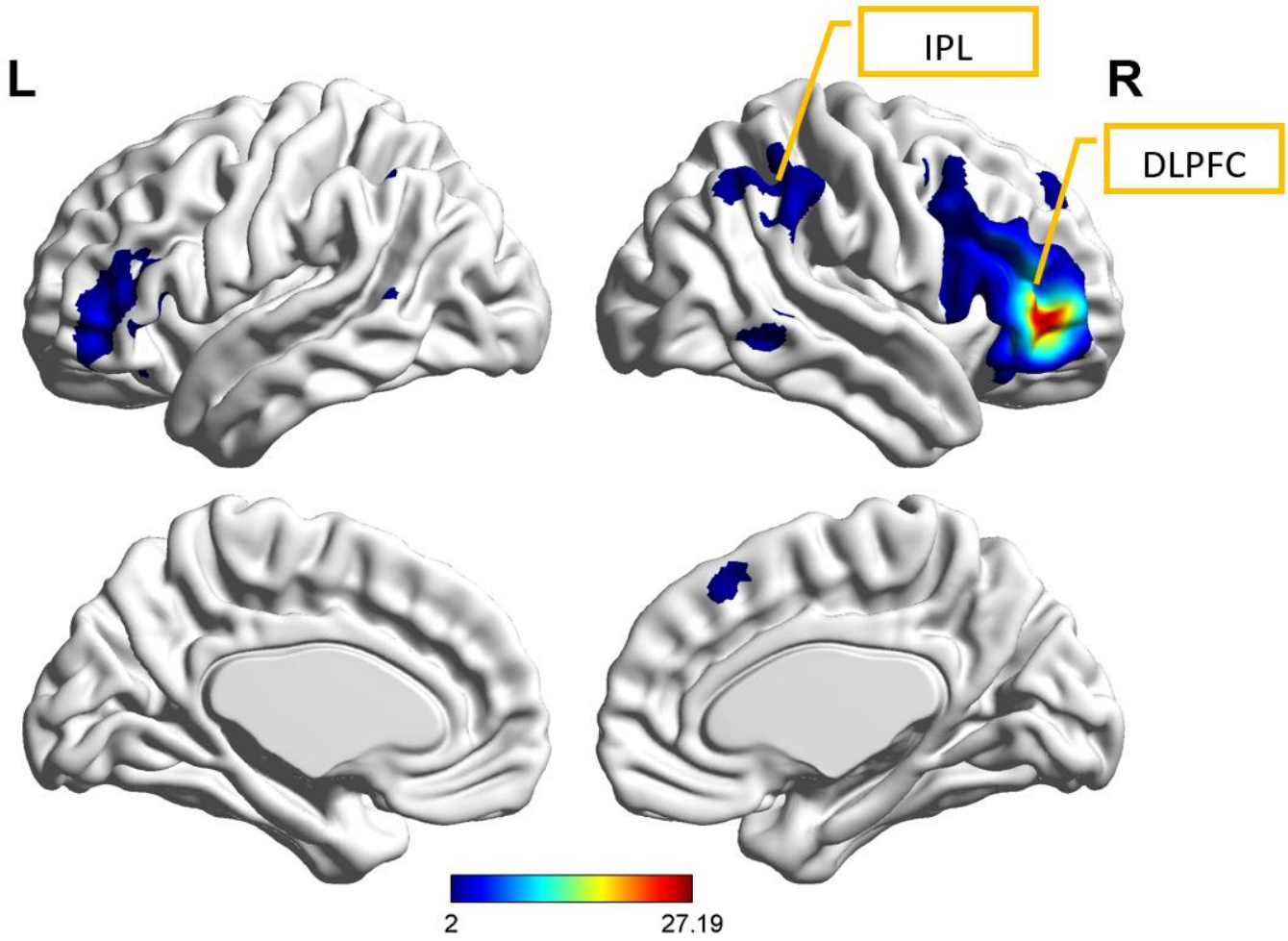

Fig. 4.9 Spatial map of the group-level component, S_p^x from PTSD + PCS group, that was found to have the highest spatial correlation with and correspondence to P^x. DLPFC (Dorsolateral prefrontal cortex) and IPL (inferior parietal lobe) have been identified.

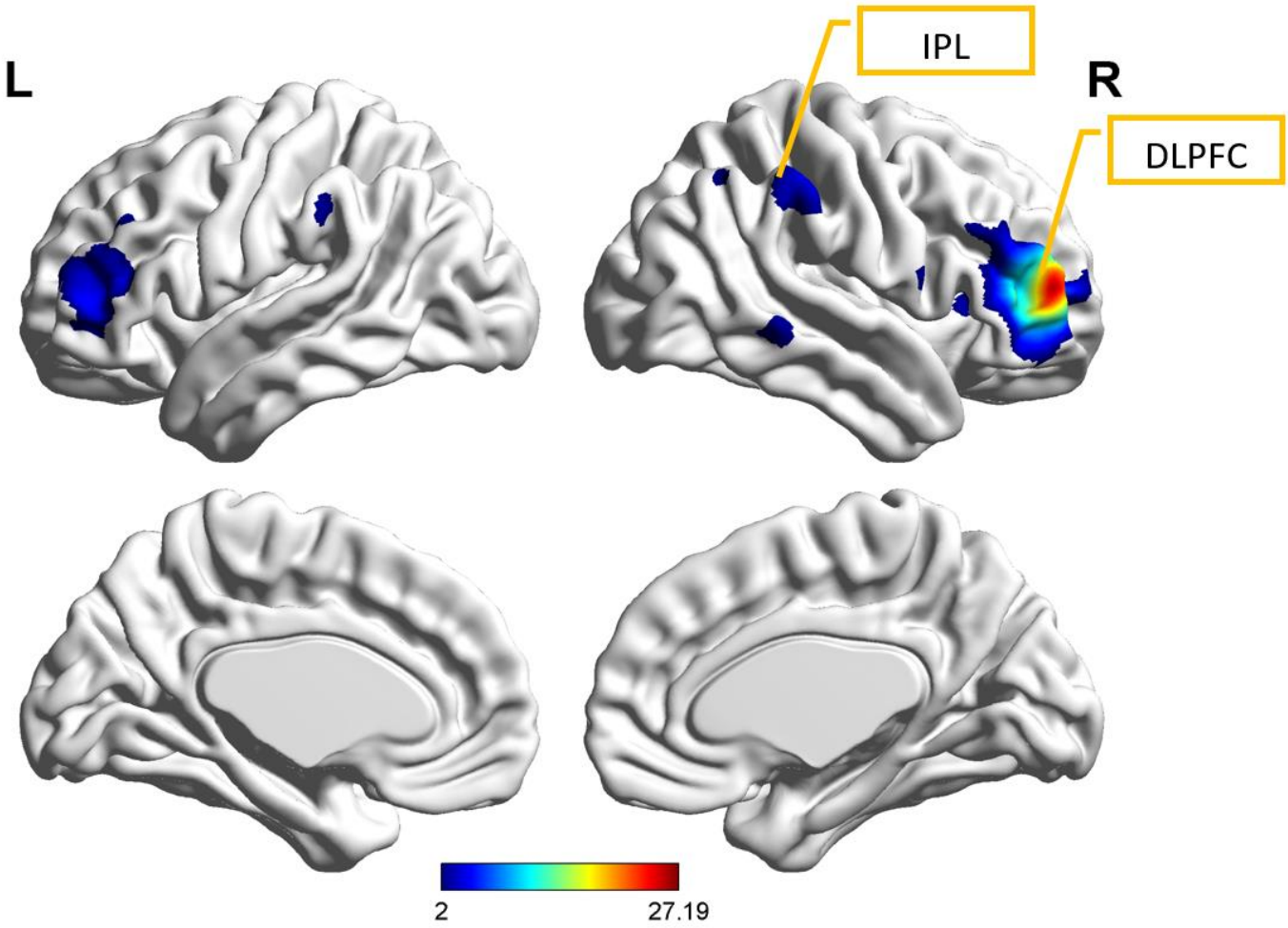

Fig. 4.10 Spatial map of the group-level component, C_p^x from the controls group, that was found to have the highest spatial correlation with and correspondence to P^x. DLPFC (Dorsolateral prefrontal cortex) and IPL (inferior parietal lobe) have been identified.

S^x was then combined with P_s^x and C_s^x and examined using k-means clustering. This combination produced cluster purity values of 1 for PTSD group, 0.97 for PTSD + PCS group, and 1 for the control group. The correlation coefficient value between S^x and P_s^x or $\rho(S^x, P_s^x)$ was 0.55 $(p < 0.005)$ while $\rho(S^x, C_s^x)$ was 0.49 $(p < 0.005)$.

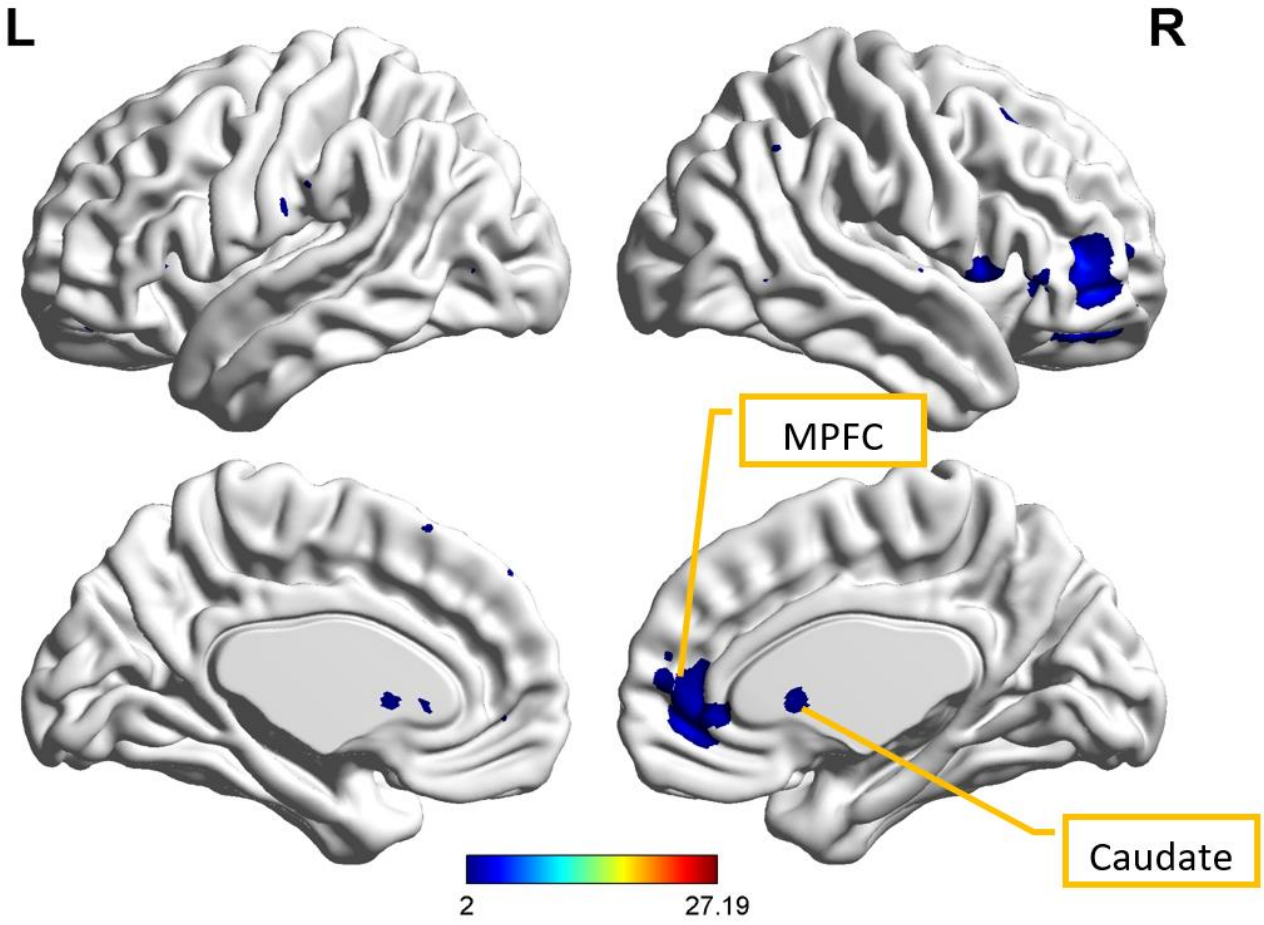

Fig. 4.11 Spatial map of the group-level component, P_s^x from PTSD group, which was found to have the highest spatial correlation with and correspondence to S^x. Caudate and MPFC (medial prefrontal cortex) have been identified as well.

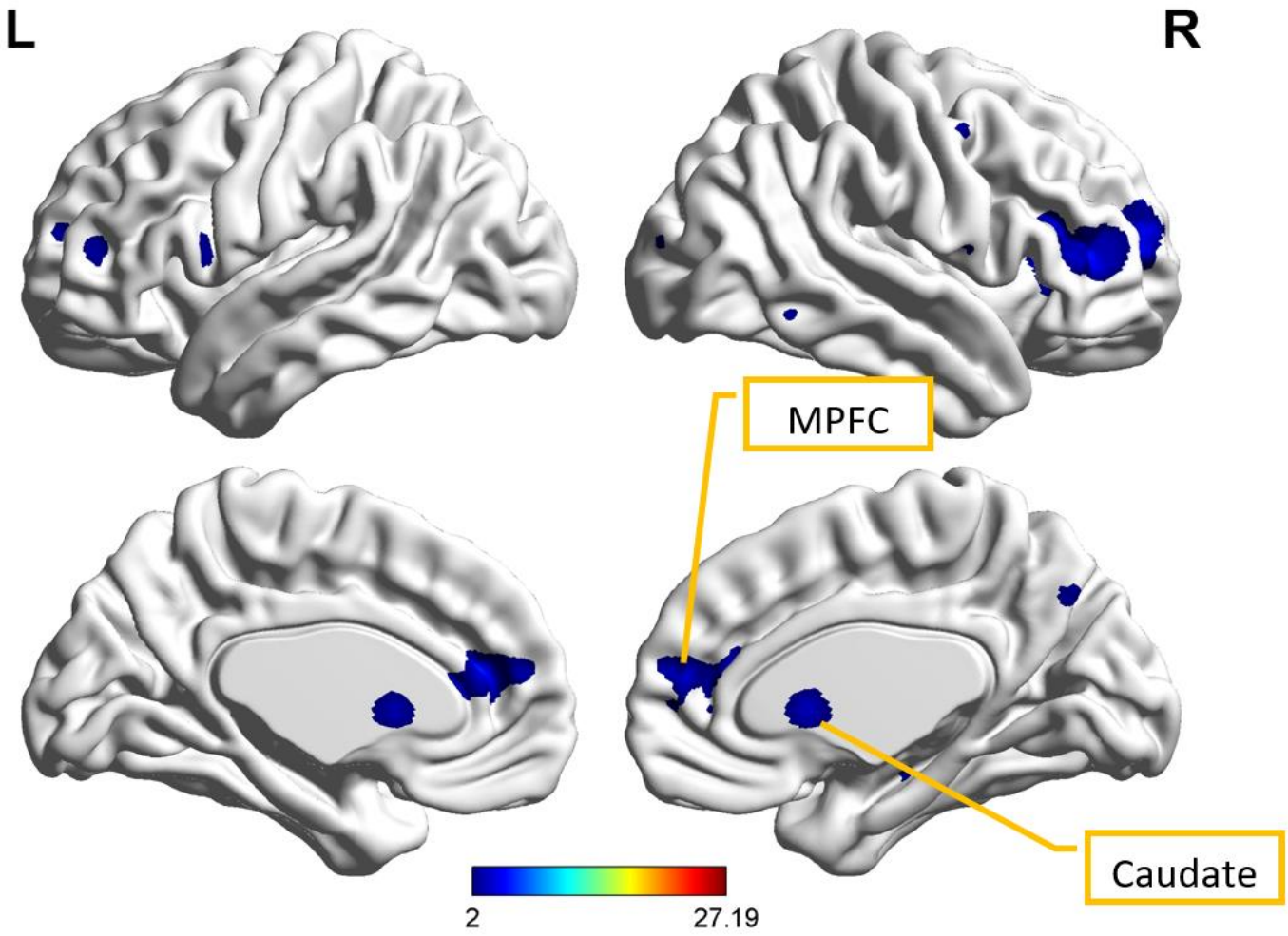

Fig. 4.12 Spatial map of the group-level component, C_s^x from the controls group, which was found to have the highest spatial correlation with and correspondence to S^x (shown in Fig.12). Caudate and MPFC (medial prefrontal cortex) have been identified as well.

Finally, we combined C^x with P_c^x and S_c^x and examined this combination using k-means clustering. This combination produced cluster purity values of 0.87 for PTSD group, 0.97 for PTSD + PCS group, and 0.92 for the control group. The correlation coefficient value between C^x and P_c^x or $\rho(C^x, P_c^x)$ was 0.65 $(p < 0.005)$ while $\rho(C^x, S_c^x)$ was 0.62 $(p < 0.005)$.

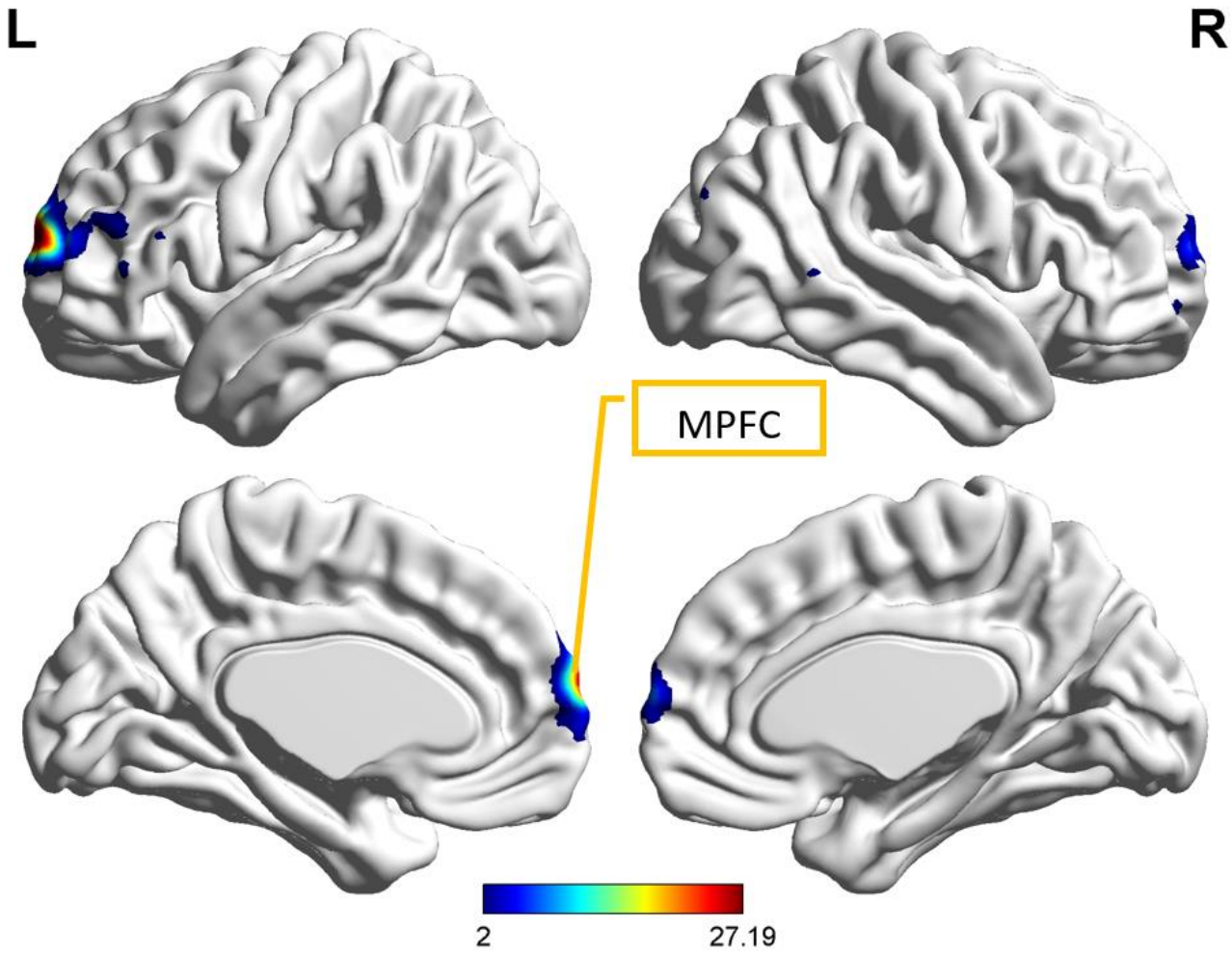

Fig. 4.13 Spatial map of the group-level component, P_c^x from PTSD group, which was found to have the highest spatial correlation with and correspondence to C^x. MPFC (Medial prefrontal cortex) has been identified as well.

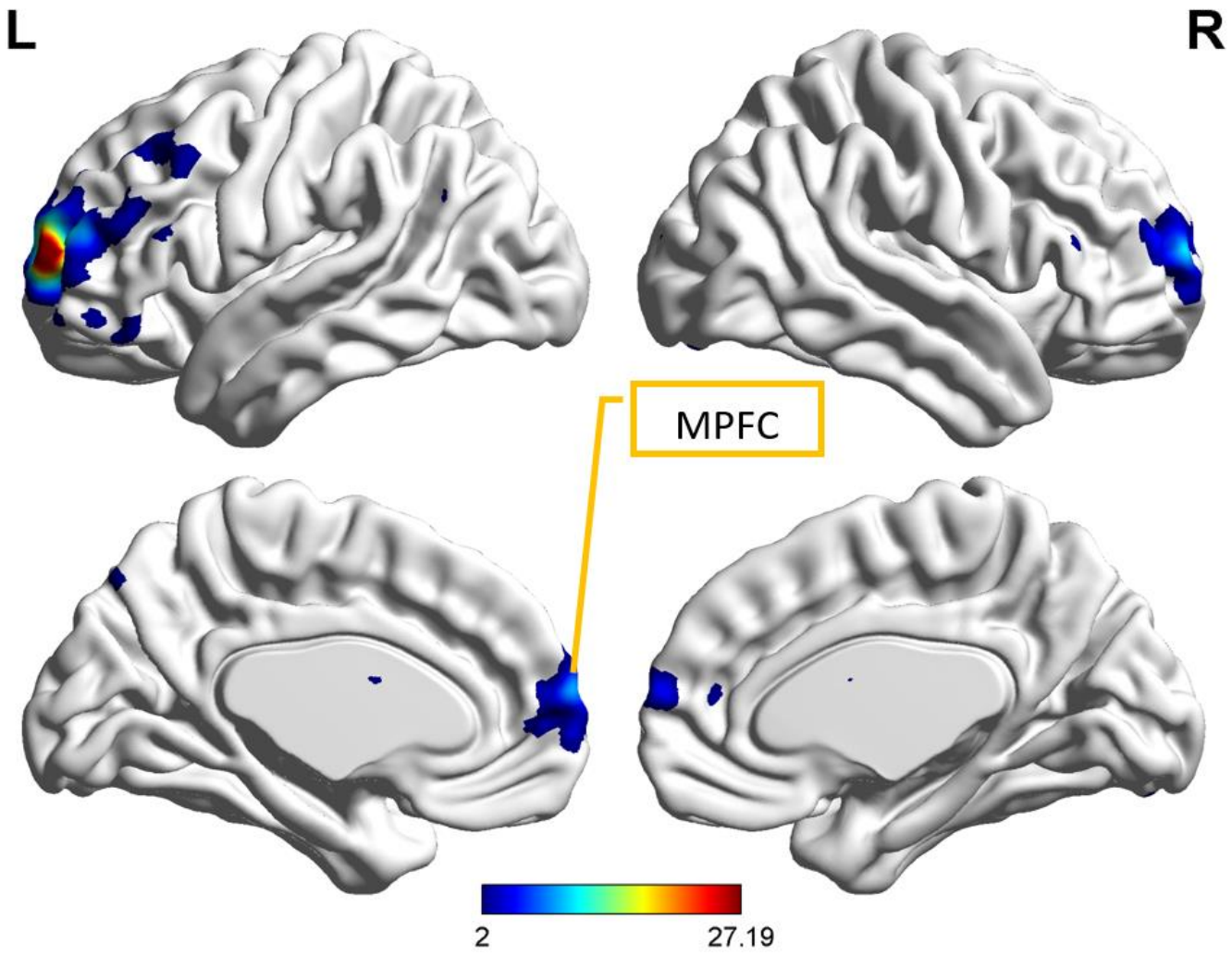

Fig. 4.14 Spatial map of the group-level component, S_c^x from PTSD + PCS group, that was found to have the highest spatial correlation with and correspondence to C^x (shown in Fig.13). MPFC (Medial prefrontal cortex) has been identified as well.

We then completed a series of two sample t-tests as described in the previous section. The goal was to examine whether there were significant between-group differences in the strength of the reproducible network(s) discovered in P^x, S^x, and C^x, as well as their spatial homologues. This round of tests indicated that these networks comprising medial prefrontal cortex as shown in C^x

were significantly stronger in controls as compared to both PTSD *($p < 0.05$ unc., $t = 1.67$)* and PTSD + PCS *($p < 0.05$ unc., $t = 1.67$)* groups. Also, functional networks comprising dorsolateral prefrontal cortex and inferior parietal lobe, shown in P^x, were significantly stronger as compared to PTSD + PCS *($p < 0.05$, $t = 1.68$).*

4.6 Discussion

In this section, we discuss the main findings of our study. We first present the unique and beneficial features of our gMedICA software package. Next, we discuss the significance of the results we have obtained from gMedICA analysis of resting state fMRI data acquired from PTSD, PTSD + PCS and controls groups, and whether they support the hypotheses described earlier in this paper. gMedICA provides users the ability to examine the reproducibility of group-level independent components using the gRAICAR algorithm, and the ability of these group-level components to distinguish between groups using unsupervised learning algorithms such as k-means clustering. A variety of neuroimaging software provide the ability to view and analyze fMRI data. Functionality in existing software packages include, but are not limited to, viewing fMRI data, format conversions such as from DICOM to NIfTI, brain extraction, tissue-type segmentation, segmentation of subcortical structures, linear and nonlinear registration, voxelwise analysis of multi-subject grey-matter density, longitudinal and cross-sectional analysis of structural changes, and structural analysis and include well respected packages such as DPARSF, SPM, FSL, Mango, AFNI, Brainnetviewer, and Brain Voyager among others [44] [45] [46] [111] [116] [117] [118]. Taking analyses a step further are standalone packages and sub-packages of the aforementioned ones, such as Sci-kit based software, MELODIC, GIFT, and CONN, a functional connectivity toolbox, among others, that apply various multivariate functional connectivity

techniques to fMRI data sets including ICA and group ICA to fMRI data sets [119] [112] [120] [121] [122] .

We are implementing our methodology in its entirety in gMedICA with no such implementation available in the literature currently. Therefore, a direct comparison with packages mentioned earlier is beyond the scope of the current report. However, we highlight how our software takes analyzing fMRI data sets a step further. In addition to providing and automating all phases of pre-processing, it incorporates mechanisms or systems to determine and analyze the reproducibility of group-level independent components using the gRAICAR algorithm [43] and k-means clustering. In gMedICA, the user just needs to complete two tasks to setup the analysis: a pre-determined directory structure where individual subject level images are arranged in group-level directories that the subjects belong to and the availability of the required analysis environment. Other tasks are accomplished seamlessly by gMedICA in the background and user responsibilities are minimized. gMedICA completes all pre-processing steps emulating our approach and processing parameters we used. It then uses a “discover-confirm” approach wherein, during the “discover” phase, it uses gRAICAR to retrieve reproducible components in each group. During the “confirm” phase, it uses unsupervised learning to determine the separation between groups based on the reproducible components in each group. This is a novel methodological framework for investigating discriminative features between diagnostic groups, as opposed to performing group-wise statistical tests or supervised classification. gMedICA then compares group-level components to find the ones that produce high cluster purities. Once a combination with one group-level component from each group that produces the highest cluster purity has been identified, group-level components with similar networks in opposite groups for each component in this combination are identified using spatial correlation. The software

combines components with similar networks (i.e. spatial distributions) and determines cluster purity once more, per network, to evaluate separation between groups based upon these networks. The current version of gMedICA has been written in MATLAB version 2014a but tested with the 2016 version as well. It runs on a UNIX platform (although, it can run on Windows platform with some modifications, which will be forthcoming in the future) and takes advantage of multi-processor environments for faster processing.

The brain regions involved in the most reproducible components in the three groups, i.e. P^x, C^x and S^x, are frontal regions including the dorsolateral prefrontal cortex and medial prefrontal cortex, the caudate and inferior parietal lobe. These regions are generally known to be involved in executive control. Furthermore, t-tests indicated that these networks were the strongest in controls, weaker in PTSD, and the weakest in PTSD + PCS. This observation is in agreement with the fact that brain regions involved in executive control are impaired in these disorders [22] [23] [24] [25]. PTSD + PCS appears to be more extreme than PTSD, mirroring prior findings [23]. The functional connectivity patterns were comparable in general to previous studies [123] [124] [125]. Specifically, they are in agreement with previous studies which implicate the prefrontal cortex [26] [27] [28] [29], parietal lobe [30] [31] [32] [33], and caudate [34] [35] [36] [37] in these disorders.

We now point out some technical limitations of the current version of gMedICA. This version has been developed in MATLAB 2014a and 2016, and is not standalone in its current shape and form. It also has dependencies on pre-processing software such as DPARSF, FSL, SPM, and REST. Even though these software are provided as a part of the gMedICA package, technical and performance impediments in these software, such as processing times, unavoidably affect the overall performance of gMedICA. The current version has been limited to the evaluation of up to

three groups, as illustrated in our example application described in this paper. This and other limitations will be reviewed in future versions and, hopefully, mitigated.

CHAPTER 5

Conclusion

The main purpose of this study was to investigate brain network alterations in heterogeneous mental (neurological, psychiatric) disorders such as Autism, PTSD and PCS. Not only did we apply a novel approach to accomplish this goal, but also produced a software package that implements our methodology.

We can summarize the main contributions of this work as follows:

i. We hypothesized that functional brain networks that are most reproducible within patients and healthy controls separately, but not when the groups are merged, may possess the ability to distinguish effectively between the groups. We then proposed a methodology based upon the assessment of the reproducibility of independent components obtained from resting state fMRI followed by a clustering analysis of these components to evaluate their ability to discriminate between groups. We demonstrated that the aforementioned networks were successfully able to distinguish between patients with a heterogeneous neurological disorder and healthy controls.

ii. We presented a self-organizing map (SOM) based approach to visualize high-dimension subject population and its ability to display separation between the groups based upon clustering analysis of the population. The approach has been demonstrated in chapter 3

where not many intuitive ways existed to visualize a large subject sample in the feature space.

iii. We produced a software package, gMedICA, which implements our methodology to examine the reproducibility of independent components obtained from resting state fMRI followed by a clustering analysis of these components to evaluate their ability to discriminate between groups. This package provides a graphical user interface (GUI) accepting group imaging data. It then pre-, para-, and post-processes the data producing results for the users, automating our proposed work flow, and minimizing user effort.

iv. We demonstrated the power and utility of our approach through this software package, gMedICA, by applying it to a subject population comprised PTSD, PCS and healthy controls. We include results of this analysis in this dissertation.

CHAPTER 6

Information on Published and Submitted Papers

6.1 Peer-reviewed *Journal* Publications

Accepted:

i. *Mohammed A. Syed,* Zhi Yang, Xiaoping Hu and Gopikrishna Deshpande, *"Investigating Brain Connectomic Alterations in Autism using the Reproducibility of Independent Components derived from Resting State functional MRI Data",* Frontiers in Neuroscience, 2017

Under construction:

ii. *Mohammed Syed,* D Rangaprakash, Xiaoping Hu Michael N. Dretsch, Thomas S. Denney Jr., Jeffrey S. Katz and Gopikrishna Deshpande, "*Investigating Brain Connectomic Alterations in PTSD and PCS using the Reproducibility of Independent Components obtained from Resting State Functional MRI Data*"

6.2 Peer-reviewed *Conference* Proceedings (Published)

i. *Mohammed Syed*, Zhi Yang, and Gopikrishna Deshpande, "*Investigating Brain Connectomic Alterations in Autism using Reproducibility of Independent Components derived from Resting State fMRI*", Proceedings of the Annual Meeting of the International Society for Magnetic Resonance in Medicine, ISMRM 2015, Toronto, ON, Canada, May 2015

ii. *Mohammed Syed,* D Rangaprakash, Xiaoping Hu**,** Michael N. Dretsch, Thomas S. Denney Jr., Jeffrey S. Katz and Gopikrishna Deshpande, "*Investigating Brain Connectomic Alterations in PTSD and PCS using the Reproducibility of Independent Components obtained from Resting State Functional MRI Data",* Proceedings of the Annual Meeting of the International Society for Magnetic Resonance in Medicine, ISMRM 2017, Hawaii, HI, U. S. A., April 2017

6.3 Author Contributions

Author Abbreviations:

M. S.	Mohammed Syed
Z. Y.	Zhi Yang
G. D.	Gopikrishna Deshpande
S. B.	Sanjeev Baskiyar
X. H.	Xiaoping Hu
T. S. D.	Thomas S Denney Jr.
D. R.	D Rangaprakash
M. N. D.	Michael N Dretsch
J. S. K.	Jeffrey S Katz

Contributions:

PTSD Project Conceptualization:	G. D., M. N. D., T. S. D. and J. S. K.
Funding Acquisition:	S. B., T. S. D., M. N. D. and G. D.
Data Acquisition:	T. A. D. and G. D.
Resting-state fMRI Data Pre-processing:	**M. S.** and D. R.
Imaging Data Analysis Methodology:	G. D., Z. Y., X. H. and **M. S.**
Resting-state fMRI Data Analysis:	**M. S.**
Investigation:	**M. S.** and G. D.
Primary Manuscript Preparation:	**M. S.**
Writing:	**M. S.**, G. D., Z. Y., X. H., T. S. D., D. R., M. N. D. and J. S. K.
Resources:	G. D. and Z. Y.
Supervision:	G. D.

REFERENCES

[1] B. Casey, J. Cohen, D. Noll, W. Schneider, J. Giedd and J. Rapoport, "Functional Magnetic Resonance Imaging," in *Neuroimaging II*, Springer, 1996, pp. 299-300.

[2] J. Sanders and W. Orrison, "Functional Magnetic Resonance Imaging," in *Functional Brain Imaging*, 1995.

[3] P. Matthews and P. Jezzard, "Functional magnetic resonance imaging," *Journal of Neurology, Neurosurgery & Psychiatry* , vol. 75, pp. 6-12, 2004.

[4] J. Binder, A. Frost, T. Hammeke, R. Cox, S. Rao and T. Prieto, "Human Brain Language Areas Identified by Functional Magnetic Resonance Imaging," *Journal of Neuroscience*, vol. 17, no. 1, pp. 353-362, 1997.

[5] S. Rao, J. Binder, P. Bandettini, T. Hammeke, F. Yetkin, A. Jesmanowicz, L. Lisk, G. Morris, W. Mueller, L. Estkowski, E. Wong, V. Haughton and J. Hyde, "Functional magnetic resonance imaging of complex human movements," *Neurology*, vol. 43, no. 11, 1993.

[6] S. Ogawa, D. Tank, R. Menon, J. Ellermann, S. Kim, H. Merkle and K. Ugurbil, "Intrinsic signal changes accompanying sensory stimulation: Functional brain mapping with magnetic resonance imaging," *Proceedings of National Academy of Sciences of U.S.A.*, vol. 89, no. 13, p. 5951–5955, 1992.

[7] D. Kapogiannis, G. Deshpande, F. Krueger, M. Thornburg and J. Grafman, "Brain networks shaping religious belief.," *Brain Connectivity*, vol. 4, no. 1, pp. 70-79, 2014.

[8] H. Jia, O. Pustovyy, Y. Wang, P. Waggoner, R. Beyers, J. Schumacher, C. Wildey, E. Morrison, N. Salibi, T. Denney, V. Vodyanoy and G. Deshpande, "Enhancement of Odor-Induced Activity in the Canine Brain by Zinc Nanoparticles: A Functional MRI Study in Fully Unrestrained Conscious Dogs.," *Chem Senses*, vol. 41, no. 1, pp. 53-67, 2016.

[9] K. Lv, Y. Fan, L. Xu and M. Xu, "Brain changes detected by functional magnetic resonance imaging and spectroscopy in patients with Crohn's disease.," *World journal of Gastroenterology*, vol. 23, no. 20, pp. 3607-3614, 2017.

[10] M. Dreyfuss, M. Riegel, G. Pedersen, A. Cohen, M. Silverman, J. Dyke, L. Mayer, B. Walsh, B. Casey and B. AI, "Patients with bulimia nervosa do not show typical neurodevelopment of cognitive control under emotional influences.," *Psychiatry research*, vol. 266, pp. 59-65, 2017.

[11] N. Hubbard, Y. Sanchez Araujo, C. Caballero, M. Ouyang, M. Turner, L. Himes, F. S, B. Thomas, J. Hart, H. Huang, D. Okuda and B. Rypma, "Evaluation of Visual-Evoked Cerebral Metabolic Rate of Oxygen as a Diagnostic Marker in Multiple Sclerosis.," *Brain Sciences*, vol. 7, no. 6, 2017.

[12] C. Jin, H. Jia, P. Lanka, D. Rangaprakash, L. Li, T. Liu, X. Hu and G. Deshpande, "Dynamic brain connectivity is a better predictor of PTSD than static connectivity," *Human Brain Mapping*, 2017.

[13] D. Rangaprakash, G. Deshpande, T. Daniel, A. Goodman, J. Robinson, N. Salibi, J. Katz, T. J. Denney and M. Dretsch, "Compromised hippocampus-striatum pathway as a potential imaging biomarker of mild-traumatic brain injury and posttraumatic stress disorder.," *Human Brain Mapping,* vol. 38, no. 6, pp. 2843-2864, 2017.

[14] R. Emerson, C. Adams, T. Nishino, H. Hazlett, J. Wolff, L. Zwaigenbaum, J. Constantino, M. Shen, M. Swanson, J. Elison, S. Kandala, A. Estes, K. Botteron, L. Collins, S. Dager, A. Evans, G. Gerig, H. Gu, R. McKinstry and S. Paterson, "Functional neuroimaging of high-risk 6-month-old infants predicts a diagnosis of autism at 24 months of age," *Science translational medicine,* vol. 9, no. 393, 2017.

[15] A. Retico, S. Arezzini, P. Bosco, S. Calderoni, A. Ciampa, S. Coscetti, S. Cuomo, L. De Santis, D. Fabiani, M. Fantacci, A. Giuliano, E. Mazzoni, P. Mercatali, G. Miscali, M. Pardini, M. Prosperi, F. Romano, E. Tamburini, M. Tosetti and F. Muratori, "ARIANNA: A research environment for neuroimaging studies in autism spectrum disorders.," *Computers in biology and medicine,* vol. 87, pp. 1-7, 2017.

[16] M. Failla, E. Moana-Filho, G. Essick, G. Baranek, B. Rogers and C. Cascio, "Initially intact neural responses to pain in autism are diminished during sustained pain.," *Autism,* 2017.

[17] X. Gu, T. Zhou, E. Anagnostou, L. Soorya, A. Kolevzon, P. Hof and J. Fan, "Heightened brain response to pain anticipation in high-functioning adults with autism spectrum disorder.," *The European Journal of Neuroscience,* 2017.

[18] M. Assaf, K. Jagannathan, V. Calhoun, L. Miller, M. Stevens, R. Sahl, J. O'Boyle, R. Schultz and G. Pearlson, "Abnormal functional connectivity of default mode sub-networks in autism spectrum disorder patients," *Neuroimage,* vol. 53, no. 1, Oct 2010.

[19] D. Kennedy and E. Courchesne, "Functional abnormalities of the default network during self- and other-reflection in autism," *Social Cognitive and Affective Neuroscience,* vol. 3, no. 2, pp. 177-190, 2008.

[20] H. Chien, S. Gau and I. W. Tseng, "Deficient visuospatial working memory functions and neural correlates of the default-mode network in adolescents with autism spectrum disorder," *Autism Research,* vol. 9, no. 10, p. 1058–1072 , 2016.

[21] Y. F, M. H, H. O, K. M, H. I and T. I, "Default mode network abnormalities in children with autism spectrum disorder detected by resting-state functional magnetic resonance imaging," *The Journal of Medical Investigation,* vol. 63, pp. 204-208, 2016.

[22] M. Kennis, A. Rademaker, S. van Rooij, R. Kahn and E. Geuze, "Resting state functional connectivity of the anterior cingulate cortex in veterans with and without post-traumatic stress disorder," *Human Brain Mapping,* vol. 36, no. 1, pp. 99-109, 2015.

[23] D. Rangaprakash, G. Deshpande, T. Daniel, A. Goodman, J. Robinson, N. Salibi, J. Katz, T. Denney and M. Dretsch, "Compromised Hippocampus-Striatum Pathway as a Potential Imaging Biomarker of Mild Traumatic Brain Injury and Posttraumatic Stress Disorder," *Human Brain Mapping,* 2017.

[24] R. Pitman, A. Rasmusson, K. Koenen, L. Shin, S. Orr, M. Gilbertson, M. Milad and I. Liberzon, "Biological studies of post-traumatic stress disorder," *National Reviews Neuroscience,* vol. 13, no. 11, pp. 769-87, 2012.

[25] L. Shin and I. Liberzon, "The neurocircuitry of fear, stress, and anxiety disorders," *Neuropsychopharmacology,* vol. 35, no. 1, pp. 169-91, 2010.

[26] K. Wrocklage, L. Averill, S. J. Cobb, C. Averill, B. Schweinsburg, M. Trejo, A. Roy, V. Weisser, C. Kelly, B. Martini, I. Harpaz-Rotem, S. Southwick, J. Krystal and C. Abdallah, "Cortical thickness reduction in combat exposed U.S. veterans with and without PTSD," *European Neuropsychopharmacology,* 2017.

[27] D. Ross, M. Arbuckle, M. Travis, J. Dwyer, G. van Schalkwyk and K. Ressler, "An Integrated Neuroscience Perspective on Formulation and Treatment Planning for Posttraumatic Stress Disorder: An Educational Review," *JAMA Psychiatry,* 2017.

[28] G. Young, "PTSD in Court II: Risk factors, endophenotypes, and biological underpinnings in PTSD," *International Journal of Law and Psychiatry,* 2017.

[29] C. Abdallah, K. Wrocklage, C. Averill, T. Akiki, B. Schweinsburg, A. Roy, B. Martini, S. Southwick, J. Krystal and J. Scott, "Anterior hippocampal dysconnectivity in posttraumatic stress disorder: a dimensional and multimodal approach," *Translational Psychiatry,* 2017.

[30] Y. Zhang, B. Xie, H. Chen, M. Li, X. Guo and H. Chen, "Disrupted resting-state insular subregions functional connectivity in post-traumatic stress disorder," *Medicine,* vol. 95, no. 27, 2016.

[31] L. Yang, L. Baojuan, F. Na, P. Huangsheng, Z. Xi, L. Hongbing and Y. Hong, "Perfusion Deficits and Functional Connectivity Alterations in Memory-Related Regions of Patients with Post-Traumatic Stress Disorder," *PLoS One,* vol. 11, no. 5, 2016.

[32] Y. Zhang, B. Xie, H. Chen, M. Li, F. Liu and H. Chen, "Abnormal Functional Connectivity Density in Post-traumatic Stress Disorder," *Brain Topography,* vol. 29, no. 3, pp. 405-11, 2016.

[33] J. DiGangi, A. Tadayyon, D. Fitzgerald, C. Rabinak, A. Kennedy, H. Klumpp, S. Rauch and K. Phan, "Reduced default mode network connectivity following combat trauma," *Neuroscience Letters,* vol. 615, pp. 37-43, 2016.

[34] D. Waltzman, S. Soman, N. Hantke, J. Fairchild, L. Kinoshita, M. Wintermark, J. Ashford, J. Yesavage, L. Williams, M. Adamson and A. Furst, "Altered Microstructural Caudate Integrity in Posttraumatic Stress Disorder but Not Traumatic Brain Injury," *PLoS One,* vol. 12, no. 1, 2017.

[35] A. Kaczkurkin, P. Burton, S. Chazin, A. Manbeck, T. Espensen-Sturges, S. Cooper, S. Sponheim and S. Lissek, "Neural Substrates of Overgeneralized Conditioned Fear in PTSD," *The American Journal of Psychiatry,* vol. 174, no. 2, pp. 125-34, 2017.

[36] E. Choi, Y. Tanimura, P. Vage, E. Yates and S. Haber, "Convergence of prefrontal and parietal anatomical projections in a connectional hub in the striatum," *Neuroimage,* vol. 146, pp. 821-32, 2017.

[37] D. Sussman, E. Pang, R. Jetly, B. Dunkley and M. Taylor, "Neuroanatomical features in soldiers with post-traumatic stress disorder," *BMC Neuroscience,* vol. 17, 2016.

[38] J. Anderson, J. Nielsen, A. Froehlich, M. DuBray, T. Druzgal, A. Cariello, J. Cooperrider, B. Zielinski, C. Ravichandran, P. Fletcher, A. Alexander, E. Bigler, N. Lange and J. Lainhart, "Functional connectivity magnetic resonance imaging classification of Autism," *Brain: A Journal of Neurology,* vol. 134, Dec 2011.

[39] M. Plitt, A. Kelly and A. Martina, "Functional connectivity classification of autism identifies highly predictive brain features but falls short of biomarker standards," *Neuroimage: Clinical,* vol. 7, p. 359–366, 2015.

[40] A. Bell and T. Sejnowski, "An Information-Maximization Approach to Blind Separation and Blind Deconvolution," *Neural Computation,* vol. 7, no. 6, pp. 1129-1159, Nov 1995.

[41] H. E. von dem, R. Stoyanova, S. Baron-Cohen and A. Calder, "Reduced functional connectivity within and between 'social' resting state networks in autism spectrum conditions," *Social Cognitive and Affective Neuroscience,* vol. 8, no. 6, Aug 2013.

[42] M. Greicius, B. Krasnow, A. Reiss and V. Menon, "Functional connectivity in the resting brain: A network analysis of the default mode hypothesis," *Proceedings of the National Academy of Sciences (PNAS),* vol. 100, no. 1, Jan 2003.

[43] Z. Yang, X. Zuo, P. Wang, Z. Li, S. LaConte, P. Bandettini and X. Hu, "Generalized RAICAR: discover homogeneous subject (sub)groups by reproducibility of their intrinsic connectivity networks," *Neuroimage,* vol. 63, no. 1, 2012.

[44] J. Pluim, J. Maintz and M. Viergever, "Mutual-information-based registration of medical images: a survey," *IEEE Trans. Med. Imaging,* vol. 22, no. 8, pp. 986-1004, 2003.

[45] F. Maes, A. Collignon, D. Vandermeulen, G. Marchal and P. Suetens, "Multimodality image registration by maximization of mutual information," *IEEE Trans. Med. Imaging,* vol. 16, no. 2, pp. 187-198, 1997.

[46] A. Kraskov, H. Stogbauer and P. Grassberger, "Estimating mutual information," *Physical Review - statistical, nonlinear, and soft matter physics,* June 2004.

[47] American Psychiatric Association, Diagnostic and Statistical Manual of Mental Disorders, Arlington, VA: American Psychiatric Publishing, 2013.

[48] M. Wingate, B. Mulvihill , R. S. Kirby, S. Pettygrove, C. Cunniff, F. Meaney, E. Schulz, L. Miller, C. Robinson, G. Quintana, M. Y. Kaiser, L. C. Lee, R. Landa, C. Newschaffer, J. Constantino, R. Fitzgerald, W. Zahorodny, J. Daniels, E. Giarelli, J. Pinto-Martin, S. E. Levy, J. Nicholas, J. Charles, J. Zimmerman, M. J. Maenner, M. Durkin, C. Rice, J. Baio, K. Van Naarden Braun , K. Phillips, N. Doernberg and M. Yeargin-Allsopp, "Prevalence of autism spectrum disorders--Autism and Developmental Disabilities Monitoring Network, 14 sites, United States, 2008," *Morbidity and Mortality Weekly Report,* vol. 61, no. 3, pp. 1-19, 30 March 2012.

[49] J. Baio, "Prevalence of Autism Spectrum Disorder Among Children Aged 8 Years - Autism and Developmental Disabilities Monitoring Network, 11 Sites, United States, 2010," *Morbidity and Mortality Weekly Report (MMWR),* vol. 63, pp. 1-21, 2014.

[50] R. Muhle , S. V. Trentacoste and I. Rapin , "The genetics of Autism," *Pediatrics,* vol. 113, no. 5, 2004.

[51] S. Ozonoff, G. S. Young , A. Carter , D. Messinger , N. Yirmiya, L. Zwaigenbaum, S. Bryson, L. J. Carver , J. N. Constantino , K. Dobkins, T. Hutman, J. M. Iverson, R. Landa, S. J. Rogers, M. Sigman and W. L. Stone, "Recurrence risk for autism spectrum disorders: a Baby Siblings Research Consortium study," *Pediatrics,* vol. 128, no. 3, Sep 2011.

[52] C. Ecker, A. Marquand, J. Mourão-Miranda, P. Johnston , E. M. Daly, M. J. Brammer, S. Maltezos, C. M. Murphy, D. Robertson, S. C. Williams and D. G. Murphy, "Describing the brain in autism in five dimensions--magnetic resonance imaging-assisted diagnosis of autism spectrum disorder using a multiparameter classification approach," *The Journal of Neuroscience,* vol. 30, no. 32, Aug 2010.

[53] Y. Jiao, R. Chen, X. Ke, K. Chu, Z. Lu and E. H. Herskovits, "Predictive models of autism spectrum disorder based on brain regional cortical thickness," *Neuroimage,* vol. 50, no. 2, April 2010.

[54] L. Q. Uddin, V. Menon, C. B. Young, S. Ryali, T. Chen, T. Khouzam, N. J. Minshew and A. Y. Hardan, "Multivariate searchlight classification of structural magnetic resonance imaging in children and adolescents with autism," *Biological Psychiatry,* vol. 70, no. 9, Nov 2011.

[55] S. Calderoni, A. Retico, L. Biagi, R. Tancredi, F. Muratori and M. Tosetti, "Female children with autism spectrum disorder: an insight from mass-univariate and pattern classification analyses," *Neuroimage,* vol. 59, no. 2, Jan 2012.

[56] J. R. Sato, M. Q. Hoexter, P. P. Oliveira, M. J. Brammer, MRC AIMS Consortium, C. Murphy and D. Ecker, "Inter-regional cortical thickness correlations are associated with autistic symptoms: a machine-learning approach," *Journal of Psychiatric Research,* vol. 47, no. 4, Apr 2013.

[57] L. Libero, T. DeRamus, A. Lahti, G. Deshpande and R. Kana, "Multimodal neuroimaging based classification of Autism Spectrum Disorder using anatomical, neurochemical and white matter correlates," *Cortex,* vol. 66, pp. 46-59, 2015.

[58] M. Coutanche, S. Thompson-Schill and R. Schultz, "Multi-voxel pattern analysis of fMRI data predicts clinical symptom severity," *Neuroimage,* vol. 57, no. 1, Jul 2011.

[59] H. Wang, C. Chen and H. Fushing, "Extracting multiscale pattern information of fMRI based functional brain connectivity with application on classification of autism spectrum disorders," *PLoS One,* vol. 7, no. 10, 2012.

[60] G. Deshpande, L. Libero, K. Sreenivasan, H. Deshpande and R. Kana, "Identification of neural connectivity signatures of autism using machine learning," *Frontiers in Human Neuroscience,* Oct 2013.

[61] J. Nielsen, B. Zielinski, P. Fletcher, A. Alexander, N. Lange, E. Bigler, J. Lainhart and J. Anderson, "Multisite functional connectivity MRI classification of autism: ABIDE results," *Frontiers in Human Neuroscience,* Sep 2013.

[62] J. Maximo, C. Keown, A. Nair and R. Müller, "Approaches to local connectivity in autism using resting state functional connectivity MRI," *Frontiers in Human Neuroscience,* Oct 2013.

[63] K. Supekar, L. Uddin, A. Khouzam, J. Phillips, W. Gaillard, L. Kenworthy, B. Yerys, C. Vaidya and V. Menon, "Brain hyper-connectivity in children with autism and its links to social deficits," *Cell Reports,* vol. 5, no. 3, p. 738–747, 2013.

[64] Z. Yang, X. Zuo, P. Wang, Z. Li, S. LaConte, P. Bandettini and X. Hu, "Generalized RAICAR: discover homogeneous subject (sub)groups by reproducibility of their intrinsic connectivity networks," *Neuroimage,* vol. 63, no. 1, Oct 2012.

[65] Z. Yang, S. LaConte, X. Weng and X. Hu, "Ranking and averaging independent component analysis by reproducibility (RAICAR)," *Human Brain Mapping,* vol. 29, no. 6, Jun 2008.

[66] Z. Yang, C. Chang, T. Xu, L. Jiang, D. Handwerker, F. Castellanos, M. Milham, P. Bandettini and X. Zuo, "Connectivity trajectory across lifespan differentiates the precuneus from the default network," *NeuroImage,* vol. 89, pp. 45-56, Apr 2014.

[67] Z. Yang, Y. Xu, T. Xu, C. Hoy, D. Handwerker, G. Chen, G. Northoff, X. Zuo and P. Bandettini, "Brain network informed subject community detection in early-onset schizophrenia," *Scientific Reports,* Jul 2014.

[68] A. Di Martino, C. Yan, Q. Li, E. Denio, F. Castellanos, K. Alaerts, J. Anderson, M. Assaf, S. Bookheimer, M. Dapretto, B. Deen, S. Delmonte, I. Dinstein, B. Ertl-Wagner, D. Fair, L. Gallagher, D. Kennedy, C. Keown, C. Keysers, J. Lainhart, C. Lord, B. Luna, V. Menon and Mi, "The autism brain imaging data exchange: towards a large-scale evaluation of the intrinsic brain architecture in autism," *Molecular Psychiatry,* vol. 19, no. 6, Jun 2014.

[69] C. Yan and Y. Zang, "DPARSF: A MATLAB Toolbox for "Pipeline" Data Analysis of Resting-State fMRI," *Frontiers in Systems Neuroscience,* vol. 4, no. 13, May 2010.

[70] X. Song, Z. Dong, X. Long, S. Li, X. Zuo, C. Zhu, Y. He, C. Yan and Y. Zang, "REST: a toolkit for resting-state functional magnetic resonance imaging data processing," *PLoS One,* vol. 6, no. 9, 2011.

[71] M. Jenkinson, C. Beckmann, T. Behrens, M. Woolrich and S. Smith, "the FMRIB Software Library (FSL)," *Neuroimage,* vol. 62, no. 2, pp. 782-90, Aug 2012.

[72] M. Woolrich, S. Jbabdi, B. Patenaude, M. Chappell, S. Makni, T. Behrens, C. Beckmann, M. Jenkinson and S. Smith, "Bayesian analysis of neuroimaging data in FSL," *Neuroimage,* vol. 45, no. 1 Suppl, Mar 2009.

[73] C. Beckman and S. Smith, "Probabilistic Independent Component Analysis," *IEEE Transactions on Medical Imaging,* vol. 23, pp. 137-52, 2004.

[74] C. Beckman, M. DeLuca, J. Devlin and S. Smith, "Investigations into resting-state connectivity using independent component analysis," *Philosophical Transactions of the Royal Society,* vol. 360, no. 1457, May 2005.

[75] E. Allen, E. Damaraju, S. Plis, E. Erhardt, T. Eichele and V. Calhoun, "Tracking whole-brain connectivity dynamics in the resting state," *Cerebral Cortex,* vol. 24, no. 3, pp. 663-76, 2014.

[76] W. Liu, S. Awate and P. Fletcher, "Group Analysis of Resting-State fMRI by Hierarchical Markov Random Fields," in *Medical Image Computing and Computer-Assisted Intervention - Lecturer Notes in Computer Science*, Nice, 2012.

[77] S. Zhang and C. Li, "Functional connectivity mapping of the human precuneus by resting state fMRI," *NeuroImage,* vol. 59, no. 4, p. 3548–3562, Feb 2012.

[78] T. Kohonen, Self-Organization and Associative Memory, vol. 8, Springer-Verlag, 1988.

[79] T. Kohonen, Self-Organizing Maps, 3rd ed., Springer-Verlag, 2001.

[80] K. Chantiluke, N. Barrett, V. Giampietro, P. Santosh, M. Brammer, A. Simmons, D. Murphy and K. Rubia, "Inverse fluoxetine effects on inhibitory brain activation in non-comorbid boys with ADHD and with ASD," *Psychopharmacology,* 2014.

[81] P. Chiu, M. Kayali, K. Kishida, D. Tomlin, L. Klinger, M. Klinger and P. Montague, "Self responses along cingulate cortex reveal quantitative neural phenotype for high-functioning autism.," *Neuron,* vol. 57, no. 3, p. 463–473, 2008.

[82] J. Kestemont, N. Ma, K. Baetens, N. Clément, F. Van Overwalle and M. Vandekerckhove, "Neural correlates of attributing causes to the self, another person and the situation," *Social Cognitive and Affective Neuroscience,* vol. 10, no. 1, pp. 114-121, 2014.

[83] M. Nebel, A. Eloyan, A. Barber and S. Mostofsky, "Precentral gyrus functional connectivity signatures of autism.," *Frontiers in Systems Neuroscience,* vol. 8, 2014.

[84] A. Bell and T. Sejnowski, "An Information Maximization Approach to Blind Separation and Blind Deconvolution," *Neural Computation,* vol. 7, no. 6, pp. 1129-1159, 1995.

[85] E. von dem Hagen, R. Stoyanova, S. Baron-Cohen and A. Calder, "Reduced functional connectivity within and between 'social' resting state networks in autism spectrum conditions," *Social Cognitive and Affective Neuroscience,* vol. 8, no. 6, pp. 694-701, 2012.

[86] M. Greicius, B. Krasnow, A. Reiss and V. Menon, "Functional connectivity in the resting brain: A network analysis of the default mode hypothesis," *Proceedings of the National Academy of Sciences (PNAS),* vol. 100, no. 1, Jan 2003.

[87] M. Assaf, K. Jagannathan, V. Calhoun, L. Miller, M. Stevens, R. Sahl, J. O'Boyle, R. Schultz and G. Pearlson, "Abnormal functional connectivity of default mode sub-networks in autism spectrum disorder patients," *Neuroimage,* vol. 53, no. 1, Oct 2010.

[88] D. von Rhein, C. Beckmann, B. Franke, J. Oosterlaan, D. Heslenfeld, P. Hoekstra, C. Hartman, M. Luman, S. Faraone, R. Cools, J. Buitelaar and M. Mennes, "Network-level assessment of reward-related activation in patients with ADHD and healthy individuals," *Human Brain Mapping,* 2017.

[89] R. Patriat, R. Birn, T. Keding and R. Herringa, "Default-Mode Network Abnormalities in Pediatric Posttraumatic Stress Disorder," *Journal of the American Academy of Child and Adolescent Psychiatry,* vol. 55, no. 4, pp. 319-327, April 2016.

[90] J. Shang, S. Lui, Y. Meng, H. Zhu, C. Qiu, Q. Gong, W. Liao and W. Zhang, "Alterations in Low-Level Perceptual Networks Related to Clinical Severity in PTSD after an Earthquake: A Resting-State fMRI Study," *PLoS One,* vol. 9, no. 5, May 2014.

[91] J. Thome, P. Frewen, J. Daniels, M. Densmore and R. Lanius, "Altered connectivity within the salience network during direct eye gaze in PTSD," *Borderline Personality Disorder and Emotion Dysregulation,* November 2014.

[92] I. Shu, J. Onton, N. Prabhakar, R. O'Connell, A. Simmons and S. Matthews, "Combat veterans with PTSD after mild TBI exhibit greater ERPs from posterior-medial cortical areas while appraising facial features," *Journal of Affective Disorders,* vol. 155, pp. 234-240, February 2014.

[93] J. Cisler, S. J. Scott, S. Smitherman, J. Lenow and C. Kilts, "Neural processing correlates of assaultive violence exposure and PTSD symptoms during implicit threat processing: a network-level analysis among adolescent girls," *Psychiatry Research,* vol. 214, no. 3, pp. 238-246, December 2013.

[94] J. Schulz, M. Cookson and L. Hausmann, "The impact of fraudulent and irreproducible data to the translational research crisis – solutions and implementation," *Journal of Neurochemistry,* vol. 139, no. S2, pp. 253-70, 2016.

[95] M. Macleod, S. Michie, I. Roberts, U. Dirnagl, I. Chalmers, J. Ioannidis, R. Salman, A. Chan and P. Glasziou, "Biomedical research: increasing value, reducing waste," *The Lancet,* vol. 383, no. 9912, pp. 101-4, 2014.

[96] M. Baker, "1,500 scientists lift the lid on reproducibility," *Nature,* vol. 533, no. 7604, pp. 452-4, 2016.

[97] I. Chalmers and P. Glasziou, "Avoidable waste in the production and reporting of research evidence," *The Lancet,* vol. 374, pp. 86-9, 2009.

[98] D. Moher, P. Glasziou, I. Chalmers, M. Nasser, P. Bossuyt, D. Korevaar, I. Graham, P. Ravaud and I. Boutron, "Increasing value and reducing waste in biomedical research: who's listening?," *The Lancet,* vol. 387, pp. 1573-86, 2016.

[99] K. Gorgolewski and R. Poldrack, "A Practical Guide for Improving Transparency and Reproducibility in Neuroimaging Research," *PLoS Biology,* vol. 14, no. 7, 2016.

[100] Z. Yang, S. LaConte, X. Weng and X. Hu, "Ranking and averaging independent component analysis by reproducibility (RAICAR)," *Human Brain Mapping,* vol. 29, no. 6, June 2008.

[101] Z. Yang, Y. Xu, T. Xu, C. Hoy, D. Handwerker, G. Chen, G. Northoff, X. Zuo and P. Bandettini, "Brain network informed subject community detection in early-onset schizophrenia," 2014.

[102] Z. Yang, C. Chang, T. Xu, L. Jiang, D. Handwerker, F. Castellanos, M. Milham, P. Bandettini and X. Zuo, "Connectivity trajectory across lifespan differentiates the precuneus from the default network," *Neuroimage,* vol. 89, pp. 45-56, 2014.

[103] K. Adams, P. Hester, J. Bradley, T. Meyers and C. Keating, "Systems Theory as the Foundation for Understanding Systems," *Systems Engineering,* vol. 17, no. 1, pp. 112-123, May 2013.

[104] C. Yan and Y. Zang, "DPARSF: A MATLAB Toolbox for Pipeline Data Analysis of Resting-State fMRI," *Frontiers in Systems Neuroscience,* vol. 4, no. 13, May 2010.

[105] X. Song, Z. Dong, X. Long, S. Li, X. Zuo, C. Zhu, Y. He, C. Yan and Y. Zang, "REST: a toolkit for resting-state functional magnetic resonance imaging data processing," *PLoS One,* vol. 6, no. 9, 2011.

[106] M. Jenkinson, C. Beckmann, T. Behrens, M. Woolrich and S. Smith, "the FMRIB Software Library (FSL)," *Neuroimage,* vol. 62, no. 2, pp. 782-90, August 2012.

[107] M. Woolrich, S. Jbabdi, B. Patenaude, M. Chappell, S. Makni, T. Behrens, C. Beckmann, M. Jenkinson and S. Smith, "Bayesian analysis of neuroimaging data in FSL," *Neuroimage,* vol. 45, no. 1 Suppl, March 2009.

[108] C. Beckman and S. Smith, "Probabilistic Independent Component Analysis," *IEEE Transactions on Medical Imaging,* vol. 23, pp. 137-52, 2004.

[109] C. Beckman, M. DeLuca, J. Devlin and S. Smith, "Investigations into resting-state connectivity using independent component analysis," *Philosophical Transactions of the Royal Society,* vol. 360, no. 1457, May 2005.

[110] S. Wold, "Principal component analysis," *Chemometrics and Intelligent Laboratory Systems,* vol. 2, no. 1-3, pp. 37-52, 1987.

[111] S. Zhang and C. Li, "Functional connectivity mapping of the human precuneus by resting state fMRI," *NeuroImage,* vol. 59, no. 4, pp. 3548-3562, Feb 2012.

[112] W. Liu, S. Awate and P. Fletcher, "Group Analysis of Resting-State fMRI by Hierarchical Markov Random Fields," *Medical Image Computing and Computer-Assisted Intervention - Lecturer Notes in Computer Science,* 2012.

[113] E. Allen, E. Damaraju, S. Plis, E. Erhardt, T. Eichele and V. Calhoun, "Tracking whole-brain connectivity dynamics in the resting state," *Cerebral Cortex,* vol. 24, no. 3, pp. 663-76, 2014.

[114] A. P. Association, Diagnostic and Statistical Manual of Mental Disorders: DSM IV, 4 ed., Washington DC, 1994.

[115] C. Hoge, C. Castro, S. Messer, D. McGurk, D. Cotting and R. Koffman, "Combat duty in Iraq and Afghanistan, mental health problems, and barriers to care," *The New England Journal of Medicine,* vol. 351, pp. 13-22, July 2004.

[116] U. Research Imaging Institute, "Multi-image Analysis GUI," Research Imaging Institute, University of Texas Health Science Center, [Online]. Available: http://rii.uthscsa.edu/mango/mango.html.

[117] N. I. o. M. Health, "Analysis of Functional NeuroImages," NIH, [Online]. Available: https://afni.nimh.nih.gov/.

[118] R. Goebel, "BrainVoyager," Brain Innovation B.V., 2015. [Online]. Available: http://www.brainvoyager.com/products/brainvoyager.html.

[119] A. Abraham, F. Pedregosa, M. Eickenberg, P. Gervais, A. Mueller, J. Kossaifi, A. Gramfort, B. Thirion and G. Varoquaux, "Machine learning for neuroimaging with scikit-learn," *Frontiers in Neuroinformatics,* vol. 8, no. 14, 2014.

[120] V. Calhoun and T. Adali, "Group ICA Of fMRI Toolbox(GIFT)," Medical Image Analysis Lab, [Online]. Available: http://mialab.mrn.org/software/gift/index.html.

[121] S. Whitfield-Gabrieli and A. Nieto-Castanon, "Conn: A functional connectivity toolbox for correlated and anticorrelated brain networks," *Brain Connectivity,* 2012.

[122] X. Chai, A. Nieto-Castanon, D. Ongur and S. Whitfield-Gabrieli, "Anticorrelations in resting state networks without global signal regression," *NeuroImage 59(2):,* vol. 59, no. 2, pp. 1420-1428, 2012.

[123] J. Camchong, A. 3. MacDonald, B. Nelson, C. Bell, B. Mueller, S. Specker and K. Lim, "Frontal hyperconnectivity related to discounting and reversal learning in cocaine subjects," *Biological Psychiatry,* vol. 69, no. 11, pp. 1117-23, 2011.

[124] C. Davey, B. Harrison, M. Yücel and N. Allen, "Regionally specific alterations in functional connectivity of the anterior cingulate cortex in major depressive disorder," *Psychological Medicine,* vol. 42, no. 10, pp. 2071-81, 2012.

[125] A. Kelly, A. Di Martino, L. Uddin, Z. Shehzad, D. Gee, P. Reiss, D. Margulies, F. Castellanos and M. Milham, "Development of anterior cingulate functional connectivity from late childhood to early adulthood," *Cerebral Cortex,* vol. 19, no. 3, pp. 640-57, 2009.

[126] H. Ross and D. Murray, (Ed. and Transl.) E.H.Weber on the tactile senses., 2nd ed., Hove: Erlbaum (UK) Taylor & Francis., 1996.

[127] [Online]. Available: http://www.nitrc.org/projects/bnv/.

[128] Functional Imaging Lab (FIL), The Welcome Trust Centre for NeuroImaging, in the Institute of Neurology at University College London (UCL), UK., [Online]. Available: http://www.fil.ion.ucl.ac.uk/spm/software/spm8/.

[129] B. Ward. [Online]. Available: http://afni.nimh.nih.gov/pub../pub/dist/doc/manual/AlphaSim.pdf.

[130] T. Fletcher and T. Saveraid, "Canine Brain MRI Atlas," [Online]. Available: http://vanat.cvm.umn.edu/mriBrainAtlas/index.html.

[131] R. Fulbright, P. Skudlarski, C. Lacadie, S. Warrenburg, A. Bowers, J. Gore and B. Wexler, "Functional MR imaging of regional brain responses to pleasant and unpleasant odors.," *American Journal of Neuroradiology,* vol. 19, no. 9, pp. 1721-1726, 1998.

[132] G. Berns, A. Brooks and M. Spivak, "Functional MRI in awake unrestrained dogs.," *PLoS One,* vol. 7, no. 5, p. e38027, 2012.

[133] D. Zald and J. Pardo, "Functional neuroimaging of the olfactory system in humans.," *International Journal of Psychophysiology,* vol. 36, no. 2, pp. 165-181, 2000.

[134] T. Kellermann, S. Caspers, P. Fox, K. Zilles, C. Roski, A. Laird, B. Turetsky and S. Eickhoff, "Task- and resting-state functional connectivity of brain regions related to affection and susceptible to concurrent cognitive demand.," *Neuroimage,* vol. 72, pp. 69-82, 2013.

[135] S. Rombouts, F. Barkhof, R. Goekoop, C. Stam and P. Scheltens, "Altered resting state networks in mild cognitive impairment and mild Alzheimer's disease: an fMRI study.," *Human Brain Mapping,* vol. 26, no. 4, pp. 231-239, 2005.

[136] C. Chang, X. Shen and G. Glover, "Behavioral correlates of temporal variations in brain network connectivity.," in *Proceedings of Human Brain Mapping*, 2011.

[137] C. Chang, C. Metzger, G. Glover, J. Duyn, H. Heinze and M. Walter, "Association between heart rate variability and fluctuations in resting-state functional connectivity.," *Neuroimage,* vol. 68, pp. 93-104, 2013.

[138] V. Kiviniemi, T. Vire, J. Remes, A. Elseoud, T. Starck, O. Tervonen and J. Nikkinen, "A sliding time-window ICA reveals spatial variability of the default mode network in time.," *Brain Connectivity,* vol. 1, pp. 339-347, 2011.

[139] J. He, O. Carmichael, E. Fletcher, B. Singh, A. Iosif, O. Martinez, B. Reed, A. Yonelinas and C. Decarli, "Influence of functional connectivity and structural MRI measures on episodic memory.," *Neurobiology of Aging,* vol. 33, no. 11, p. 2612–2620, 2012.

[140] M. Filippi, F. Agosta, E. Scola, E. Canu, G. Magnani, A. Marcone, P. Valsasina, F. Caso, M. Copetti, G. Comi, S. Cappa and A. Falini, "Functional network connectivity in the behavioral variant of frontotemporal dementia.," *Cortex,* vol. 49, no. 9, pp. 2389-2401, 2012.

[141] C. Han, S. Yoo, S. Seo, D. Na and J. Seong, "Cluster-based statistics for brain connectivity in correlation with behavioral measures.," *PLoS One,* vol. 8, no. 8, p. e72332, 2013.

[142] N. Andreasen, D. O'Leary, S. Paradiso, T. Cizadlo, S. Arndt, G. Watkins, L. Ponto and R. Hichwa, "The cerebellum plays a role in conscious episodic memory retrieval.," *Human Brain Mapping,* vol. 8, no. 4, pp. 226-234, 1999.

[143] K. Jimura, M. Chushak and T. Braver, "Impulsivity and self-control during intertemporal decision making linked to the neural dynamics of reward value representation.," *Journal of Neuroscience,* vol. 33, no. 1, pp. 344-357, 2013.

[144] K. Louie and P. Glimcher, "Separating value from choice: delay discounting activity in the lateral intraparietal area.," *Journal of Neuroscience,* vol. 30, no. 16, pp. 5498-5507, 2010.

[145] J. Kinnison, S. Padmala, J. Choi and L. Pessoa, "Network analysis reveals increased integration during emotional and motivational processing.," *Journal of Neuroscience,* vol. 32, no. 24, pp. 8361-8372, 2012.

[146] T. Breckel, C. Thiel, E. Bullmore, A. Zalesky, A. Patel and C. Giessing, "Long-term effects of attentional performance on functional brain network topology.," *PLoS One,* vol. 8, no. 9, p. e74125, 2013.

[147] S. Olbrich, C. Mulert, S. Karch, M. Trenner, G. Leicht, O. Pogarell and U. Hegerl, "EEG-vigilance and BOLD effect during simultaneous EEG/fMRI measurement.," *Neuroimage,* vol. 45, no. 2, pp. 319-332, 2009.

[148] L. Seidman, H. Breiter, J. Goodman, J. Goldstein, P. Woodruff, K. O'Craven, R. Savoy, M. Tsuang and B. Rosen, "A functional magnetic resonance imaging study of auditory vigilance with low and high information processing demands.," *Neuropsychology,* vol. 12, no. 4, pp. 505-518, 1998.

[149] O. Devinsky, M. Morrell and B. Vogt, "Contributions of anterior cingulate cortex to behaviour.," *Brain,* vol. 118, no. 1, pp. 279-306, 1995.

[150] H. Karnath, B. Baier and T. Nägele, "Awareness of the functioning of one's own limbs mediated by the insular cortex?," *Jounal of Neuroscience,* vol. 25, no. 31, pp. 7134-7138, 2005.

[151] T. Ishizu and S. Zeki, "Toward a brain-based theory of beauty.," *PLoS One,* vol. 6, no. 7, p. e21852, 2011.

[152] M. Liljeström, A. Tarkiainen, T. Parviainen, J. Kujala, J. Numminen, J. Hiltunen, M. Laine and R. Salmelin, "Perceiving and naming actions and objects.," *Neuroimage,* vol. 41, no. 3, pp. 1132-1141, 2008.

[153] T. Bliss and G. Collingridge, "A synaptic model of memory: long-term potentiation in the hippocampus.," *Nature,* vol. 361, no. 6407, pp. 31-39, 1993.

[154] J. Bogousslavsky, J. Miklossy, J. Deruaz, G. Assal and F. Regli, "Lingual and fusiform gyri in visual processing: a clinico-pathologic study of superior altitudinal hemianopia.," *Journal of Neurology, Neurosurgery, Psychiatry.,* vol. 50, no. 5, pp. 607-614, 1987.

[155] J. Cisler, J. Steele, J. Lenow, S. Smitherman, B. Everett, E. Messias and C. Kilts, "Functional reorganization of neural networks during repeated exposure to the traumatic memory in posttraumatic stress disorder: an exploratory fMRI study.," *Journal of Psychiatric Research,* vol. 48, no. 1, pp. 47-55, 2014.

[156] K. Moores, C. Clark, A. McFarlane, G. Brown, A. Puce and D. Taylor, "Abnormal recruitment of working memory updating networks during maintenance of trauma-neutral information in post-traumatic stress disorder.," *Psychiatry Research,* vol. 163, no. 2, pp. 156-170, 2008.

[157] A. Kemp, K. Felmingham, E. Falconer, B. Liddell, R. Bryant and L. Williams, "Heterogeneity of non-conscious fear perception in posttraumatic stress disorder as a function of physiological arousal: an fMRI study.," *Psychiatry Research,* vol. 174, no. 2, pp. 158-161, 2009.

[158] M. Shaw, K. Moores, R. Clark, A. McFarlane, S. Strother, R. Bryant, G. Brown and J. Taylor, "Functional connectivity reveals inefficient working memory systems in post-traumatic stress disorder.," *Psychiatry Research,* vol. 172, no. 3, pp. 235-241, 2009.

[159] R. Viviani, G. Grön and M. Spitzer, "Functional principal component analysis of fMRI data.," *Human Brain Mapping,* vol. 24, no. 2, pp. 109-129, 2005.

[160] D. Bassett, N. Wymbs, M. Porter, P. Mucha, J. Carlson and S. Grafton, "Dynamic reconfiguration of human brain networks during learning.," *Proceedings of National Academy of Sciences of U.S.A.*, vol. 108, no. 18, pp. 7641-7646, 2011.

[161] Y. Yeshurun and N. Sobel, "An odor is not worth a thousand words: from multidimensional odors to unidimensional odor objects.," *Annual Review of Psychology,* vol. 61, pp. 219-241, C211-215, 2010.

[162] J. Mainland and N. Sobel, "The sniff is part of the olfactory percept.," *Chemical Senses,* vol. 31, no. 2, pp. 181-196, 2006.

[163] T. Kondoh, S. Yamada, S. Shioda and K. Torii, "Central olfactory pathway in response to olfactory stimulation in rats detected by magnetic resonance imaging.," vol. 30, no. Suppl. 1, pp. i172-i173, 2005.

[164] A. Kruse, "Defense Sciences Research and Technology Special Focus Area: RealNose.," 2007. [Online]. Available: https://www.fbo.gov/index?s=opportunity&mode=form&tab=core&id=32bb6977f45cc0b870f0837f32ad7fcf&_cview=0..

[165] "FreeSurfer," [Online]. Available: http://surfer.nmr.mgh.harvard.edu/.

[166] M. Williams and J. Johnston, "Training and maintaining the performance of dogs (Canis familiaris) on an increasing number of odor discriminations in a controlled setting.," *Applied Animal Behaviour Science,* vol. 78, pp. 55-65, 2002.

[167] K. Ridderinkhof, M. Ullsperger, E. Crone and S. Nieuwenhuis, "The role of the medial frontal cortex in cognitive control.," *Science,* vol. 306, no. 5695, pp. 443-447, 2004.

[168] C. Studzinski, J. Araujo and N. Milgram, "The canine model of human cognitive aging and demintia: pharmacological validity of the model for assessment of human cognitive-enhancing drugs.," *Progress in Neuro-Psychopharmacology & Biological Psychiatry,* vol. 29, pp. 489-498, 2005.

[169] M. Kujala, H. Törnqvist, S. Somppi, L. Hänninen, C. Krause, O. Vainio and J. Kujala, "Reactivity of dogs' brain oscillations to visual stimuli measured with non-invasive electroencephalography.," *PLoS One,* vol. 8, no. 5, p. e61818, 2013.

[170] E. Kandel, J. Schwartz and T. Jessell, Priciples of neural science, 4th ed., New York: McGraw-Hill, 2000.

[171] S. Youngentob, B. Johnson and M. Leon, "Predicting odorant quality from multidimensional scaling of olfactory bulb glomerular activity patterns.," *Behavioral Neuroscience,* vol. 120, no. 6, pp. 1337-1345, 2006.

[172] L. Haberly, "Parallel-distributed processing in olfactory cortex: new insights from morphological and physiological analysis of neuronal circuitry.," *Chemical Senses,* vol. 26, no. 5, pp. 551-576, 2001.

[173] J. Gottfried and D. Zald, "On the scent of human olfactory orbitofrontal cortex: meta-analysis and comparison to non-human primates.," *Brain Research Reviews,* vol. 50, no. 2, pp. 287-304, 2005.

[174] R. Popp, M. Sommer, J. Müller and G. Hajak, "Olfactometry in fMRI studies: odor presentation using nasal continuous positive airway pressure.," *Acta Neurobiologiae Experimentalis,* vol. 64, no. 2, pp. 171-176, 2004.

[175] A. Samoylov, T. Samoylova, O. Pustovyy, A. Samoylov, M. Toivio-Kinnucan, N. Morrison, L. Globa, W. Gale and V. Vodyanoy, "Novel metal clusters isolated from blood are lethal to cancer cells.," *Cells,Tissues,Organs,* vol. 179, no. 3, pp. 115-124, 2005.

[176] K. Friston, A. Mechelli, R. Turner and C. Price, "Nonlinear responses in fMRI: the Ballon model, Volterra kernels, and other hemodynamics.," *Neuroimage,* vol. 12, pp. 466-477, 2000.

[177] D. Walker, J. Walker, P. Cavnar, J. Talyor, D. Pickel, S. Hall and J. Suarez, "Naturalistic quantification of canine olfactory sensitivity.," *Applied Animal Behaviour Scinece,* vol. 97, pp. 241-254, 2006.

[178] J. Jadauji, J. Djordjevic, J. Lundström and C. Pack, "Modulation of olfactory perception by visual cortex stimulation.," *Journal of Neuroscience,* vol. 32, no. 9, pp. 3095-3100, 2012.

[179] S. Forman, J. Cohen, M. Fitzgerald, W. Eddy, M. Mintun and D. Noll, "Improved assessment of significant activation in functional magnetic resonance imaging (fMRI): use of a cluster-size threshold.," *Magnetic Resonance in Medicine,* vol. 33, no. 5, pp. 636-647, 1995.

[180] G. Orban, "Imaging image processing in the human brain.," *Current Opinion in Neurology,* vol. 14, no. 1, pp. 47-54, 2001.

[181] D. Wilson, "Habituation of odor responses in the rat anterior piriform cortex.," *Journal of Neurophysiology,* vol. 79, no. 3, pp. 1425-1440, 1998.

[182] G. De Groof, E. Jonckers, O. Güntürkün, P. Denolf, J. V. Auderkerke and A. V. Der Linden, "Functional MRI and functional connectivity of the visual system of awake pigeons.," *Behavioural Brain Research,* vol. 239, pp. 43-50, 2013.

[183] C. Martin, D. Grenier, M. Thévenet, M. Vigouroux, B. Bertrand, M. Janier, N. Ravel and P. Litaudon, "fMRI visualization of transient activations in the rat olfactory bulb using short odor stimulations.," *Neuroimage,* vol. 36, no. 4, pp. 1288-1293, 2007.

[184] C. Stoodley and J. Schmahmann, "Evidence for topographic organization in the cerebellum of motor control versus cognitive and affective processing.," *Cortex,* vol. 46, no. 7, pp. 831-844, 2010.

[185] J. Vincent, I. Kahn, A. Snyder, M. Raichle and R. Buckner, "Evidence for a frontoparietal control system revealed by intrinsic functional connectivity.," *Jounal of Neurophysiology,* vol. 100, no. 6, pp. 3328-3342, 2008.

[186] D. Van de Ville, J. Britz and C. Michel, "EEG microstate sequences in healthy humans at rest reveal scale-free dynamics.," *Proceedings of National Academy of Sciences of U.S.A.*, vol. 42, pp. 18179-18184, 2010.

[187] R. Peeters, I. Tindemans, E. De Schutter and A. Van Der Linden, "Comparing BOLD fMRI signal changes in the awake and anesthetized rat during electrical forepaw stimulation.," *Magnetic Resonance Imaging,* vol. 19, pp. 821-826, 2001.

[188] M. Williams, J. Johnston, M. Cicoria, E. Paletz, P. Waggoner, C. Edge and S. Hallowell, "Canine detection odor signatures for explosives.," *SPIE Proceedings,* vol. 3575, pp. 291-301, 1998.

[189] D. Krestel, D. Passe, J. Smith and L. Jonsson, "Behavioral determination of olfactory thresholds to amyl acetate in dogs.," *Neuroscience and Biobehavioral Reviews,* vol. 8, pp. 169-174, 1984.

[190] T. Howell, R. Conduit, S. Toukhsati and P. Bennett, "Auditory stimulus discrimination recorded in dogs, as indicated by mismatch negativity (MMN).," *Behavioural Processes,* vol. 89, no. 1, pp. 8-13, 2012.

[191] D. Ottoson, "Analysis of the electrical activity of the olfactory epithelium.," *Acta physiologica Scandinavica,* vol. Supplementum 35, no. 122, pp. 1-83, 1955.

[192] G. Wintermann, M. Donix, P. Joraschky, J. Gerber and K. Petrowski, "Altered olfactory processing of stress-related body odors and artificial odors in patients with panic disorder.," *PLoS One,* vol. 8, no. 9, p. e74655, 2013.

[193] J. Sommer, W. Maboshe, M. Griebe, C. Heiser, K. Hörmann, B. Stuck and T. Hummel, "A mobile olfactometer for fMRI-studies.," *Journal of Neuroscience Methods,* vol. 209, no. 1, pp. 189-194, 2012.

[194] J. Sato, E. Junior, D. Takahashi, F. M. de Maria, M. Brammer and P. Morettin, "A method to produce evolving functional connectivity maps during the course of an fMRI experiment using wavelet-based time-varying Granger causality.," *Neuroimage,* vol. 31, no. 1, pp. 187-196, 2006.

[195] U. Sakoğlu, G. Pearlson, K. Kiehl, Y. Wang, A. Michael and V. Calhoun, "A method for evaluating dynamic functional network connectivity and task-modulation: application to schizophrenia.," *MAGMA,* vol. 23, no. 5-6, pp. 351-366, 2010.

[196] S. Lowen and S. Lukas, "A low-cost, MR-compatible olfactometer.," *Behavior Research Methods,* vol. 38, no. 2, pp. 307-313, 2006.

[197] B. Kent, J. Drane, B. Blumenstein and J. Manning, "A mathematical model to assess changes in the baroreceptor reflex.," *Cardiology,* vol. 57, no. 5, pp. 295-310, 1972.

[198] S. Hu, N. Wei, Q. Wang, L. Yan, E. Wei, M. Zhang, J. Hu, M. Huang, W. Zhou and Y. Xu, "Patterns of brain activation during visually evoked sexual arousal differ between homosexual and heterosexual men.," *American Journal of Neuroradiology,* vol. 29, no. 10, pp. 1890-1896, 2008.

[199] S. Bookheimer, T. Zeffiro, T. Blaxton, P. Gaillard and W. Theodore, "Activation of language cortex with automatic speech tasks.," *Neurology*, vol. 8, pp. 1151-1157, 2000.

[200] A. Garrett and R. Maddock, "Separating subjective emotion from the perception of emotion-inducing stimuli: an fMRI study.," *Neuroimage,* vol. 33, no. 1, pp. 263-274, 2006.

[201] J. Ellermann, J. Siegal, J. Strupp, T. Ebner and K. Ugurbil, "Activation of visuomotor systems during visually guided movements: a functional MRI study.," *Journal of Magnetic Resonance,* vol. 131, no. 2, pp. 272-285, 1998.

[202] Research Imaging Institute, UT Health Science Center San Antonio, [Online]. Available: http://www.brainmap.org/sleuth/.

[203] C. Yan and Y. Zang, 2010. [Online]. Available: http://www.restfmri.net.

[204] R. S. Patel, F. D. Bowman and J. K. Rilling, "A Bayesian approach to determining connectivity of the human brain.," *Human Brain Mapping,* vol. 27, no. 3, pp. 267-276, 2006.

[205] W. Pan, "A comparative review of statistical methods for discovering differentially expressed genes in replicated microarray experiments.," *Bioinformatics,* vol. 18, no. 4, pp. 546-554, 2002.

[206] T. Lorig, D. Elmes, D. Zald and J. Pardo, "A computer-controlled olfactometer for fMRI and electrophysiological studies of olfaction.," *Behavior Research Methods, Instruments & Computers,* vol. 31, pp. 370-375, 1999.

[207] A. Schlogl, S. Roberts and G. Pfurtscheller, "A criterion for adaptive autoregressive models.," in *IEEE (Ed.), Proceedings of the 22nd IEEE International Conference on Engineering in Medicine and Biology*, 2000.

[208] R. Datta, J. Lee, J. Duda, B. Avants, C. Vite, B. Tseng, J. Gee, G. Aguirre and G. Aguirre, "A digital atlas of the dog brain.," *PLoS One,* vol. 7, no. 12, p. e52140, 2012.

[209] M. García-Cabezas and H. Barbas, "A direct anterior cingulate pathway to the primate primary olfactory cortex may control attention to olfaction.," *Brain, Structures & Function,* (DOI 10.1007/s00429-013-0598-3), 2013.

[210] N. Wang, W. Zeng and L. Chen, "A fast-FENICA method on resting state fMRI data.," *Journal of Neuroscience Methods,* vol. 209, no. 1, pp. 1-12, 2012.

[211] L. Qin, Z. Wang, Y. Sun, J. Wan, S. Su, Y. Zhou and J. Xu, "A preliminary study of alterations in default network connectivity in post-traumatic stress disorder patients following recent trauma.," *Brain Research,* vol. 1484, pp. 50-56, 2012.

[212] K. Stephan and A. Roebroeck, "A short history of causal modeling of fMRI data.," *NeuroImage,* vol. 62, no. 2, pp. 856-863, 2012.

[213] R. Craddock, G. James, P. Holtzheimer, X. Hu and H. Mayberg, "A whole brain fMRI atlas generated via spatially constrained spectral clustering.," *Human Brain Mapping,* vol. 33, no. 8, pp. 1914-1928, 2012.

[214] R. Bednarski, K. Grimm, R. Harvey, V. Lucasik, W. Penn, B. Sargent, K. Spelts and Association American Animal Hospital, "AAHA anesthesia guidelines for dogs and cats.," *Journal of American Animal Hospital Association,* vol. 47, no. 6, pp. 377-385, 2011.

[215] D. Wotruba, L. Michels, R. Buechler, S. Metzler, A. Theodoridou, M. Gerstenberg, S. Walitza, S. Kollias, W. Rössler and K. Heekeren, "Aberrant coupling within and across the default mode, task-positive, and salience network in subjects at risk for psychosis.," *Schizophrenia Bulletin,* (DOI: 10.1093/schbul/sbt161), 2013.

[216] B. Hampstead, A. Stringer, R. Stilla, G. Deshpande, X. Hu, A. Moore and K. Sathian, "Activation and effective connectivity changes following explicit-memory training for face-name pairs in patients with mild cognitive impairment: a pilot study.," *Neurorehabilitation and Neural Repair,* vol. 25, no. 3, pp. 210-222, 2011.

[217] A. Poellinger, R. Thomas, P. Lio, A. Lee, N. Makris, B. Rosen and K. Kwong, "Activation and habituation in olfaction--an fMRI study.," *NeuroImage,* vol. 13, no. 4, pp. 547-560, 2001.

[218] M. Arnold, W. Miltner, H. Witte, R. Bauer and C. Braun, "Adaptive AR modeling of nonstationary time series by means of Kalman filtering.," *IEEE Transactions on Biomedical Engineering,* vol. 45, no. 5, pp. 553-562, 1998.

[219] K. S. Xu, M. Kliger and A. O. Hero III, "Adaptive evolutionary clustering.," *Data Mining and Knowledge Discovery,* vol. 28, pp. 304-336, 2014.

[220] T. Hirai, S. Kojima, A. Shimada, T. Umemura, M. Sakai and C. Itakurat, "Age-related changes in the olfactory system of dogs.," *Neuropathology and Applied Neurobiology,* vol. 22, no. 6, p. 531–539, 1996.

[221] P. Liang, Z. Li, G. Deshpande, Z. Wang, X. Hu and K. Li, "Altered causal connectivity of resting state brain networks in amnesic MCI.," *PLoS One,* 2014 (in press).

[222] W. Liao, C. Qiu, C. Gentili, M. Walter, Z. Pan, J. Ding, W. Zhang, Q. Gong and H. Chen, "Altered effective connectivity network of the amygdala in social anxiety disorder: a resting-state fMRI study.," *PLoS One,* vol. 12, p. e15238, 2010.

[223] Y. Yin, C. Jin, L. T. Eyler, H. Jin, X. Hu, L. Duan, H. Zheng, B. Feng, X. Huang, B. Shan, Q. Gong and L. Li, "Altered regional homogeneity in post-traumatic stress disorder: a resting-state functional magnetic resonance imaging study.," *Neuroscience Bulletin,* vol. 28, no. 5, pp. 541-549, 2012.

[224] C. Inman, G. James, S. Hamann, J. Rajendra, G. Pagnoni and A. Butler, "Altered resting-state effective connectivity of fronto-parietal motor control systems on the primary motor network following stroke.," *Neuroimage,* vol. 1, pp. 227-237, 2012.

[225] Y. Yin, C. Jin, X. Hu, L. Duan, Z. Li, M. Song, H. Chen, B. Feng, T. Jiang, H. Jin, C. Wong, Q. Gong and L. Li, "Altered resting-state functional connectivity of thalamus in earthquake-induced posttraumatic stress disorder: a functional magnetic resonance imaging study.," *Brain Research,* vol. 1411, pp. 98-107, 2011.

[226] S. Dimitriadis, N. Laskaris, V. Tsirka, M. Vourkas and S. Micheloyannis, "An EEG study of brain connectivity dynamics at the resting state.," *Nonlinear dynamics, Psychology, and Life sciences,* vol. 16, no. 1, pp. 5-22, 2012.

[227] M. Whalley, M. Kroes, Z. Huntley, M. Rugg, S. Davis and C. Brewin, "An fMRI investigation of posttraumatic flashbacks.," *Brain and Cognition,* vol. 81, no. 1, pp. 151-159, 2013.

[228] S. Frey, D. Pandya, M. Chakravarty, L. Bailey, M. Petrides and D. Collins, "An MRI based average macaque monkey stereotaxic atlas and space (MNI monkey space).," *Neuroimage,* vol. 55, no. 4, pp. 1435-1442, 2011.

[229] S. Price, "Anisole binding protein from dog olfactory epithelium.," *Chemical Senses,* vol. 3, no. 1, pp. 51-55, 1978.

[230] N. Ramnani and A. Owen, "Anterior prefrontal cortex: insights into function from anatomy and neuroimaging.," *Nature Reviews. Neuroscience,* vol. 5, no. 3, pp. 184-194, 2004.

[231] V. Vodyanoy and E. Morrison, "Apparatus and method for the measurement of the aerodynamics of olfaction in animals and man.". US Patent 6,979,298, 27 12 2005.

[232] G. Deshpande, K. Sathian and X. Hu, "Assessing and compensating for zero-lag correlation effects in time-lagged Granger causality analysis of fMRI.," *IEEE Transactions on Biomedical Engineering,* vol. 57, no. 6, pp. 1446-1456, 2010.

[233] W. Orrison, Atlas of brain function, Thieme, 2008.

[234] J. Lancaster, D. Tordesillas-Gutiérrez, M. Martinez, F. Salinas, A. Evans, K. Zilles, J. Mazziotta and P. Fox, "Bias between MNI and Talairach coordinates analyzed using the ICBM-152 brain template.," *Human Brain Mapping,* vol. 11, pp. 1194-1205, 2007.

[235] N. A. Shapira, Y. Liu, A. He, M. M. Bradley, M. C. Lessig, G. A. James, D. J. Stein, P. J. Lang and W. K. Goodman, "Brain activation by disgust-inducing pictures in obsessive-compulsive disorder.," *Biological Psychiatry,* vol. 54, no. 7, pp. 751-756, 2003.

[236] I. Savic, "Brain imaging studies of the functional organization of human olfaction.," *Chemical Senses,* Vols. 30, Supplement 1, pp. i222-i223, 2005.

[237] J. Britz, D. Van De Ville and C. Michel, "BOLD correlates of EEG topography reveal rapid resting-state network dynamics.," *Neuroimage,* vol. 52, p. 1162–1170, 2010.

[238] S. Ogawa, T. Lee, A. Kay and D. Tank, "Brain magnetic resonance imaging with contrast dependent on blood oxygenation.," *Proceedings of National Academy of Sciences of U.S.A.*, vol. 87, no. 24, pp. 9868-9872, 1990.

[239] A. Rack-Gomer and T. Liu, "Caffeine increases the temporal variability of resting-state BOLD connectivity in the motor cortex.," *Neuroimage,* vol. 59, pp. 2994-3002, 2012.

[240] L. McDowall and R. Dampney, "Calculation of threshold and saturation points of sigmoidal baroreflex function curves.," *American Journal of Physiology, Heart and Circulatory Physiology,* vol. 291, no. 4, pp. H2003-H2007, 2006.

[241] K. Coffman, R. Dum and P. Strick, "Cerebellar vermis is a target of projections from the motor areas in the cerebral cortex.," *Proceedings of National Academy of Sciences of U.S.A.*, vol. 108, no. 38, pp. 16068-16073, 2011.

[242] M. D. De Bellis and M. Kuchibhatla, "Cerebellar volumes in pediatric maltreatment-related posttraumatic stress disorder.," *Biological Psychiatry,* vol. 60, no. 7, pp. 697-703, 2006.

[243] K. Azuma, I. Uchiyama, H. Takano, M. Tanigawa, M. Azuma, I. Bamba and T. Yoshikawa, "Changes in cerebral blood flow during olfactory stimulation in patients with multiple chemical sensitivity: a multi-channel near-infrared spectroscopic study.," *PLoS One,* vol. 8, no. 11, p. e80567, 2013.

[244] M. Murray and M. Wallace, "Chapter 13: Characterization of multisensory integration with fMRI.," in *The Neural Bases of Multisensory Processes.*, Boca Raton (FL), CRC Press, 2012.

[245] S. Pathirana, W. Neely, L. Myers and V. Vodyanoy, "Chiral recognition of odorants (+)-carvone and (-)-carvone by phospholipid monolayers.," *Journal of the American Chemical Society*, vol. 114, pp. 1404-1405, 1992.

[246] N. Kriegeskorte, W. Simmons, P. Bellgowan and C. Baker, "Circular analysis in systems neuroscience: the dangers of double dipping.," *Nature Neuroscience*, vol. 12, no. 5, p. 535–540, 2009.

[247] S. A. Rombouts, F. Barkhof and P. Scheltens, Clinical applications of functional brain MRI., UK: Oxford University Press, 2007.

[248] J. Xiong, J. Gao, J. L. Lancaster and P. T. Fox, "Clustered pixels analysis for functional MRI activation studies of the human brain.," *Human Brain Mapping*, vol. 3, no. 4, pp. 287-301, 1995.

[249] M. Lee, C. Hacker, A. Snyder, M. Corbetta, D. Zhang, E. Leuthardt and J. Shimony, "Clustering of resting state networks.," *PLoS One*, vol. 7, no. 7, p. e40370, 2012.

[250] D. Garrett, D. A. Peterson, C. W. Anderson and M. H. Thaut, "Comparison of linear, nonlinear, and feature selection methods for EEG signal classification.," *IEEE Transactions on Neural Systems and Rehabilitation Engineering*, vol. 11, no. 2, pp. 141-144, 2003.

[251] A. Kelly, L. Uddin, B. Biswal, F. Castellanos and M. Milham, "Competition between functional brain networks mediates behavioral variability.," *Neuroimage*, vol. 39, pp. 527-537, 2008.

[252] A. Fornito, B. Harrison, A. Zalesky and J. Simons, "Competitive and cooperative dynamics of large-scale brain functional networks supporting recollection.," *Proceedings of National Academy of Sciences of U.S.A.*, vol. 109, p. 12788–12793., 2012.

[253] M. Deck, C. Henschke, B. Lee, R. Zimmerman, R. Hyman, J. Edwards, L. Saint Louis, P. Cahill, H. Stein and J. Whalen, "Computed tomography versus magnetic resonance imaging of the brain. A collaborative interinstitutional study.," *Clinical Imaging*, vol. 1, pp. 2-15, 1989.

[254] G. Deshpande, S. LaConte, S. Peltier and X. Hu, "Connectivity analysis of human functional MRI data: from linear to nonlinear and static to dynamic.," *Lecture Notes in Computer Science*, vol. 4091, pp. 17-24, 2006.

[255] J. Zhuang, S. LaConte, S. Peltier, K. Zhang and X. Hu, "Connectivity exploration with structural equation modeling: an fMRI study of bimanual motor coordination.," *NeuroImage*, vol. 25, no. 2, pp. 462-470, 2005.

[256] M. Moussa, M. Steen, P. Laurienti and S. Hayasaka, "Consistency of network modules in resting-state fMRI connectome data.," *PLoS One*, vol. 7, no. 8, p. e44428, 2012.

[257] J. Damoiseaux, S. Rombouts, F. Barkhof, P. Scheltens, C. Stam, S. Smith and C. Beckmann, "Consistent resting-state networks across healthy subjects.," *Proceedings of National Academy of Sciences of U.S.A.*, vol. 103, no. 37, pp. 13848-13853, 2006.

[258] G. Lohmann, K. Erfurth, K. Muller and R. Turner, "Critical comments on dynamic causal modelling.," *NeuroImage*, vol. 59, no. 3, pp. 2322-2329, 2012.

[259] R. Morecraft, C. Geula and M. Mesulam, "Cytoarchitecture and neural afferents of orbitofrontal cortex in the brain of the monkey.," *Journal of Comparative Neurology,* vol. 323, no. 3, pp. 341-358, 1992.

[260] K. Bush and J. Cisler, "Decoding neural events from fMRI BOLD signal: a comparison of existing approaches and development of a new algorithm.," *Magnetic Resonance Imaging,* vol. 6, pp. 976-989, 2013.

[261] W. Shirer, S. Ryali, E. Rykhlevskaia, V. Menon and M. Greicius, "Decoding subject-driven cognitive states with whole-brain connectivity patterns.," *Cerebral Cortex,* vol. 22, no. 1, pp. 158-165, 2012.

[262] A. L. Bokde, M. Karmann, S. J. Teipel, C. Born, M. Lieb, M. F. Reiser, H. J. Moller and H. Hampel, "Decreased activation along the dorsal visual pathway after a 3-month treatment with galantamine in mild Alzheimer disease: a functional magnetic resonance imaging study.," *Journal of Clinical Psychopharmacology,* vol. 29, no. 2, pp. 147-156, 2009.

[263] I. Strigo, S. Matthews and A. Simmons, "Decreased frontal regulation during pain anticipation in unmedicated subjects with major depressive disorder.," *Translational Psychiatry,* vol. 3, p. e239, 2013.

[264] R. Kleiger, J. Miller, J. Bigger and A. Moss, "Decreased heart rate variability and its association with increased mortality after acute myocardial infarction.," *American Journal of Cadiology,* vol. 59, no. 4, p. 256–262, 1987.

[265] J. Oxley and P. Waggoner, "Detection of explosives by dogs.," in *Marshall, M., and Oxley, J. eds., Aspects of Explosives Detection, Elsevier: Amsterdam*, 2009, pp. 27-40.

[266] R. Kus, M. Kaminski and K. Blinowska, "Determination of EEG activity propagation: pair-wise versus multichannel estimate.," *IEEE Transactions on Biomedical Engineering,* vol. 51, no. 9, pp. 1501-1510, 2004.

[267] American Psychiatric Association, Diagnostic and statistical manual of mental disorders (DSM IV). 4th ed., Washington D.C.: American Psychiatric Association, 1994.

[268] G. Shepherd, "Discrimination of molecular signals by the olfactory receptor neuron.," *Neuron,* vol. 13, pp. 771-790, 1994.

[269] R. Craddock, P. Holtzheimer III, X. Hu and H. Mayberg, "Disease state prediction from resting state functional connectivity.," *Magnetic Resonance in Medicine,* vol. 62, no. 6, p. 1619–1628, 2009.

[270] A. Dove, M. Brett, R. Cusack and A. Owen, "Dissociable contributions of the mid-ventrolateral frontal cortex and the medial temporal lobe system to human memory.," *NeuroImage,* vol. 31, no. 4, pp. 1790-1801, 2006.

[271] A. Jatzko, A. Schmitt, T. Demirakca, E. Weimer and D. Braus, "Disturbance in the neural circuitry underlying positive emotional processing in post-traumatic stress disorder (PTSD). An fMRI study.," *European Archives of Psychiatry & Clinical Neuroscience,* vol. 256, no. 2, pp. 112-114, 2006.

[272] K. Sathian, S. Lacey, R. Stilla, G. Gibson, G. Deshpande, X. Hu, S. LaConte and C. Glielmi, "Dual pathways for haptic and visual perception of spatial and texture information.," *NeuroImage,* vol. 57, no. 2, pp. 462-475, 2011.

[273] E. Tagliazucchi, F. von Wegner, A. Morzelewski, V. Brodbeck and H. Laufs, "Dynamic BOLD functional connectivity in humans and its electrophysiological correlates.," *Frontiers in Human Neuroscience,* vol. 6, p. 339, 2012.

[274] K. Friston, L. Harrison and W. Penny, "Dynamic causal modeling.," *NeuroImage,* vol. 19, no. 4, pp. 1273-1302, 2003.

[275] C. Büchel and K. Friston, "Dynamic changes in effective connectivity characterized by variable parameter regression and Kalman filtering.," *Human Brain Mapping,* vol. 6, no. 5-6, pp. 403-408, 1998.

[276] I. Cribben, R. Haraldsdottir, L. Atlas, T. Wager and M. Lindquist, "Dynamic connectivity regression: determining state-related changes in brain connectivity.," *Neuroimage,* vol. 61, pp. 907-920, 2012.

[277] R. Hutchison, T. Womelsdorf, E. Allen, P. Bandettini, V. Calhoun, M. Corbetta, P. S. Della, J. Duyn, G. Glover, J. Gonzalez-Castillo and et al., "Dynamic functional connectivity: promise, issues, and interpretations.," *Neuroimage,* vol. 80, pp. 360-378, 2013.

[278] M. Havlicek, J. Jan, B. Milan and V. D. Calhoun, "Dynamic Granger causality based on Kalman filter for evaluation of functional network connectivity in fMRI data.," *NeuroImage,* vol. 53, no. 1, pp. 65-77, 2010.

[279] X. Yang, R. Renken, F. Hyder, M. Siddeek, C. Greer, G. Shepherd and R. Shulman, "Dynamic mapping at the laminar level of odor-elicited responses in rat olfactory bulb by functional MRI.," *Proceedings of Natioal Academy of Sciences of U.S.A.,* vol. 95, no. 13, pp. 7715-7720, 1998.

[280] S. Keilholz, M. Magnuson, W. Pan, M. Willis and G. Thompson, "Dynamic properties of functional connectivity in the rodent.," *Brain Connectivity,* vol. 3, no. 1, pp. 31-40, 2013.

[281] C. Chang, Z. Liu, M. Chen, X. Liu and J. Duyn, "EEG correlates of time-varying BOLD functional connectivity.," *NeuroImage,* vol. 72, pp. 227-236, 2013.

[282] G. Deshpande, X. Hu, R. Stilla and K. Sathian, "Effective connectivity during haptic perception: a study using Granger causality analysis of functional magnetic resonance imaging data.," *NeuroImage,* vol. 40, no. 4, pp. 1807-1814, 2008.

[283] F. Krueger, S. Landgraf, E. van der Meer, G. Deshpande and X. Hu, "Effective connectivity of the multiplication network: a functional MRI and multivariate Granger causality mapping study.," *Human Brain Mapping,* vol. 32, no. 9, pp. 1419-1431, 2011.

[284] P. Valdes-Sosa, A. Roebroeck and J. F. K. Daunizeau, "Effective connectivity: influence, causality and biophysical modeling.," *NeuroImage,* vol. 58, no. 2, pp. 339-361, 2011.

[285] S. Fu, Y. Chen, S. M. Smith, S. D. Iversen and P. M. Matthews, "Effects of word form on brain processing of written chinese.," *Neuroimage,* vol. 17, no. 3, pp. 1538-1548, 2002.

[286] D. Zald and J. Pardo, "Emotion, olfaction, and the human amygdala: amygdala activation during aversive olfactory stimulation.," *Proceedings of National Academy of Sciences of U.S.A.,* vol. 94, no. 8, pp. 4119-4124, 1997.

[287] N. Viswaprakash, J. Dennis, L. Globa, O. Pustovyy, E. Josephson, P. Kanju, E. Morrison and V. Vodyanoy, "Enhancement of odorant-induced response in olfactory recptor neurons by zinc nanoparticles.," *Chemical Senses,* vol. 34, pp. 547-557, 2009.

[288] G. Lowe, T. Nakamura and G. Gold, "Eog amplitude is correlated with odor-stimulated adenylate-cyclase activity in the bullfrog olfactory epithelium.," *Chemical Senses,* vol. 13, no. 4, p. 710, 1988.

[289] G. Schwartz, "Estimating the dimension of a model.," *The Annals of Statistics,* vol. 5, no. 2, pp. 461-464, 1978.

[290] M. Kaminski, M. Ding, W. A. Truccolo and S. L. Bressler, "Evaluating causal relations in neural systems: Granger causality, directed transfer function and statistical assessment of significance.," *Biological Cybernetics,* vol. 85, no. 2, pp. 145-157, 2001.

[291] U. Wolf, M. Rapoport and T. Schweizer, "Evaluating the affective component of the cerebellar cognitive affective syndrome.," *Journal of Neuropsychiatry & Clinical Neuroscience,* vol. 21, no. 3, pp. 245-253, 2009.

[292] I. Inza, P. Larranaga, R. Blanco and A. J. Cerrolaza, "Filter versus wrapper gene selection approches in DNA microarray domains.," *Artificial Intelligence in Medicine,* vol. 31, no. 2, pp. 91-103, 2004.

[293] F. Pruesse, E. van der Meer, G. Deshpande, F. Krueger and I. Wartenburger, "Fluid intelligence allows flexible recruitment of the parieto-frontal network in analogical reasoning.," *Frontiers in Human Neuroscience,* vol. 5, p. 22, 2011.

[294] D. Macfarlane and C. Wildey, "fMRI headtracking using a single camera and a lightweight fiducial.," *Conference Proceedings: IEEE Engineering in Medicine & Biology Society,* pp. 5673-5676, 2010.

[295] M. De Luca, C. Beckmann, N. De Stefano, P. Matthews and S. Smith, "fMRI resting state networks define distinct modes of long-distance interactions in the human brain.," *Neuroimage,* vol. 29, no. 4, pp. 1359-1367, 2006.

[296] P. Fox and M. Raichle, "Focal physiological uncoupling of cerebral blood flow and oxidative metabolism during somatosensory stimulation in human subjects.," *Proceedings of National Academy of Sciences of U.S.A.,* vol. 4, pp. 1140-1144, 1986.

[297] H. Carr, Free precession techniques in nuclear magnetic resonance, PhD thesis (Cambridge, MA: Harvard University), 1952.

[298] M. Strenziok, F. Krueger, G. Deshpande, R. Lenroot, E. van der Meer and J. Grafman, "Fronto-parietal regulation of media violence exposure in adolescents: a multi-method study.," *Social Cognitive and Affective Neuroscience,* vol. 6, no. 5, pp. 537-547, 2011.

[299] V. Schöpf, C. Kasess, R. Lanzenberger, F. Fischmeister, C. Windischberger and E. Moser, "Fully exploratory network ICA (FENICA) on resting-state fMRI data.," *Jounal of Neuroscience Methods,* vol. 192, no. 2, pp. 207-213, 2010.

[300] K. Kalcher, W. Huf, R. Boubela, P. Filzmoser, L. Pezawas, B. Biswal, S. Kasper, E. Moser and C. Windischberger, "Fully exploratory network independent component analysis of the 1000 functional connectomes database.," *Frontiers in Human Neuroscience,* vol. 6, no. 301, pp. 1-11, 2012.

[301] K. Friston, "Functional and effective connectivity in neuroimaging: a synthesis.," *Human Brain Mapping,* vol. 2, no. 1-2, pp. 56-78, 1994.

[302] P. Fusar-Poli, A. Placentino, F. Carletti, P. Landi, P. Allen, S. Surguladze, F. Benedetti, M. Abbamonte, R. Gasparotti, F. Barale, J. Perez, P. McGuire and P. Politi, "Functional atlas of emotional faces processing: a voxel-based meta-analysis of 105 functional magnetic resonance imaging studies.," *Journal of Psychiatry Neuroscience,* vol. 34, no. 6, pp. 418-432, 2009.

[303] J. Boyett-Anderson, D. Lyons, A. Reiss, A. Schatzberg and V. Menon, "Functional brain imaging of olfactory processing in monkeys.," *NeuroImage,* vol. 20, pp. 257-264, 2003.

[304] V. van de Ven, E. Formisano, D. Prvulovic, C. Roeder and D. Linden, "Functional connectivity as revealed by spatial independent component analysis of fMRI measurements during rest.," *Human Brain Mapping,* vol. 22, no. 3, pp. 165-178, 2004.

[305] M. Lowe, B. Mock and J. Sorenson, "Functional connectivity in single and multislice echoplanar imaging using resting-state fluctuations.," *NeuroImage,* vol. 7, no. 2, pp. 119-132, 1998.

[306] M. Greicius, B. Krasnow, A. Reiss and V. Menon, "Functional connectivity in the resting brain: a network analysis of the default mode hypothesis.," *Proceedings of National Academy of Sciences of U.S.A.*, vol. 100, no. 1, pp. 253-258, 2003.

[307] A. Shinn, J. Baker, B. Cohen and D. Ongür, "Functional connectivity of left Heschl's gyrus in vulnerability to auditory hallucinations in schizophrenia.," *Schizophrenia Research,* vol. 143, no. 2-3, pp. 260-268, 2013.

[308] K. Friston, C. Frith, P. Liddle and R. Frackowiak, "Functional connectivity: the principal-component analysis of large (PET) data sets.," *Journal of Cerebral Blood Flow & Metabolism,* vol. 13, no. 1, pp. 5-14, 1993.

[309] S. A. Huettel, A. W. Song and G. McCarthy, Functional Magnetic Resonance Imaging, Sinauer Associates, Incorporated, 2009.

[310] C. Hattingh, J. Ipser, S. Tromp, S. Syal, C. Lochner, S. Brooks and D. Stein, "Functional magnetic resonance imaging during emotion recognition in social anxiety disorder: an activation likelihood meta-analysis.," *Frontiers in Human Neuroscience,* vol. 6, p. 347, 2013.

[311] C. Ferris, B. Smerkers, P. Kulkarni, M. Caffrey, O. Afacan, S. Toddes, T. Stolberg and M. Febo, "Functional magnetic resonance imaging in awake animals.," *Reviews in Neurosciences,* vol. 22, no. 6, pp. 665-674, 2011.

[312] S. Kim and K. Ugurbil, "Functional magnetic resonance imaging of the human brain.," *Journal of Neuroscience Methods,* vol. 74, no. 2, pp. 229-243, 1997.

[313] B. P. Rogers, S. B. Katwald, V. L. Morgana, C. L. Asplunde and J. C. Gore, "Functional MRI and multivariate autoregressive models.," *Magnetic Resonance Imaging,* vol. 28, no. 8, pp. 1058-1065, 2010.

[314] L. Levy, R. Henkin, A. Hutter, C. Lin, D. Martins and D. Schellinger, "Functional MRI of human olfaction.," *Journal of Computer Assisted Tomography,* vol. 21, no. 6, pp. 849-856, 1997.

[315] M. Cole, T. Yarkoni, G. Repovs, A. Anticevic and T. Braver, "Global connectivity of prefrontal cortex predicts cognitive control and intelligence.," *Journal of Neuroscience,* vol. 32, no. 26, pp. 8988-8999, 2012.

[316] M. Guye, G. Bettus, F. Bartolomei and P. Cozzone, "Graph theoretical analysis of structural and functional connectivity MRI in normal and pathological brain networks.," *MAGMA,* Vols. 5-6, pp. 409-421, 2010.

[317] H. Joe and J. Ward, "Hierarchical grouping to optimize an objective function.," *Journal of the American Statistical Association,* vol. 58, no. 301, p. 236–244, 1963.

[318] [Online]. Available: http://emedicine.medscape.com/article/835585-overview.

[319] Warner Instruments, [Online]. Available: http://vt-8-valve-timer.software.informer.com/.

[320] Smiths Medical, [Online]. Available: http://www.surgivet.com/pet-oxygen-masks/index.html.

[321] R. Doty, D. Kreiss and R. Frye, "Human odor intensity perception: correlation with frog epithelial adenylate cyclase activity and transepithelial voltage response.," *Brain Research,* vol. 527, no. 1, pp. 130-134, 1990.

[322] G. Deshpande, L. Libero, K. Sreenivasan, H. Deshpande and R. Kana, "Identification of neural connectivity signatures of autism using machine learning.," *Frontiers in Human Neuroscience,* vol. 7, p. 670, 2013.

[323] L. Zeng, H. Shen, L. Liu, L. Wang, B. Li, P. Fang, Z. Zhou, Y. Li and D. Hu, "Identifying major depression using whole-brain functional connectivity: a multivariate pattern analysis.," *Brain,* vol. 135, no. 5, pp. 1498-1507, 2012.

[324] U. Sailer, S. Robinson, F. Fischmeister, E. Moser, I. Krypsin-Exner and H. Bauer, "Imaging the changing role of feedback during learning in decision-making.," *Neuroimage,* vol. 37, no. 4, pp. 1474-1486, 2007.

[325] T. Lee, O. Josephs, R. Dolan and H. Critchley, "Imitating expressions: emotion-specific neural substrates in facial mimicry.," *Social Cognitive and Affective Neuroscience,* vol. 1, no. 2, pp. 122-135, 2006.

[326] Y. Miyashita, "Inferior temporal cortex: where visual perception meets memory.," *Annual Review of Neuroscience,* vol. 16, no. 1, pp. 245-263, 1993.

[327] J. Zhang, X. Li, C. Li, Z. Lian, X. Huang, G. Zhong, D. Zhu, K. Li, C. Jin, X. Hu, J. Han, L. Guo, X. Hu, L. Li and T. Liu, "Inferring functional interaction and transition patterns via dynamic bayesian variable partition models.," *Human Brain Mapping,* (DOI: 10.1002/hbm.22404), 2013.

[328] P. Lledo, G. Gheusi and J. Vincent, "Information processing in the mammalian olfactory system.," *Physiological Reviews,* vol. 85, no. 1, pp. 281-317, 2005.

[329] G. Deshpande, P. Santhanam and X. Hu, "Instantaneous and causal connectivity in resting state brain networks derived from functional MRI data.," *NeuroImage,* vol. 54, no. 2, pp. 1043-1052, 2011.

[330] K. Butts, S. J. Riederer, R. L. Ehman, R. M. Thompson and C. R. Jack, "Interleaved echo planar imaging on a standard MRI system.," *Magnetic Resonance in Medicine,* vol. 31, no. 1, p. 67–72, 1994.

[331] A. K. Roy, J. L. Fudge, C. Kelly, J. S. Perry, T. Daniele, C. Carlisi, B. Benson, F. Castellanos, M. P. Milham, D. S. Pine and M. Ernst, "Intrinsic functional connectivity of amygdala-based networks in adolescent generalized anxiety disorder.," *Journal of American Academy of Child & Adolescent Psychiatry,* vol. 52, no. 3, pp. 290-299.e2, 2013.

[332] R. B. Buxton, Introduction to Functional Magnetic Resonance Imaging. Principles and Techniques. 2nd Edition., University of California, San Diego., 2009.

[333] C. Granger, "Investigating causal relations by econometric models and cross-spectral methods.," *Econometrica,* vol. 37, p. 424–438, 1969.

[334] G. Deshpande and X. Hu, "Investigating effective brain connectivity from fMRI data: past findings and current issues with reference to Granger causality analysis.," *Brain Connectivity,* vol. 2, no. 5, pp. 235-245, 2012.

[335] S. Zobel, T. Hummel, J. Ilgner, A. Finkelmeyer, U. Habel, D. Timmann, J. Schulz and M. Kronenbuerger, "Involvement of the human ventrolateral thalamus in olfaction.," *Journal of Neurology,* vol. 257, no. 12, pp. 2037-2043, 2010.

[336] N. S. Nadi, J. D. Hirsch and F. L. Margolis, "Laminar distribution of putative neurotransmitter amino acids and ligand binding sites in the dog olfactory bulb.," *Journal of Neurochemistry,* vol. 34, no. 1, p. 138–146, 1980.

[337] E. Sanz-Arigita, M. Schoonheim, J. Damoiseaux, S. Rombouts, E. Maris, F. Barkhof, P. Scheltens and C. Stam, "Loss of 'small-world' networks in Alzheimer's disease: graph analysis of fMRI resting-state functional connectivity.," *PLoS One,* vol. 5, no. 11, p. e13788, 2010.

[338] E. M. Haacke, R. F. Brown, M. Thompson and R. Venkatesan, Magnetic resonance imaging: physical principles and sequence design., New York: J. Wiley & Sons., 1999.

[339] W. Golder, "Magnetic resonance spectroscopy in clinical oncology.," *Onkologie,* vol. 3, p. 304–309, 2007.

[340] A. Roebroeck, E. Formisano and R. Goebel, "Mapping directed influence over the brain using Granger causality and fMRI.," *NeuroImage,* vol. 25, p. 230–242, 2005.

[341] G. Wu, S. Stramaglia, H. Chen, W. Liao and D. Marinazzo, "Mapping the voxel-wise effective connectome in resting state fMRI.," *PLoS One,* vol. 8, no. 9, p. e73670, 2013.

[342] J. Geweke, "Measurement of linear dependence and feedback between multiple time series.," *Journal of the American Statistical Association,* vol. 77, no. 378, pp. 304-313, 1982.

[343] U. Bingel, J. Lorenz, E. Schoell, C. Weiller and C. Büchel, "Mechanisms of placebo analgesia: rACC recruitment of a subcortical antinociceptive network.," *Pain,* vol. 120, no. 1-2, pp. 8-15, 2006.

[344] T. Tsukiura, T. Fujii, T. Takahashi, R. Xiao, M. Sugiura, J. Okuda, T. Iijima and A. Yamadori, "Medial temporal lobe activation during context-dependent relational processes in episodic retrieval: an fMRI study. Functional magnetic resonance imaging.," *Human Brain Mapping,* vol. 17, no. 4, pp. 203-213, 2002.

[345] V. Schöpf, C. Windischberger, S. Robinson, C. Kasess, F. Fischmeister, R. Lanzenberger, J. Albrecht, A. Kleemann, R. Kopietz, M. Wiesmann and E. Moser, "Model-free fMRI group analysis using FENICA.," *Neuroimage,* vol. 55, no. 1, pp. 185-193, 2011.

[346] M. Brant-Zawadzki, G. Gillan and W. Nitz, "MP RAGE: a three-dimensional,T1-weighted, gradient-echo sequence–initial experience in the brain.," *Radiology,* vol. 182, p. 769–775, 1992.

[347] G. Deshpande, S. LaConte, G. James, S. Peltier and X. Hu, "Multivariate Granger causality analysis of fMRI data.," *Human Brain Mapping,* vol. 30, no. 4, pp. 1361-1373, 2009.

[348] M. Bensafi, E. Iannilli, J. Gerber and T. Hummel, "Neural coding of stimulus concentration in the human olfactory and intranasal trigeminal systems.," *Neuroscience,* vol. 154, no. 2, pp. 832-838, 2008.

[349] A. Achim and M. Lepage, "Neural correlates of memory for items and for associations: an event-related functional magnetic resonance imaging study.," *Journal of Cognitive Neuroscience,* vol. 17, no. 4, pp. 652-667, 2005.

[350] C. Wiggs, J. Weisberg and A. Martin, "Neural correlates of semantic and episodic memory retrieval.," *Neuropsychologia,* vol. 37, no. 1, pp. 103-118, 1999.

[351] E. Ricciardi, D. Bonino, C. Gentili, L. Sani, P. Pietrini and T. Vecchi, "Neural correlates of spatial working memory in humans: a functional magnetic resonance imaging study comparing visual and tactile processes.," *Neuroscience,* vol. 139, no. 1, pp. 339-349, 2006.

[352] R. Stilla, R. Hanna, E. Mariola, G. Deshpande, X. Hu and K. Sathian, "Neural processing underlying tactile microspatial discrimination in the blind: a functional magnetic resonance imaging study.," *Journal of Vision,* vol. 8, no. 10, pp. 13.1-19, 2008.

[353] J. Radua, M. Phillips, T. Russell, N. Lawrence, N. Marshall, S. Kalidindi, W. El-Hage, C. McDonald, V. Giampietro, M. Brammer, A. David and S. Surguladze, "Neural response to specific components of fearful faces in healthy and schizophrenic adults.," *NeuroImage,* vol. 49, no. 1, pp. 939-946, 2010.

[354] M. Bear, B. Connors and M. Paradiso, Neuroscience: Exploring the Brain, Baltimore: Lippincott Williams & Wilkins, 2007, p. 265–275.

[355] J. Ashburner and K. Friston, "Nonlinear spatial normalization using basis functions.," *Human Brain Mapping,* vol. 7, no. 4, pp. 254-266, 1999.

[356] M. van den Heuvel, R. Mandl and H. Hulshoff Pol, "Normalized cut group clustering of resting-state fMRI data.," *PLoS One,* vol. 3, no. 4, p. e2001, 2008.

[357] G. Deshpande, X. Hu, S. Lacey, R. Stilla and K. Sathian, "Object familiarity modulates effective connectivity during haptic shape perception.," *NeuroImage,* vol. 49, no. 3, pp. 1991-2000, 2010.

[358] K. Mori, Y. Takahashi, K. Igarashi and S. Nagayama, "Odor maps in the dorsal and lateral surfaces of the rat olfactory bulb.," *Chemical Senses,* vol. Suppl.1, pp. i103-i104, 2005.

[359] B. Slotnick and D. Restrepo, "Olfactometry with Mice.," unit 8.20., Hoboken (NJ), Wiley InterScience, 2005.

[360] I. Savic, B. Gulyas, M. Larsson and P. Roland, "Olfactory functions are mediated by parallel and hierarchical processing.," *Neuron,* vol. 26, no. 3, pp. 735-745, 2000.

[361] C. Moore, O. Pustovyy, J. Dennis, T. Moore, E. Morrison and V. Vodyanoy, "Olfactory responses to explosives associated odorants are enhanced by zinc nanoparticles.," *Talanta,* vol. 88, pp. 730-733, 2012.

[362] I. Mutschler, T. Ball, J. Wankerl and I. Strigo, "Pain and emotion in the insular cortex: evidence for functional reorganization in major depression.," *Neuroscience Letters,* vol. 520, no. 2, pp. 204-209, 2012.

[363] D. Handwerker, V. Roopchansingh, J. Gonzalez-Castillo and P. Bandettini, "Periodic changes in fMRI connectivity.," *NeuroImage,* vol. 63, no. 3, pp. 1712-1719, 2012.

[364] R. Stilla, G. Deshpande, S. Laconte, X. Hu and K. Sathian, "Posteromedial parietal cortical activity and inputs predict tactile spatial acuity.," *Journal of Neuroscience,* vol. 27, no. 41, pp. 11091-11102, 2007.

[365] R. Yehuda, "Post-traumatic stress disorder.," *New England Journal of Medicine,* vol. 346, no. 2, pp. 108-114, 2002.

[366] R. Herringa, M. Phillips, J. Almeida, S. Insana and A. Germain, "Post-traumatic stress symptoms correlate with smaller subgenual cingulate, caudate, and insula volumes in unmedicated combat veterans.," *Psychiatry Research,* vol. 203, no. 2-3, pp. 139-145, 2012.

[367] N. Leonardi, J. Richiardi, M. Gschwind, S. Simioni, J. Annoni, M. Schluep, P. Vuilleumier and D. Van De Ville, "Principal components of functional connectivity: a new approach to study dynamic brain connectivity during rest.," *NeuroImage,* vol. 83, pp. 937-950, 2013.

[368] L. Qin, P. van Gelderen, J. Derbyshire, F. Jin, J. Lee, J. de Zwart, Y. Tao and J. Duyn, "Prospective head movement correction for high resolution MRI using an in-bore optical tracking system.," *Magnetic Resonance in Medicine,* vol. 62, pp. 924-934, 2009.

[369] F. Esposito, E. Seifritz, E. Formisano, R. Morrone, T. Scarabino, G. Tedeschi, S. Cirillo, R. Goebel and F. Di Salle, "Real-time independent component analysis of fMRI time-series.," *Neuroimage,* vol. 20, no. 4, pp. 2209-2224, 2003.

[370] M. Yousef, S. Jung, L. Showe and M. Showe, "Recursive cluster elimination (RCE) for classification and feature selection from gene expression data.," *BMC Bioinformatics,* vol. 8, p. 144, 2007.

[371] G. Deshpande, Z. Li, P. Santhanam, C. D. Coles, M. E. Lynch, S. Hamann and X. Hu, "Recursive cluster elimination based support vector machine for disease state prediction using resting state functional and effective brain connectivity.," *PLoS One,* vol. 5, no. 12, p. e14277, 2010.

[372] G. Malhi, J. Lagopoulos, A. Owen, B. Ivanovski, R. Shnier and P. Sachdev, "Reduced activation to implicit affect induction in euthymic bipolar patients: an fMRI study.," *Journal of Affective Disorders,* vol. 97, no. 1-3, pp. 109-122, 2007.

[373] L. Baldacara, A. Jackowski, A. Schoedl, M. Pupo, S. Andreoli, M. Mello, A. Lacerda, J. Mari and R. Bressan, "Reduced cerebellar left hemisphere and vermal volume in adults with PTSD from a community sample.," *Journal of Psychiatric Research,* vol. 45, no. 12, pp. 1627-1633, 2011.

[374] E. Lindemer, D. Salat, E. Leritz, R. McGlinchey and W. Milberg, "Reduced cortical thickness with increased lifetime burden of PTSD in OEF/OIF veterans and the impact of comorbid TBI.," *Neuroimage: Clinical,* vol. 2, pp. 601-611, 2013.

[375] E. von dem Hagen, R. Stoyanova, S. Baron-Cohen and A. Calder, "Reduced functional connectivity within and between 'social' resting state networks in autism spectrum conditions.," *Social Cognitive and Affective Neuroscience,* vol. 8, no. 6, pp. 694-701, 2013.

[376] K. Sicard, Q. Shen, M. Brevard, R. Sullivan, C. Ferris, J. King and T. Duong, "Regional cerebral blood flow and BOLD responses in conscious and anesthetized rats under basal and hypercapnic conditions: implications for functional MRI studies.," *Journal of Cerebral Blood Flow & Metabolism,* vol. 23, no. 4, pp. 472-481, 2003.

[377] G. Baylis and E. Rolls, "Responses of neurons in the inferior temporal cortex in short term and serial recognition memory tasks.," *Experimental Brain Research,* vol. 65, no. 3, pp. 614-622, 1987.

[378] M. Greicius, B. Flores, V. Menon, G. Glover, H. Solvason, H. Kenna, A. Reiss and A. Schatzberg, "Resting-state functional connectivity in major depression: abnormally increased contributions from subgenual cingulate cortex and thalamus.," *Biological Psychiatry,* vol. 5, pp. 429-437, 2007.

[379] M. Greicius, K. Supekar, V. Menon and R. Dougherty, "Resting-state functional connectivity reflects structural connectivity in the default mode network.," *Cerebral Cortex,* vol. 1, pp. 72-78, 2009.

[380] R. Hutchison, T. Womelsdorf, J. Gati, S. Everling and R. Menon, "Resting-state networks show dynamic functional connectivity in awake humans and anesthetized macaques.," *Human Brain Mapping,* vol. 34, no. 9, pp. 2154-2177, 2012.

[381] Y. Komura, R. Tamura, T. Uwano, H. Nishijo, K. Kaga and T. Ono, "Retrospective and prospective coding for predicted reward in the sensory thalamus.," *Nature,* vol. 412, no. 6846, pp. 546-549, 2001.

[382] M. Tremblay, F. Tam and S. Graham, "Retrospective coregistration of functional magnetic resonance imaging data using external monitoring.," *Magnetic Resonance in Medicine,* vol. 53, pp. 141-149, 2005.

[383] A. Aron, H. Fisher, D. Mashek, G. Strong, H. Li and L. Brown, "Reward, motivation, and emotion systems associated with early-stage intense romantic love.," *Journal of Neurophysiology,* vol. 94, no. 1, pp. 327-337, 2005.

[384] S. Lissek, M. Hausmann, F. Knossalla, S. Peters, V. Nicolas, O. Güntürkün and M. Tegenthoff, "Sex differences in cortical and subcortical recruitment during simple and complex motor control: an fMRI study.," *Neuroimage,* vol. 37, no. 3, pp. 912-926, 2007.

[385] P. J. Rousseeuw, "Silhouettes: a graphical aid to the interpretation and validation of cluster analysis.," *Journal of Computational and Applied Mathematics,* vol. 20, pp. 53-65, 1987.

[386] C. Wildey, D. MacFarlane, A. Goyal, K. Gopinath, S. Cheshkov and R. Briggs, "Single-camera motion measurement and monitoring for magnetic resonance applications.," *Applied Optics,* vol. 50, no. 14, pp. 2088-2097, 2011.

[387] M. van den Heuvel, C. Stam, M. Boersma and H. Hulshoff Pol, "Small-world and scale-free organization of voxel-based resting-state functional connectivity in the human brain.," *Neuroimage,* vol. 43, no. 3, pp. 528-539, 2008.

[388] N. Sobel, V. Prabhakaran, J. Desmond, G. Glover, R. Goode, E. Sullivan and J. Gabrieli, "Sniffing and smelling: separate subsystems in the human olfactory cortex.," *Nature,* vol. 392, no. 6673, pp. 282-286, 1998.

[389] W. Majeed, M. Magnuson, W. Hasenkamp, H. Schwar, E. Schumacher, L. Barsalou and S. Keilholz, "Spatiotemporal dynamics of low frequency BOLD fluctuations in rats and humans.," *Neuroimage,* vol. 54, pp. 1140-1150, 2011.

[390] F. Musso, J. Brinkmeyer, A. Mobascher, T. Warbrick and G. Winterer, "Spontaneous brain activity and EEG microstates. A novel EEG/fMRI analysis approach to explore resting-state networks.," *Neuroimage,* vol. 52, no. 4, pp. 1149-1161, 2010.

[391] A. McIntosh and F. Gozales-Lima, "Structural equation modelling and its application to network analysis in functional brain imaging.," *Human Brain Mapping,* vol. 2, pp. 2-22, 1994.

[392] B. R. Frederick, K. J. Edward and J. Markee, "Studies on olfactory discrimination in dogs: II. Discriminatory behavior in a free environment.," *Journal of Comparative and Physiological Psychology,* vol. 55, no. 5, pp. 773-780, 1962.

[393] L. Wang, Support Vector Machines: Theory and Applications, New York: Springer, 2005.

[394] J. Theiler, S. Eubank, A. Longtin, B. Galdrikian and D. Farmer, "Testing for nonlinearity in time series: the method of surrogate data.," *Physica D: Nonlinear Phenomena,* vol. 58, no. 1-4, pp. 77-94, 1992.

[395] S. E. Said and D. A. Dickey, "Testing for unit roots in autoregressive moving average models of unknown order.," *Biometrika,* vol. 71, no. 3, pp. 599-607, 1984.

[396] A. Graybiel, "The basal ganglia: learning new tricks and loving it.," *Current Opinion in Neurobiology,* vol. 15, no. 6, pp. 638-644, 2005.

[397] P. Jensen, The Behavioral Biology of Dogs., Cambridge, MA: CAB International, 2007.

[398] R. Buckner, J. Andrews-Hanna and D. Schacter, "The brain's default network: anatomy, function, and relevance to disease.," *Annuals of the New York Academy of Sciences,* vol. 1124, pp. 1-38, 2008.

[399] J. Grahn, J. Parkinson and A. Owen, "The cognitive functions of the caudate nucleus.," *Progress in Neurobiology,* vol. 86, no. 3, pp. 141-155, 2008.

[400] K. Hadland, M. Rushworth, D. Gaffan and R. Passingham, "The effect of cingulate lesions on social behaviour and emotion.," *Neuropsychologia,* vol. 41, no. 8, pp. 919-931, 2003.

[401] M. Kringelbach and E. Rolls, "The functional neuroanatomy of the human orbitofrontal cortex: evidence from neuroimaging and neuropsychology.," *Progress in Neurobiology,* vol. 72, no. 5, pp. 341-372, 2004.

[402] D. B. Twieg, "The k-trajectory formulation of the NMR imaging process with applications in analysis and synthesis of imaging methods.," *Medical Physics,* vol. 5, p. 610–621, 1983.

[403] J. Medaglia, K. Chiou, J. Slocomb, N. Fitzpatrick, B. Wardecker, D. Ramanathan, J. Vesek, D. Good and F. Hillary, "The less BOLD, the wiser: support for the latent resource hypothesis after traumatic brain injury.," *Human Brain Mapping,* vol. 33, no. 4, pp. 979-993, 2012.

[404] M. Kim, R. Loucks, A. Palmer, A. Brown, K. Solomon, A. Marchante and P. Whalen, "The structural and functional connectivity of the amygdala: from normal emotion to pathological anxiety.," *Behavioral Brain Research,* vol. 2, pp. 403-410, 2011.

[405] P. Bandettini, E. Wong, R. Hinks, R. Tifosky and J. Hyde, "Time course EPI of human brain function during task activation.," *Magnetic Resonance in Medicine,* vol. 25, pp. 390-398, 1992.

[406] C. Chang and G. H. Glover, "Time–frequency dynamics of resting-state brain connectivity measured with fMRI.," *Neuroimage,* vol. 50, no. 1, pp. 81-98, 2010.

[407] D. Harel, L. Carmel and D. Lancet, "Towards an odor communication system.," *Computational Biology and Chemistry,* vol. 27, pp. 121-133, 2003.

[408] H. Lee, B. Zahneisen, T. Hugger, P. LeVan and J. Hennig, "Tracking dynamic resting-state networks at higher frequencies using MR-encephalography.," *Neuroimage,* vol. 65, pp. 216-222, 2013.

[409] E. Allen, E. Damaraju, S. Plis, E. Erhardt, T. Eichele and V. Calhoun, "Tracking whole-brain connectivity dynamics in the resting state.," *Cerebral Cortex,* vol. 24, no. 3, pp. 663-676, 2014.

[410] T. Wragg, Univariate and Multivariate Methods for the Analysis of Repeated Measures Data., GRIN Verlag, 2011.

[411] D. D. Langleben and J. C. Moriarty, "Using brain imaging for lie detection: where science, law, and policy collide.," *Psychology, Public policy & Law,* vol. 19, no. 2, pp. 222-234., 2013.

[412] H. Törnqvist, M. Kujala, S. Somppi, L. Hänninen, M. Pastell, C. Krause, J. Kujala and O. Vainio, "Visual event-related potentials of dogs: a non-invasive electroencephalography study.," *Animal Cognition,* vol. 16, no. 6, pp. 973-982, 2013.

[413] L. Strathearn, J. Li, P. Fonagy and P. Montague, "What's in a smile? maternal brain responses to infant facial cues.," *Pediatrics,* vol. 122, no. 1, pp. 40-51, 2008.

[414] V. Szetei, Á. Miklósi, J. Topál and V. Csányi, "When dogs seem to lose their nose: an investigation on the use of visual and olfactory cues in communicative context between dog and owner.," *Applied Animal Behaviour Science,* vol. 83, p. 141–152, 2003.

[415] S. Bressler and A. Seth, "Wiener-Granger causality: a well established methodology.," *Neuroimage,* vol. 58, no. 2, pp. 323-329, 2011.

[416] V. Vodyanoy, "Zinc nanoparticles interact with olfactory receptor neurons.," *Biometals,* vol. 23, pp. 1097-1103, 2010.

[417] A. G. Filler, "The history, development and impact of computed imaging in neurological diagnosis and neurosurgery: CT, MRI, and DTI," *The Internet Journal of Neurosurgery,* vol. 7, no. 1, pp. 1-76, 2010.

[418] A. Anderson, K. Christoff, I. Stappen, D. Panitz, D. Ghahremani, G. Glover, J. Gabrieli and N. Sobel, "Dissociated neural representations of intensity and valence in human olfaction.," *Nature Neuroscience,* vol. 6, no. 2, pp. 196-202, 2003.

[419] X. Li, D. Zhu, X. Jiang, C. Jin, X. Zhang, L. Guo, J. Zhang, X. Hu, L. Li and T. Liu, "Dynamic functional connectomics signatures for characterization and differentiation of PTSD patients.," *Human Brain Mapping,* (DOI: 10.1002/hbm.22290), 2013.

[420] N. Soldati, V. Calhoun, L. Bruzzone and J. Jovicich, "The use of a priori information in ICA-based techniques for real-time fMRI: an evaluation of static/dynamic and spatial/temporal characteristics.," *Frontiers in Human Neuroscience,* vol. 7, p. 64, 2013.

[421] G. Thompson, M. Magnuson, M. Merritt, H. Schwarb, W. Pan, A. McKinley, L. Tripp, E. Schumacher and S. Keilholz, "Short-time windows of correlation between large-scale functional brain networks predict vigilance intraindividually and interindividually.," *Human Brain Mapping,* vol. 34, no. 12, pp. 3280-3298, 2013.

[422] S. Lacey, H. Hagtvedt, V. Patrick, A. Anderson, R. Stilla, G. Deshpande, X. Hu, J. Sato, S. Reddy and K. Sathian, "Art for reward's sake: visual art recruits the ventral striatum," *Neuroimage,* vol. 55, no. 1, pp. 420-433, 2011.

[423] V. Vapnik, The Nature of Statistical Learning Theory, New York: Springer, 1995.

[424] J. Schmahmann and D. Pandya, "The cerebrocerebellar system.," in *The Cerebellum and Cognition*, San Diego, California, USA, Academic Press, 1997, pp. 31-60.

[425] S. Ogawa, D. Tank, R. Menon, J. Ellermann, S. Kim, H. Merkle and K. Ugurbil, "Intrinsic signal changes accompanying sensory stimulation: functional brain mapping with magnetic resonance imaging," *Proceedings of the National Academy of Sciences of the United States of America,* vol. 89, no. 13, 1992.

[426] D. Kapogiannis, G. Deshpande, F. Krueger, M. Thornburg and J. Grafman, "Brain networks shaping religious belief.," *Brain Connect* , vol. 4, no. 1, pp. 70-9, 2013.